SURFACE MODIFICATION OF CHITOSAN FILMS/MESHES FOR BIOMATERIAL APPLICATIONS

A Thesis Submitted to
the Graduate School of Engineering and Sciences of
İzmir Institute of Technology
in Partial Fulfillment of the Requirements for the Degree of

MASTER OF SCIENCE

in Biotechnology

by
Berçin IŞIKLI

October 2019
İZMİR

We approve the thesis of **Berçin IŞIKLI**

Examining Committee Members:

Prof. Dr. Funda TIHMINLIOĞLU
Department of Chemical Engineering, İzmir Institute of Technology

Prof. Dr. Banu ÖZEN
Department of Food Engineering, İzmir Institute of Technology

Asst. Prof. Dr. Emel SOKULLU
Department of Biophysics, Koç University

15 October 2019

Prof. Dr. Funda TIHMINLIOĞLU
Supervisor,
Department of Chemical Engineering,
Izmir Institute of Technology

Prof. Dr. Gülşah ŞANLI MOHAMED
Head of the Department of Biotechnology
and Bioengineering

Prof. Dr. Mehtap EANES
Dean of the Graduate School of
Engineering and Sciences

ACKNOWLEDGMENTS

Firstly, I would like to express my warmest gratitude to Prof. Dr. Funda Tıhmınlıoğlu for constant insightful advice, guidance and support during my thesis studies. She was my role model for me from the beginning of my undergraduate and graduate studies as a leader, researcher and finally as my thesis advisor.

I would like to offer special thanks to Prof. Dr. Ahmet Öztarhan, who, although no longer with us, continues to inspire by his example and dedication to all of his students. Also, I would like to thank Dr. Emel Sokullu for her help, suggestions and guidance in Ion Implantation process.

I also acknowledge to Asst. Prof. Dr. Didem Şen Karaman, Dr.Yekta Günay and Asst. Prof. Dr. Çisem Bulut Albayrak for their valuable recommendations and friendship. I am thankful to my lab and office mates Dr. Hale Oğuzlu, Dr. Sedef Tamburacı and Sibel Değer for their help and support. They were always more than a colleague throughout this thesis.

I cannot begin to express my gratitude to my parents, Nevin Cavlak and Barış Cavlak for all of the love, support, encouragement and prayers they have sent my way along this journey. Your unconditional love and support has meant the world to me, I hope that I have made you proud. To my daughter, Bilge Işıklı, you are my inspiration to achieve greatness. I wish you will do better than me on whole of your life.

This study was financially supported by The Scientific and Technological Research Council of Turkey (TUBITAK) under the Project Number of 108M391.

ABSTRACT

SURFACE MODIFICATION OF CHITOSAN FILMS/MESHES FOR BIOMATERIAL APPLICATIONS

Modification of surface of biomaterials is a great interest for many years due to first contact of surface of materials with the biological fluids. This thesis aims to investigate surface modification effect on the chemical, surface wettability, protein adsorption as well biodegradability properties of dense chitosan (Ch) and asymmetric chitosan films (ACh). The surfaces of chitosan dense and asymmetric films were modified by ion implantation technique using carbon and carbon-nitrogen hybrid ions at a fluence of $1x10^{15}$ ions/cm^2 and ion energy of 20kV.

Chemical compositions of the film surfaces were analyzed by Fourier transform infrared spectroscopy (FTIR-ATR). Surface hydrophobicity measurements were conducted by static contact angle measurements. Protein adsorption on unmodified and modified surfaces on films was investigated as a function of time at various pH conditions. After ion implantation on chitosan films, both C and C-Nitrogen ion implantation, the surfaces become rougher and hydrophobic having moderate wettability (Θ values in the range of 72-85°) and in good agreement with FTIR-ATR data findings. It was found pH dependence of the amount of protein adsorbed on the dense chitosan films as a function of time for both un-implanted and implanted films. BSA and fibrinogen were more adsorbed on the chitosan films at pH 5. The amount of BSA and fibrinogen protein adsorption was 0.97 and 1.33 $g_{protein}/g_{film}$, respectively for 60 min incubation period. Protein adsorption enhanced for C and C+N_2 ion implanted samples for BSA and fibrinogen, respectively due to the hydrophobic protein surface interaction effect. *In vitro* degradation results showed that ACh films degrade much faster (mass loss 57 %) than Ch films (40 %) due to the porous structure at the end of 3 weeks. However, the ion implanted Ch samples degraded much slower having mass loss of 30% and 17.7% for C+N_2 and C implanted samples, respectively at the end of 3 weeks compared to un-implanted Ch films as 40 %. The results are in good agreement with water sorption and surface hydrophobicity of the implanted films. This study demonstrated that surface modification, as well as structure, changes the protein sorption, wettability and biodegradation properties of the chitosan films.

ÖZET

BİYOMALZEME UYGULAMALARI İÇİN KİTOSAN FİLM VE AĞLARIN YÜZEY MODİFİKASYONU

Biyomalzemelerin yüzeylerinin değiştirilmesi, biyolojik ortam ile ilk teması malzeme yüzeyinin yapması nedeniyle büyük ilgi görmektedir. Bu tez, yoğun ve asimetrik kitosan filmlerin kimyasal, yüzey ıslanabilirliği, protein adsorpsiyonu ve biyolojik olarak parçalanabilirlik özellikleri üzerindeki yüzey modifikasyon etkisini araştırmayı amaçlamaktadır. Kitosan (Ch) yoğun ve asimetrik (ACh) filmlerin yüzeyleri, 20kV iyon enerjisi ve $1x10^{15}$ions/cm^2 yoğunlukta karbon ve karbon-azot hibrit iyonları ile iyon implantasyon tekniği ile geliştirildi.

Film yüzeylerinin kimyasal bileşimleri, Fourier dönüşümü kızılötesi spektroskopisi (FTIR-ATR) ile analiz edildi. Statik kontak açısı ölçümleri ile yüzey hidrofobikliği ölçümleri yapıldı. Modifiye edilmiş ve edilmemiş filmlerde protein adsorpsiyonu çeşitli pH koşullarında zamanın bir fonksiyonu olarak incelenmiştir. Kitosan filmlere, hem C hem de C-Azot iyon iyon implantasyonundan sonra, yüzeyler daha pürüzlü ve hidrofobik hale gelmiş olup, kontak açıları orta ıslanabilirliğe ($72 \leq \Theta \leq 85°$) çıkmıştır. Bu veriler ile FTIR-ATR bulguları uyum içindedir. Yoğun kitosan filmlerine adsorbe edilen protein miktarının, hem implante edilmemiş hem de implante edilmiş filmler için zamanın bir fonksiyonu olarak pH etkisi çalışılmış, pH 5'te tutunmanın daha fazla olduğu görülmüştür. BSA ve Fibrinogen protein adsorpsiyon miktarı, 60 dakika inkübasyon sonrası 0,97 ve 1,33 $g_{protein}/g_{film}$ olarak bulunmuştur. Protein, hidrofobik yüzey etkileşiminden dolayı BSA ve Fibrinogen için C ve C+N_2 iyonuyla implante edilmiş örnekler için protein adsorpsiyonu artmıştır. İn vitro bozunma sonuçlarına göre, ACh filmler 3 hafta sonunda gözenekli yapıları nedeniyle yoğun kitosan filmlerden (%40) daha hızlı kütle kaybı gösterdi. Bununla birlikte, implante edilen C+N_2 ve C ile implante edilen Ch filmler 3 hafta da %30 ve %17,7'lik kütle kaybı yaşamıştır. Implante edilmemiş Ch film numuneleri ise, çok daha yavaş bir şekilde, 3 hafta sonunda %40 bozulma görülmüştür. Bu sonuçlar, implante edilmiş filmlerin su emilimi ve yüzey hidrofobikliği sonuçları ile iyi bir uyum içindedir. Bu çalışma yüzey modifikasyonunun, yapının yanı sıra, kitosan filmlerinin protein emilimini, ıslanabilirliğini ve biyolojik bozunma özelliklerini etkilediğini göstermiştir.

TABLE OF CONTENTS

LIST OF FIGURES

Figure **Page**

Figure **Page**

LIST OF TABLES

Table **Page**

LIST OF ABBREVIATIONS

Ch	Dense Chitosan Film
ChG	Dense Chitosan Film plastized with glycerol
ACh	Asymmetric Chitosan Film
AChG	Asymmetric Chitosan Film with glycerol
C-Ch	C ion implanted Dense Chitosan Film
CN_2-Ch	C-N_2 hybrid ion implanted Dense Chitosan Film
C-ChG	C ion implanted Dense Chitosan Film plastized with glycerol
CN_2-ChG	C-N_2 hybrid ion implanted Dense Chitosan Film plastized with glycerol
CN_2- ACh	C-N_2 hybrid ion implanted Asymmetric Chitosan Film
MEVVA	Metal vapor vacuum arc
FTIR-ATR	Attenuated Total Reflectance Fourier Transform Infrared Spectroscopy
DSC	Differential Scanning Calorimeter
TGA	Thermo Gravimetric Analysis
SEM	Scanning Electron Microscopy
BSA	Bovine serum albumin
RBS	Rutherford Backscattering
FDA	Food and drug administration
XRD	X-Ray Diffractometer
AFM	Atomic Force Microscopy
SBF	Simulated Body Fluid
MIC	Minimum inhibitory concentration
EDGE	Ethylene glycol diglycidylet

CHAPTER 1

INTRODUCTION

With prolonged human life, medical applications have increased as a result of the importance of biomaterials increase. Biomaterials are the materials that are used for displaying the function of a tissue and/or used for therapeutic purposes such as strengthening the tissue, increasing healing speed, or releasing drugs. Up to now, through the world, the life quality of millions of patients has been improved by using these implanted biomaterials. So, recently, biomaterials have been focused on trans-dermal drug delivery systems (Lavon and Kost, 2004; Tsai et al., 2019; Takeuchi et al., 2017; Jeong et al., 2019) , nasal drug delivery (Q. Wang et al., 2019) , oral drug delivery systems (He et al., 2019; Shamekhi et al., 2018; Lee et al., 2016; Fonseca-Santos and Chorilli, 2017), scaffolds (Tamburaci and Tihminlioglu, 2018; Kara et al., 2019; Tamburaci and Tihminlioglu, 2017; Tamburaci et al., 2019) , wound dressings (Saporito et al., 2018; Ranjith et al., 2019; Güneş and Tıhmınlıoğlu, 2017) , nerve guides/conduits (Sanhueza et al., 2019; Quan et al., 2019; Shen et al., 2011; Cheong et al., 2019; Jing et al., 2018; Singh et al., 2018; Sun et al., 2019; Vijayavenkataraman et al., 2019; Wang et al., 2017), and micro fluidic devices (Zhou et al., 2019; Yu and Choudhury, 2019; Björnmalm et al., 2014; Konwarh et al., 2016; Ahn et al., 2018; Ning et al., 2016).

Today, biomaterials used in medical applications can have various forms. They can be in the form of ceramic, metal, polymer or composites and also they can be originated from synthetic or natural sources. Among these, polymers have advantages due to the biocompatibility and biodegradability properties which allow them to be used in widespread medical applications. In some areas of application, the surface properties of the material appear to be the property that limits the performance of the application since surface properties directly affects the cell interaction within the surface. So, the desired surface properties depending on the biomaterial application area could be obtained by using surface modification techniques. Widely used surface modification techniques are electron beam (Ramya et al., 2018; Zhang et al., 2010; Jiang et al., 2006;

Zhang et al., 2018) , ion beam (Malyer and Oztarhan, 2005; Patel et al., 2019; Yotoriyama et al., 2005; Selvi et al., 2005; Tanaka et al., 2011; Vasenina et al., 2018; Kaya et al., 2007), plasma (Mahajan and Sidhu, 2018; Siow, 2018), x-rays, chemical grafting and a combination of these methods. Improvement of the surface properties is critical to the application area. Due to this, various chemical surface modification methods have been used to change the physicochemical and biological properties of chitosan biomaterials' surface (Tinwala and Wairkar, 2019).

Ion beam surface modification technology is one of the well advanced technology and has promising properties such as enhancement in mechanical properties (Selvi et al., 2005; Tek et al., 2007; Sokullu Urkac et al., 2007), wear and corrosion resistance, surface wettability and cell adhesion (Mahajan and Sidhu, 2018).

Among biopolymers, chitosan is the most abundant biodegradable polymer. It is also natural, non-toxic, biodegradable and biocompatible. Many researchers have been studying the chitosan films/meshes for biomaterial applications throughout the last two decades. Studies over the past 25 years has been focused on wound healing, hemodialysis membranes, drug targeting, pharmaceutical applications, and tissue engineering applications as well as scaffolds for regenerative medicine based on its functions as biodegradability, biocompatibility, low toxicity, preventing antimicrobial activity, suitability for fibroblast formation, hydrophilicity, gel-forming capability, high adsorption capacity and cationic nature due to the reactive functional groups. (Dash et al., 2011; Shalaby et al., 2004; Ahmed et al., 2018).

More than the form of the chitosan biomaterial, much attention has been focused on the surface modification of various forms of chitosan to impart new and improved surface properties for biomaterial applications since the surface of the biomaterial first contacts with the biological fluid.

During the past decade, surface modification methods such as plasma surface modification, grafting, etching, and chemical modification have been intensively studied on chitosan polymer. Plasma surface modification of chitosan films is a widely used technique to control a variety of their properties, such as biodegradability, protein adsorption, (Chang and Chain, 2013) permeability, haemostatic activity and ability to support cell adhesion, proliferation and growth (Demina et al., 2015; Dorraki et al., 2015). On the other hand, after plasma surface modification, the lower BSA protein adsorption amount was reported (Chang and Chian, 2013) because of the surface defects. Ion beam irradiation makes possible to design made-to-order polymer matrix

with desired properties (Patel et al., 2019). MEVVA Ion Implantation method which uses co-implantation of gas and metal reactive ions, has been studied on the surface modification few polymer surfaces. To our knowledge, there, there is no study reported related to surface modification on chitosan polymers.

Therefore, the aim of this study was to use an ion implantation technique to modify the surfaces of asymmetric and dense chitosan films for biomedical applications. Firstly, dense films were prepared with the solvent casting method. Asymmetric films were prepared by the combination of the solvent casting method followed by freeze drying. Effects of chitosan concentration as well as pre-treatment temperature and chitosan microstructure and porosity effects were studied.

Effects of ion implantation according to the type of ion (C and C-N_2 hybrid) on the chemical, thermal, surface characteristics (surface roughness, surface wettability), biodegradation, microstructure properties, and water uptake capacities of the films were investigated. The effects of the ion implantation on biodegradation mechanism and molecular weight change were also analyzed. Ion implantation impact on surface characteristics were determined with FTIR-ATR, DSC, contact angle, surface roughness, protein adsorption biodegradation mechanism and molecular weight change studies.

The thesis report consists of five chapters, which altogether aim at covering the preparation and characterization of the chitosan films for biomaterial applications. In Chapter 1, the general information about the background of the study is given. Chapter 2 gives the literature studies about biomaterials, chitosan and chitosan film production and biodegradation mechanism, surface modification methods, ion beam surface modification, and protein adsorption. Chapter 3 gives the experimental results. Before and after ion implantation chemical, thermal, surface and morphological changes are listed in this chapter. In Chapter 4 results and discussions were summarized. Finally, Chapter 5 gives the conclusions and closing comments on the study were given.

CHAPTER 2

LITERATURE REVIEW

2.1. Biomaterials

Biomaterials can be classified in different ways. According to material type, biomaterials can be classified into 4 groups. These are polymeric, metal based, ceramics, and composite biomaterials.

All of these materials have some benefits and damages that affect the application of the material. For instance, metals are strong, tough and ductile but their processing is very hard and they corrode when contacted with tissue.

Ceramic biomaterials are very suitable for biomaterial applications since they are inert, strong, and highly biocompatible. But they are also brittle and making them is very difficult.

Composites can show a combination of all of these properties but their processing is also difficult. Similarly, polymers are easily shaped and fabrication is also very easy. Some types of polymers are degradable; this can be both an advantage and a disadvantage according to the application area. They deform under pressurized mediums and they are not strong for many biomaterial applications. These benefits and disadvantages of biomaterials were tabulated in Table 2.1.

Table 2.1. Benefits and disadvantages of biomaterials.

Biomaterial	**Benefits**	**Disadvantages**
Polymers	Resilient, easily producible, degradable	Not strong, deform with time and pressure, degradable
Metals	Strong, tough, ductile.	Corrodible, dense, difficult to produce.
Ceramics	High biocompatibility, inert, robust, made-to-order	Fragile, inflexible, difficult to produce
Composites	Robust, made-to-order	Processing is difficult

Successful biomaterials require some properties such as: biocompatibility, biodegradability, biomechanical properties, surface chemistry, micro topography, and porosity, pore size criterions.

Biocompatibility minimizes the inflammatory response. The host immune system should recognize the implant as part of the host and not reject it. By using biocompatible materials, clinically useful, preferred cellular and/or host tissue response is obtained. Biocompatible biomaterials perform desired function in accordance with medical treatment. Also, they are selected to perform best healing performance in accordance with patients and tissue used. Biocompatibility is not only affected by host tissue properties such as pH, blood transport speed, etc., but also materials' surface properties. As a result, the biocompatibility characteristics of the biomaterials enable the appropriate host response after the application. When biomaterial is implanted into the body, first of all, protein adheres on and is followed by cell attachment. In other worlds, protein adsorption plays an important role in determining material biocompatibility. To control the biocompatibility of the biomaterial, researchers work on the adsorption profile studies before and after surface modification of the biomaterials.

Biodegradation rate must be engineered to comply with new the tissue growing rate and also mechanical support. Moreover, by products of the implanted foreign material expelled from the host's physiological system. Biodegradability and usage in the body without toxic effect and toxic by-products of the biomaterials are primarily concerned with the safety of the medical device/application. So that, toxicity has a major role for biocompatibility since it may cause a slight or irreversible change of the function of a cell/cells because of chemical injury. Change in the function of cell/cells may cause cell death.

Biomechanical properties of the implanted material must be suitable with application areas. *The surface chemistry* is the main factor to cellular adhesion since the cell-material interface is mediated by proteins adsorbed from the surrounding medium onto the substratum. However, a highly adhesive surface allowing for a strong cell adhesion may also result in cell immobilization. *Micro topography* of the biomaterial effects the cell growing and spreading behavior. On smooth surfaces, the cells are able to spread, perhaps forming greater number of hemi-desmosomes as anchors to the substrate. In contrast, on rougher surfaces, the cells appear to form local contacts that allow the cells to span across the space between surfaces. *Porosity, pore size* of the biomaterial is important for scaffolds. Large pore size maximizes attachment, migration

and growth, extracellular matrix production, fluid circulation, and vascularization within the pore space throughout the scaffold structure. However, porosity and pore size of the biomaterial should be adjusted for better cell proliferation depending on cell tissue.

Bostancioglu et al. work on the adhesion profile and differentiation capacity of a mesenchymal stem cell by zinc, silver and copper ions doping on hydroxyapatite surfaces. They found that the cell adhesion capability is higher on ions coated surfaces compared to non-ion coated surfaces, therefore higher biocompatibility was obtained for zinc, silver and copper ions coated surfaces (Bostancioglu et al., 2017).

Application areas of the materials are changing according to material properties. For instance, in vascular stents, orthopedic, and dental applications generally metallic biomaterials have been used. Similarly, ceramics can be used in many application areas such as dental porcelains, bonds and bonding applications. Also, polymers can be used in the joint replacements, grafts, suture, wound dressings, nerve guides, etc. These examples of main biomaterials and application areas are summarized and given in Table 2.2. Some of the biomaterials can be used in many application areas.

Table 2.2. Application areas of some biomaterials.

Materials	**Specific Type**	**Application Area**
Polymers	Polyamide (Nylon)	Packaging film, catheters, sutures, and mold parts.
	UHWPE	Articulating surfaces in joint replacements.
	Polytetrafluoroethylene	Catheter and artificial vascular grafts.
	Chitosan	Artificial skin, wound dressings and sutures. Tissue Engineering Applications
Metals	TiNi Alloys	Orthodontic arcwire, bone tissue applications, total hip an total knee arthroplasty, fracture fixation
	CoCr Alloys	Stems of prostheses for knee and hip joints.
Ceramics	Aluminum oxide	Orthopedics and dental surgery.
	Hydroxyapatite	Bone bonding applications
	Carbon, Bioinert Bioceramics	Bone plates, screws, femoral heads, and middle ear ossicles.
Composites	Carbon-carbon, wire or fiber reinforced bone cement	Joint implants and heart valves.

As a result, to be able to use the biomaterial, as long as possible, in the host tissue without side effects as infection and rejection of the implanted biomaterial, it should possess some important properties and also material's chemical, mechanical and surface properties must be suitable to the application area. To be able to gain these properties without side effect by host tissue; new materials, new engineering processes and new surface modification methods have been studied. For biomaterial applications, where applicable, polymeric biomaterials are preferred because of the advantages of the application as well as processing.

2.1.1. Polymeric Biomaterials

Polymeric biomaterials are used in the form of artificial surgical implants, dental materials, dressings, encapsulations, drug delivery systems, tissue engineering products, and medical devices to improve the life quality of the patients. Biomaterials take place and stimulate the function of defected tissue or organ. Polymeric biomaterials have many advantages. These advantages are listed below.

- Easy to manufacture in many shapes,
- Easy to processed secondarily,
- Reasonable cost, and
- Wide variety of mechanical and physical properties.

On the contrary to these advantages, sterilizing of the polymers is a problem. Sterilizing the polymeric biomaterials are difficult than ceramics and metals because of the lower thermal and chemical stability of polymers. Generally, they are sterilized by dry heat, steam sterilization, radiation, and ethylene oxide gas. Sterilization with EtO and propylene oxide gases is widely used since they can be applied at low temperatures (Park and Bronzino, 2003)

Polymeric biomaterials widely used in drug delivery systems and tissue engineering applications. Table 2.3 shows some properties of most common polymeric biomaterials as well as application areas. Appropriate material selection is made according to biomaterial properties such as mechanical, surface, biodegradability and biodegradation time.

Table 2.3. Most common polymeric biomaterial properties and application areas (Ratner, et al. 1996)

Polymer	Tensile Strength (MPa)	Water Absorption (%)	Water Contact Angle (º)	Application
Polyethylene				Tubing, shunts, catheters.
• LDPE	4-16	<0.01	93-95	Plastic surgery implants.
• HDPE	21-38	<0.01	91	Acetabulum in total hip
• UHMWPE	22-42	<0.01	-	prostheses, artificial knee prostheses.
Polypropylene	30-38	<0.01	104	Heart valve structures, oxygenator and plasmapheresis films.
Polyethylene terephtlate	59-72	0.1-0.2	101-109	Oxygenator film, tubing, shunts, burn dressings.
Polyamides	62-68	1.5	-	Hemodialysis film, non-absorbable sutures
Polystyrene	35-83	0.10	45	Tissue culture dish
Polycarbonate	55-66	0.2	62	Connectors, oxygenator, Hemodialyzer and plasmapheresis films.
Poly glycolic acid	29-35	2-6.5	-	Drug delivery devices, absorbable sutures.
Poly (lactic acid) (MW: 50000-30000)	58.6	>1	-	Drug delivery
(MW: 107000-550000)	50-100	0.2 - 1	-	Drug delivery
Cellulose acetate	610-690	-	-	Hemodialysis film.

(Cont. on next page)

Table 2.3. (Cont.)

Chitosan	60-69	100 – 1000 % *according to form*	55	Membrane, drug delivery, hemostasis, wound healing, wound dressing, immunological applications, contact lens.
Silk	-	-	-	Non-absorbable sutures.

Scaffolds for the tissue applications must have mainly three properties. First of all, they must define the proper 3D shape. Secondly, they should fulfill the role of the tissue having required properties during regeneration continues. And finally, they must enable the ingrowths' of tissue and accelerate tissue regeneration (Deb et al., 2018).

For drug delivery applications, in addition to the biocompatibility requirements, biomaterial should release of drug to the target tissue without side effects as well the desired rate. Particle size, surface charge distribution, hydrophilicity and hydrophilicity of the biomaterial effects the drug delivery performance (George, 2019).

2.1.1.1. Biodegradable Polymers

After the 1980s, biodegradable polymers have replaced biologically stable biomaterials in the application areas like biomaterial, medicine, packaging, agriculture, etc. For biomaterial and medicine applications, replacing of biologically stable biomaterials with biodegradable ones happens because of the toxic effect and biocompatibility responses of the living tissue to stable polymers. This replacement was primarily caused by the absence of residual mass of by-products of biodegradable polymers. So that, the biodegradable/biocompatible polymers were preferred since they prevent the formation of side effects such as inflammation in living tissues.

Biodegradable polymers can be natural, synthetic and a mixture of natural polymers with additives and fillers. Synthetic biodegradable polymers offer an advantage in the view of productivity over natural polymers. Synthetic biodegradable

polymers can be tailor-made by adding desired materials with predictable properties. On the other hand, most of the natural polymers offer an advantage with non-toxic effect in the tissue. So, the first polymers used as biodegradable biomaterials are natural polymers.

For the biodegradable biomaterial applications, the degradation rate of the material is a significant limitation since it must be equal to the time of the tissue formation rate of the organism (Lu, 2007). Biodegradation rate also limits the material selection for the specific applications. For instance, biodegradation time of PGA changes between 6 to 12 months whereas PGLA degrades in 5-6 months. There are also biodegradable materials which degrade more than 2 years as Poly (l-lactic acid). Beyond the biodegradation time, biocompatibility, shape, porosity, surface properties and mechanical strength of the biomaterial are very important parameters for operation and post-operation host tissue response and also to support daily activities of the patient. Mechanical strengths, thermal behavior, and by-products of degradation of the biodegradable polymers are changing according to the polymer which plays an important role to choose the suitable polymer to the application area.

Biodegradation mechanism of polymeric biomaterials based on their chemical origin is divided into eight major groups (Park and Bronzino, 2003).

1. Biodegradable aliphatic polyesters
2. Biodegradable copolymers
3. Polyorthoesters
4. Polyandhydrides
5. Poly (ester-ethers)
6. Biodegradable polysaccharides (Chitosan)
7. Polyamino acids
8. Inorganic biodegradable polymers

Biodegradation of polymeric biomaterials can be classified into two groups. These are enzymatic degradation and hydrolytically degradation. Natural polymers mostly degrade enzymatically.

Bulk degradation of biodegradable polymers starts with implantation into the host tissue. The degradation of the molecular weight of the polymer starts when it

contacts with aqueous media. On the other hand, the mass loss just starts after reducing the molecular chains to be able to diffusion thought out the polymer matrix (Liu, 2007).

For drug delivery applications, the main aim is to transport and release of drug to the target tissue without side effects. Particle size, surface charge distribution, hydrophilicity and hydrophilicity of the biomaterial effects the drug delivery performance (George, 2019). As well as drug delivery applications, natural polymers are preferred because of the high biocompatibility in tissue engineering applications. Among the natural polymers, chitosan tops the list not only in the field of drug delivery, tissue engineering applications but also in the fields of wound healing, tissue engineering, and artificial skin applications (Mohandas et al., 2018; Jeong et al., 2019; Tamburaci and Tihminlioglu, 2017; Ali and Ahmed, 2018).

2.2. Structure and Properties of Chitosan

Chitosan is one of the most abundant polymers in nature. Chitosan is a linear polysaccharide. Chitosan is obtained from chitin by alkaline deacetylation. Chitin is extracted mostly from crab, lobsters and shrimp shells (Wang, 2007). Chitin is also found in the external skeletons on insects and spiders. Based on studies in a number of fungi, the cell wall contains relatively minor amount chitin (Bowman and Free, 2006).

The structure of chitosan is a linear polymer of β-(l-4)-N-acetyl-D-glucosamine. In Figure 2.1 chemical structure of chitin and chitosan is shown.

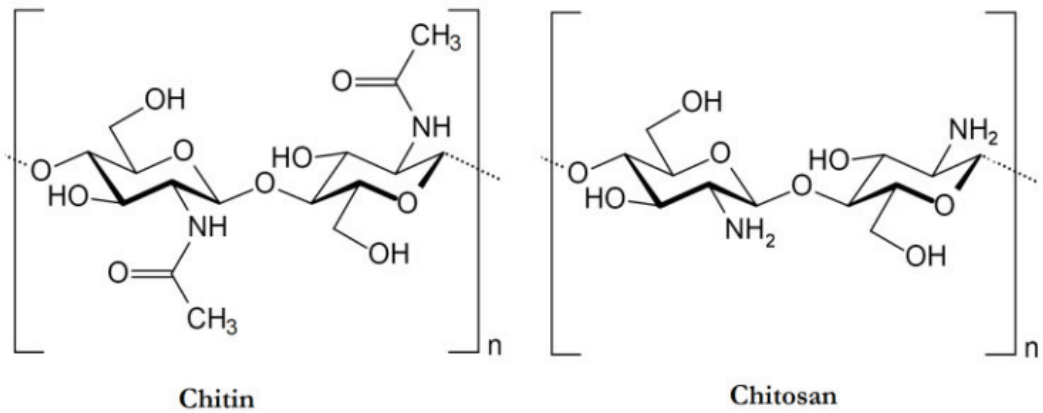

Figure 2.1. Chemical structure of Chitin and Chitosan
(Source:Younes and Rinaudo, 2015)

Chitosan has amine group, so that it becomes possible to contain a large number of hydroxyl and amino groups (Arancibia et al., 2015). These two functional groups ensure various probabilities for derivatization or grafting of desirable bioactive groups (Tangpasuthadol, 2003).

Main properties of chitosan can be listed as non-toxicity, biocompatibility, biodegradability, film-forming ability (Kaczmarek, 2019), antibacterial effects. These features make the chitosan preferred polymer in biomaterial applications (Kargarzadehetal, 2018).

Chitosan is the only pseudonatural cationic polymer. This unique property makes it suitable for many applications. Positive charge of chitosan attracts negatively charged plasma proteins. Plasma proteins lead to platelet adhesion and activation followed by thrombus formation and clot (Benesch, 2002; Martinez-Camacho, 2010). So, being positive charged under acidic conditions makes the chitosan suitable for wound healing and blood clots (Hu et al., 2018; Sun et al., 2019; Saporito et al., 2018). Chitosan is also good coagulant agent and flocculent. Negatively charged substances, such as proteins, solids, dyes, and polymers and the amino groups of chitosan can interact with each other's.

Molecular weight of the chitosan is another important characteristic. It is affecting both mechanical properties and producibility. Molecular weight of the chitosan can be determined with many methods as light scattering, chromatography, mass spectrometry and viscometry. Among those, viscometry is the simplest and most rapid method for molecular weight determination.

Antimicrobial property is another attractive biological property of chitosan from the standpoint of food and medical applications. Branched chitosan was expected to have considerable activity due to the presence of free amino groups and considered of interest as potential water-soluble antimicrobial agents (Uragami, 2006). The antimicrobial activity proved to be considerably dependent on the chemical structures of the branches and most likely on the density of free amino groups in polysaccharides (Uragami, 2006).

No et al. compares the antibacterial activity of chitosan and chitosan oligomers. In the study gram-negative and gram-positive bacteria was used. Chitosan shows, higher antibacterial activity especially to gram-positive bacteria. Study concludes that the use of chitosan at lower pH increases its antibacterial effectiveness and should be further studied as a natural food additive (No et al., 2002).

Biodegradation mechanisms according to chemical origin were mentioned in the biodegradable polymers in Section 2.1.1. According to this classification, chitosan is placed in the 6th group. Chitosan is biodegradable polysaccharide and its biodegradation can be controlled by changing following parameters.

- The ratio of glucosamine to *N*-acyl glucosamine and
- The length of the acyl side group and/or
- It's molecular weight.

Chitosan is an enzymatically degraded polymer. Chitosanase enzyme breaks chitosan down into chitosan oligosaccharides. And then, oligosaccharides are further acted upon by other enzymes to generate N-glucosamine (Figure 2.2).

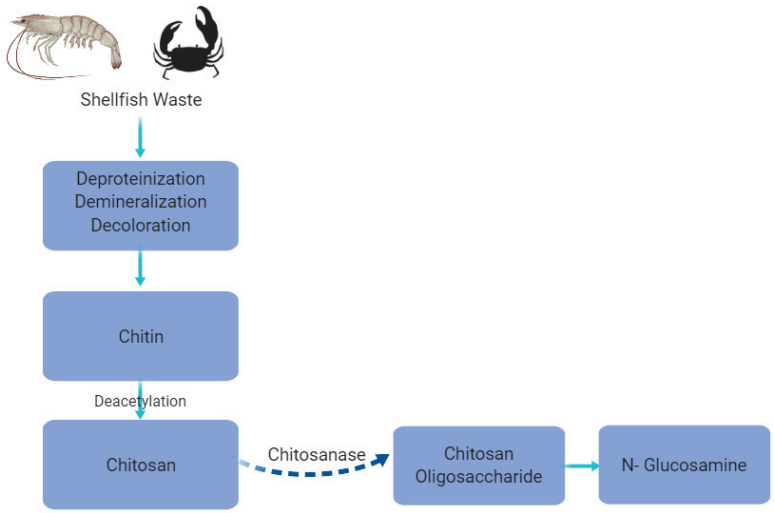

Figure 2.2. Formation and Biodegradation of Chitosan

As seen from the literature chitosan and their modified derivatives have an unlimited application potential. Chitosan is used in the fields of food preservation, material science, medical science, tissue engineering, gene therapy, microbiological, immunological, agriculture, cosmetics, polymeric nanoparticles, etc., (Harish et al., 2007; Varma et al., 2018; Shi et al., 2006; Sahoo et al., 2009; Uragami, 2006).

2.3. Chitosan Film Production

The production method of the chitosan films affects both the application area of the material and microstructure of the material. In this study, for various application areas, two different forms of chitosan films were prepared. These are dense and asymmetric films.

Asymmetric films consist of dense layer, transition area and porous sponge like layer which have high porosity while the dense films have much lower amount of pores. In the following parts, their production methods in literature were summarized.

Dense films consist of dense layer. A dense film does not contain any pores and/or sponge like layer.

2.3.1. Dense Film Production

Chitosan can be dissolved under acidic conditions where the pH < 6.3 but it is also affected by solvent mixing, deacetylation, solvation, and chemical modification (Zimet et al., 2019). Generally, acetic acid and formic acids were used to dissolve chitosan for film production. Some dilute organic acids, such as nitric acid, hydrochloric acid, per chloric acid, and phosphoric acid can also be used to prepare a chitosan solution with long stirring time and heating but those acids were not suitable for mass production.

One of the oldest film production method is the solvent casting method. In industry, the continuous solvent cast process was developed more than a hundred years ago. The main advantage of the solvent casting method is drying. The drying process does not require any additional mechanical or thermal stress while the final product has homogeneous thickness distribution, optical purity, and transparency (Siemann, 2005). Also, by this method soluble but non-melting polymers can be cast. In the literature, there are many applications of film production with the solvent casting method (Prasad, 2017; Speer, 2018; Deng, 2018).

Homez-Jara et al. have worked on the preparation and characterization of edible chitosan films with 0.5%, 1.0% and 1.5% chitosan concentration. They evaluate polymer concentration and drying temperature effects on physicochemical, mechanical

and thermal properties. Three different drying temperatures of 2°C, 25°C, and 40°C were studied. They concluded that the lower drying temperature proportionally affects the moisture content, solubility, water vapor permeability and optical property of chitosan films. Using 40°C drying temperature with higher chitosan concentration increases tensile strength, and swelling power. Optimization for food packaging or coating applications was successfully developed in the study (Homez-Jara et al., 2018).

Aider reviewed chitosan film production by extrusion and casting methods. Polymer-based packaging materials are produced by extrusion method. Polymers heated to molten state and then the resin forced to form the desired shape. After extruded material reached the room temperature, solidified product is obtained. In casting method, solvent poured into Petri dish and air dried. For further drying, the films were vacuum dried for 30 minutes at room temperature. Then the films were peeled from the dish (Aider, 2010).

Srinivasa et al. prepared the chitosan films by solvent casting method. They dissolve chitosan 2% (w/v) with 1% acetic acid solution. Dissolved solution was filtered through sieve to remove un-dissolved impurities. After the filtration, entrapped air was removed by vacuum pump. Finally, solvent was casted and dried to obtain film (Srinivasa et al., 2007).

By chemical modifications, made-to-order biomaterials can be produced. Ghosh et al. prepared modified and unmodified dense chitosan films. The study, focused on the micro structural morphology and physical performance of the chitosan films. By dissolving chitosan powder in an aqueous acetic acid solution chitosan films were obtained. After that, films were treated with methanol and EGDE. They found that the EGDE treated film's tensile modulus increase and the elongation-at-break decreased without changing the tensile strength (Ghosh et al. 2010).

Monte et al. have prepared chitosan powder from shrimp waste. They have work on the thermodynamic properties and microstructure of the dense and plasticizer (glycerol) added chitosan films prepared by solvent casting method. They investigated moisture isotherms of the films. They have used 10% (w/w) of plasticizer and found that the addition of plasticizer resulted in change at sorption isotherm. They explain this situation as plasticizer addition reduces the film's crystallinity. Due to this situation water easily drips out of the film (Monte et al., 2018).

2.3.2. Asymmetric Film Production (ACh)

Asymmetric films structure is similar with the natural skin with the ability of protection from external threats as bacterial penetration and chemicals by dense layer and also asymmetric films allows gas exchanges, adsorption, serves moist environment and supports cell proliferation (Miguel et al., 2019). Mostly used production techniques of asymmetric membrane are phase inversion, electrospinning, bioprinting, two-step phase separation and dry/wet phase separation. The dry/wet phase separation is the most widely used technique. This method requires the solution of film forming polymer with at least one volatile solvent. When solvent evaporates, film's outside undergoes to dry phase separation.

Figure 2.3 summaries the method. Solvent evaporation from the outside of the film destabilizes the film's outer side. Then, the film is immersed in coagulant tank to wet phase separation. In wet phase separation, bulk of the film structure is formed. By final evaporation of volatile solvent, solvent loss and polymer coagulation rates can be controlled. Evaporation time is very important since it affects both thickness of dense layer and also porosity. By increasing the evaporation time, porosity of the films could be decreased. And also, by increasing the evaporation time, thickness of the dry phase separation region could be increased (Mi et al., 2003).

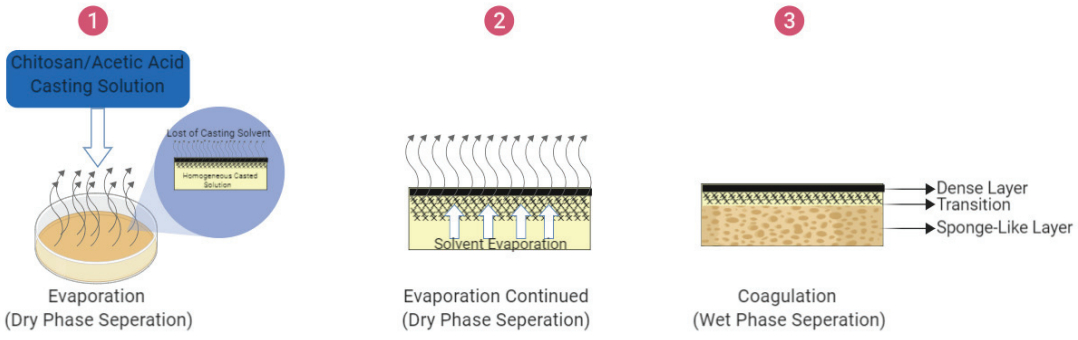

Figure 2.3. Asymmetric chitosan membrane production by dry/wet phase separation

Asymmetric chitosan based membranes were studied by several researchers for tissue engineering and wound healing applications since chitosan simulates the

migration of inflammatory cells and fibroblasts to the wound side. Ho et al. prepare asymmetric chitosan membranes for guided tissue regeneration. They produced the membranes by using the two-step phase separation. The membrane prepared showed good tissue integration having 80-120μm pore size ranges and prevented bacterial growth and suggested as promising for the treatment of guided tissue regeneration (Ho et al., 2010).

Miguel et al. reviewed the Chitosan based asymmetric membranes for wound healing studies. In the review wet-phase inversion, dry/wet phase separation, $scCO_2$-assisted phase inversion technique, electrospinning and bio-printing methods explored. They concluded that the chitosan is the one of the most promising material for wound healing with advantages of intrinsic characteristics and also producibility with different techniques despite of that no chitosan based wound dressing has been produced (Miguel et al., 2019).

Mi et al. also used dry/wet phase separation method to prepare asymmetric chitosan films (87% deacetylated, MW 70000) for antimicrobial wound dressing applications. Effect of pre-heated treatment for 10-60 minutes for dry phase separation was studied. In addition, silver sulfadiazine addition and its release were investigated. They found that dense-layer-thickness change is proportional to evaporation time. Increasing evaporation time increases the dense layer thickness. On the contrary, porosity is decreased by evaporation time increase. As evaporation time increased, water vapor and oxygen permeability of film decreased. It means that the shortest time evaporation time has a highest permeability. They suggested this film as a potential wound dressing with antimicrobial activity for infected wounds (Mi et al., 2003).

Hong et al. have studied the development of asymmetric gradational-changed chitosan films for treatment in guided periodontal tissue regeneration. In the study, they use immersion precipitate phase inversion technique to fabricate the film. They have found that the structural properties of the film effected by the concentration and solvent evaporation time. Results of the study, increasing the evaporation time degrease the porosity and water absorption amount. Solvent evaporation time increase can cause larger colloid particle inside the membrane layer, so that, membrane thickness increases. Moreover, higher porosity is resulted with higher adsorbed water percent (Hong et al., 2007).

Santos et al. have prepared chitosan dense and macro porous membranes by using silica as a porogen. Effect of silica concentration on the porosity and average pore

size was investigated in the study. Production method has two steps. First one is the, dissolving the polymer with acetic acid. Then half of the solution casted and dried in oven at 50°C for 3 h. Secondly, silica dispersion was added to the remaining solution. At the end of the 3h silica added solution were poured into the plate, which has been in the oven already, with a 1:1 ratio. Plates dried for further 24h in oven for complete solvent evaporation (Santos et al., 2008).

2.4. Surface Modification Techniques

Biomaterial surface creates a boundary between the bulk polymer and host tissue. Due to the interaction with tissue, surface modification has great interest. The change in the surface properties of the biomaterial can alter the chemical composition, surface wetting, surface roughness, crystallinity, permeability, biocompatibility, conductivity, adhesion, and cross-linking density of the polymers. Depending on the surface changes that took place, the polymers can be used for different applications such as medical and food industries, especially the biodegradable and biocompatible polymers. So, new techniques for polymers have been studied and developed to modify the surface of polymers especially used in biomedical applications.

During the past decade, surface modification methods such as grafting, light-induced modification, laser treatment, plasma treatment, etching, polyelectrolyte modification and ion implantation have been intensively studied (Prashanth and Tharanathan, 2007; Nedela et al., 2017; Liu et al., 2019; Shen et al., 2011; Silva et al., 2008). According to application area of the biomaterials suitable surface modification methods is used by considering the pros and cons of the method.

In the *plasma treatment* method, non-polymer-forming gases used to improve surface wettability and adhesion properties of polymers.

Similarly, in surface *Grafting* new functions is added to polymer. Grafting, generally consist of more than one step where the physicochemical properties and the morphology of the surface must be improved to provide appropriate interactions and sufficient bonding sites for the grafted biomaterials.

Laser irradiation of solid substrates can also add new functions to polymer. This method has an advantage of the lack of pollutants, tailor-made topography at the

microscale to nanoscale, high enhancement factor, low cost with high uniformity and reproducibility (Nedela et al., 2017; Hu et al., 2018).

Ion implantation method is fundamentally surface/near-surface processing method. Ion penetration at the same energy level is lower than electrons because of stronger interactions with target atoms. Ion implantation method can modify/improve physical and chemical properties of materials within 50 nm to 1µm surface layer. Chemical modification of ion implanted surfaces occurs since implanted chemical species different than the target. Although implanted chemical species is in a small amount, they may still reach high relative concentrations on a microscopic scale. Structural modification of ion implanted surfaces occurs because of the damage on the structure of the target caused by generating radiation defects, changes of phase, atom removal etc. (Lulli, 2014).

Some researchers found that the properties such as hardness, wear resistance, and corrosion resistance can be improved by ion implantation method (Patel et al., 2019; Nedela et al., 2017; Oks et al., 1997; Malyer and Oztarhan, 2005).

Therefore, there are many methods related to the surface modification. Also, there are numerous polymeric biomaterial studies (Table 2.4).

Table 2.4. Surface Modification Techniques in Literature

Surface Modification Method	**Results**	**Ref**
Ion implantation method (MEVVA ion source)	* Mg-ion-implantation on poly(L-lactide/caprolactone) films make the surface rougher and more hydrophilic and changes the organic structure on the surface. * Ion implantation has increased the biodegradation rate.	Sokullu et al., 2017
Surface grafting	* Improved surface hydrophobicity * Selective adsorption	Tangpasuthadol, et al., 2003

(Cont. on next page)

Table 2.4. (Cont.)

Surface grafting	* CS–CA film has good hydrophilicity and excellent biomineralization ability. * CS–CA film have potential application in bone tissue engineering	Liu et al., 2016
Ar/N_2/H_2 surface-wave plasma treatment	* Improved chitosan film functionalization.	Zhang et al., 2013
Plasma surface modification	* The 120 s plasma-modified chitosan film possesses optimal hydrophilicity, swelling property, biodegradability, and the lowest BSA protein adsorption, because pro- longed plasma treatment time may cause films surface damage.	Chang and Chian, 2013

2.4.1. Ion Implantation Methods

Chitosan surface characteristics can be changed by using modification techniques such as ion implantation. Ion implantation equipment is relatively complex equipment and needs complex components. These components are given below (Öztarhan et al., 2005)

1. Vacuum system and sample chamber,
2. Power supply,
3. Ion source assembly,
4. Voltage isolation transformer,
5. Electronic measurement instruments,
6. Second-grid power supply,
7. Faraday cage.

Ion implantation system is basically summarized in two steps. The first step is the forming a plasma. The second step is extracting the positive ions from the plasma and accelerating toward the target.

There are three methods commonly used for ion implantation. Similarly, all of these methods used in isolated high vacuum chamber.

- Mass analyzed ion implantation,
- Direct ion implantation,
- Plasma source ion implantation.

Recently, a new ion implantation technique Metal Vapor ion implantation has been used. The first MEVVA ion implantation facility of Turkey was in İzmir (Öztarhan.et al., 2005). In this thesis, the films were ion implanted in this facility.

In order to provide the desired wear resistance, corrosion resistance, surface wettability, briefly, to provide desired tissue-material response in implant applications, it is desired to replace the surface properties with the ion implantation method. In the literature several types of ions such as calcium, oxygen, nitrogen, sodium, magnesium, argon, silver, carbon, helium and combination of these ions have been studied.

Rautray et al. reviewed ion implantation of different ions on titanium based biomaterials to find the solution for metal ion releasing to tissues. They concluded that the calcium and phosphorus implantation increases the biocompatibility of the titanium biomaterials whereas the strontium and silicon improves the osteoconductive properties (Rautray et al., 2011).

Kondyurina et al. worked on cell growing onto the ion implanted PTFE. They use nitrogen ions of 20 keV energies and 10^{13}–10^{16} ions/cm^2 ion fluencies. Polymer surfaces analyzed with FTIR-ATR, XPS spectroscopy, wetting contact angle measurement and AFM images. By comparison of ion implanted and un-implanted samples with respect to cell growing and cell adherence it was found ion implanted PTFE and ePTFE are suitable for cell growing and cell spreading on the surface when the medical implant is required to be totally coated by the cells (Kondyurina et al., 2014).

Prakrajang et al. worked on the effects of ion interaction with plant cell envelope. Chitosan and cellulose membranes were bombarded with nitrogen and argon ions with energy of 15– 25keV to fluencies in an order of 10^{15} ions/cm^2 at room

temperature whereas control samples were not bombarded. The results show that surface roughness and membrane impedance is inversely proportional to each other. In other worlds, when surface roughness increases, membrane impedance decreases. Surface can accelerate the DNA transfer and increase in the membrane capacitance which raises the driving force to transfer DNA are involved in the mechanisms for ion-beam-induced gene transfer. On the contrary, the contact angle of the materials surface is oppositely effect the DNA transfer. The modification of the membrane surface morphology and the electric properties of the films are changed according to implanted ion species (Prakrajang et al., 2009)

Shin et al. worked on the effects of N^+ ion implantation on surface structures and properties of polyimide films. The polyimide films were modified by 100keV ions using an N^+ source at room temperature. They have revealed that the nitrogen and oxygen atoms originally contained in the PI films were selectively treated by the incident N^+ ion causing reduction in the relative ratios of these elements. Moreover, new C-O and O-O bond was deduced. Also, the adhesion of the PI films was increased by increasing the surface roughness and N^+ ion fluence (Shin et al., 2010).

Vasenina et al. worked on the surface physicochemical and mechanical properties of PLA (polylactic acid). PLA surfaces were modified by Silver, Argon and Carbon ions. No new bonds were observed. They reported molecular weight degradation of PLA by two times more. The micro hardness of PLA decreases by a factor of 1.3. The surface conductivity increases by 6 orders of magnitude after ion implantation. According to AFM results, surface roughness increases with irradiation dose. The highest roughness of 190 nm was found on the silver irradiated samples (Vasenina et al., 2018)

Yotoriyama et al. worked on the analysis of cell-adhesion surface induced by ion-beam irradiation into biodegradable polymer. They performed Ar^+ ion-beam irradiation into PLLA at energy of 50 keV at room temperature. In the study they used non-irradiated PLLA sheets as control material (Yotoriyama et al., 2005).

Takano et al. used ion beam modification. They use Ar^+ or He^+ ions irritate on polylactic acid (PLA) because of its high transparency property. In the study they resulted that the PLA hardness increased by He^+ ion bombardment (Takano et al., 2011).

2.5. Characterization of Surface Properties of Films

For biomaterial applications, surface hydrophobicity, surface roughness, and protein adsorption properties are very important since they affect the interactions of the biomaterial with biological fluids.

In other words, biocompatibility of the biomaterial plays an important role for choosing correct material for appropriate host response. So that material surfaces can be modified without changing their bulk properties. After these modifications, characterization techniques were studied to understand the mechanical, physicochemical, morphological and surface property changes of the biomaterial. In the following sections characterization by protein adsorption, contact angle and surface roughness is given.

2.5.1. Protein Adsorption

Protein adsorption has achieved increasing attention in the last years. It is largely controlled by surface properties and plays a key role in many processes. A protein adsorption phenomenon is still complicated to understand. From the first systematic studies on the 1970s, development of the methods and techniques is still increasing by experimental approaches. Protein adsorption is very important in biomaterial applications since material's biocompatibility, cell adhesion behavior and proliferation can be determined by protein adsorption. Protein adsorption is affected by many factors. These are can be classified in 3 groups as external parameters, protein properties and surface properties. Table 2.5 summaries the factors and sub-factors that effects protein adsorption.

Table 2.5. Factors controls protein adsorption

External Parameters	Protein Properties	Surface Properties
Temperature	Size	Surface energy
Ph	Structural stability	Polarity

(Cont. on next page)

Table 2.6. (Cont.)

Ionic strength	Composition	Charge
Buffer conditions		Morphology
		Wettability

Temperature effects both adsorption kinetic and equilibrium state. Generally, at higher temperature protein adsorption is increases. Electronic states of the proteins determined by the pH. Isoelectric point (pI) of the protein and pH of medium affects the adsorption. pH directly affects the surface charge of the adsorbent. At point of zero charge (PZC), the negatively and positively charged molecular species are present in equal concentration. Zero net charge in proteins is called isoelectric point (pI). Due to their isoelectric point or point of zero charge, molecules behave variously at different pH values. If the medium of the pH is lower than pI, surface of the adsorbent is positively charged and electrostatic interactions begin to occur between the adsorbent and adsorbate. When the medium of the pH is higher than pI, surface of the adsorbent is negatively charged and again the electrostatic interactions take place in the adsorption medium.

When the pH is equal to pI of the protein, charges are balanced. pH – Isoelectric point relationship is summarized in the Table 2.6. Higher ionic strength results with enhanced adsorption to like-charged substrates while oppositely charged substrate inhibited.

Table 2.7. pH – Isoelectric point relationship

pH< pI	**pH = pI**	**pH > Pi**
Positive charged protein	Neutral molecule	Negatively charged protein
High adsorption rate	Min. repulsion	High adsorption rate

Proteins composed of amino acids and possible side chains. Proteins are functionally and structurally complex macromolecules. Size, structural stability and composition of the proteins control the protein adsorption. Small proteins, as lysozyme, show small tendency to structure change and they can diffuse faster. Moderate size proteins, as albumin, are re-oriented when contact with the surface. Large proteins as

lipoproteins, are unstable polymers, can be re-oriented. Lipoproteins show strong affinity to hydrophobic surfaces. Another high molecular weight protein is glycoprotein. Glycoprotein cannot adsorb onto hydrophobic surfaces because of the hydrophilic structure. So that, to be able to understand the protein adsorption phenomena, properties of the proteins must be known. In the Table 2.6 physical properties of mostly studied proteins are given.

Table 2.8. Mostly studied protein's physical properties

Property	**Albumin**	**Fibrinogen**	**Lysozyme**
Mass (Da)	69,000	340,000	14,600
Isoelectric point (pH units)	4.8	5.5	11.1

Proteins can be detected with Total Nitrogen Detection (Kjeldal Method), Gravimetric Methods and Spectrometric Methods. Generally spectrophotometric methods are used for protein detection. Lowry, Biuret and BCA are the methods used in the UV region. Protein detection method is chosen according to;

- Amount of unknown protein in the sample
- Structure of sample (most appropriates are liquid samples)
- Specificity of the method for protein
- Amino acid composition of protein that is quantified.

The total protein concentration is exhibited by a color change of the sample solution in proportion to protein concentration, which can then be measured using colorimetric techniques. In order to determine the quantities of proteins adsorbed on chitosan films before and after ion implantation treatment, the films were incubated in protein solution as a function of time.

Kotwal and Schmidt worked on protein sorption on electrically conducting polymers. The study focused on the hypothesis of the electrical charge effect on nerve regeneration. Protein adsorption has been studied to control this effect. Test conducted with fibronectin solutions. In the study, proteins were marked with radiolabels to detect the adsorbed protein amount on the polymer surface. Electrical current was used on the

PC-12 cell cultured polypyrrole film surface to determine the electric stimulation. Delayed and immediate stimulation was studied. They found that the fibronectin adsorption in immediate stimulation was increased and also, PC-12 cells grown on polypyrrole films have longer neurites. Results of the delayed stimulation do not show any difference for fibronectin absorbance and neurite growth. As a result, increased fibronectin adsorption with immediate electrical stimulation may explain improved neurite extension.

Surface modification and effects of hydrophobicity on protein adsorption were studied by Tangpasuthadol et al., (2003). Surface modification changes the hydrophobicity because of the attachment of the selected molecules. For the protein adsorption BSA and lysozyme was used. Chitosan surface becomes hydrophobic after reacting with stearoyl functional group which enhances the protein adsorption. When the chitosan reacted with anhydride derivatives, BSA adsorption decreased while lysozyme adsorption was increased. Charge-charge repulsion between BSA-Chitosan happened. On the other hand, lysozyme adsorbed more since it was positively charged at pH 7.4. Hydrogen bonding and charge-charge attraction increased the lysozyme adsorption.

2.5.2. Surface Wettability

Surface wettability is one of the most important parameters which influences on biological response with biomaterials. Surface wettability measured by the air-water contact angle measurement. Contact angle measurement is a simple method. Contact angle (θ) shows the degree of hydrophobic behavior of the surface. Figure 2.4 summarizes the hydrophilic and hydrophobic behavior in between the liquid-solid interfaces.

When $\theta>90°C$ low wettability occurs. When $\theta<90°C$ surface called as hydrophilic and high wettability occurs. Cells adhere and spread more effectively on moderate contact angles which is between $30^o<\theta<90^o$ as compared to hydrophobic surfaces (Devi and Dutta 2019).

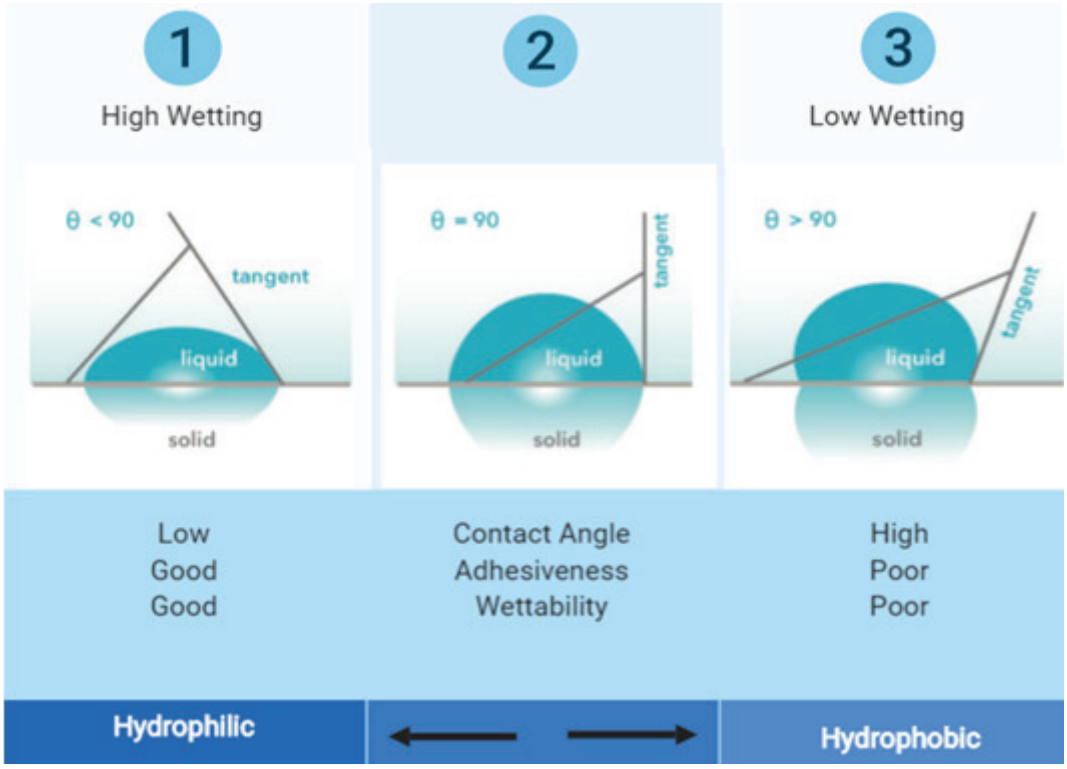

Figure 2.4. Surface Wettability illustration

2.5.3. Surface Roughness Measurement

Surface roughness is an important characteristic parameter that reflects the rough surface performance, and it is a measure of the surface quality. "*Ra*" (arithmetical mean of the surface roughness) is commonly used to indicate the level of surface roughness. For film deposition the final average roughness plays a crucial role for many applications. Contact angle of the surface and the adhesion potential is affected by surface roughness. Today, to improve accuracy and efficiency of the surface roughness measurement methods and new techniques are still studied (Chen et al., 2018).

Chou et al. works on the surface roughness and stiffness changes by changing the degree of deacetylation (DD) by investigating the rabbit corneal keratocyte migration, proliferation and differentiation on the surface. They increase DD from 75 % to 96 % and they have reported the decreased surface roughness and increased surface stiffness. They obtained enhancement of cell migration, spheroid formation, and phenotypic maintenance by increasing surface roughness.

CHAPTER 3

EXPERIMENTAL

3.1. Material and Method

3.1.1. Material

Low molecular weight chitosan powder, acetic acid with 99.7% purity, and sodium phosphate monobasic, were obtained from Sigma Aldrich. The chitosan and solvent properties are given in Table 3.1 and Table 3.2 respectively.

Table 3.1. Properties of Chitosan

Property	Information
Chemical Structure	$(C_{12}H_{24}N_2O_9)_n$
Molecular Weight (g/mol)	$(340.33)_n$
Physical Form	75-85% deacetylated

Table 3.2. Properties of Acetic Acid

Property	Information
Chemical Structure	CH_3COOH
Molecular Weight (g/mol)	60.05
Physical Form	1.05
Purity (%)	99.7

Sodium potassium tartarate tetra-hydrate, Copper II sulphate pentahydrate, and disodium hydrogen phosphate, sodium hydroxide were purchased from Merck.

Glycerol was purchased from Fluka and used as plasticizer for flexible film production. Citric acid anhydrous was purchased from Alfa and sodium chloride was purchased from Riedel. Acetic acid was used as a solvent for the preparation of polymer solution.

For protein adsorption studies BCA acid kit was purchased from Thermo – Pierce. The proteins, albumin and fibrinogen, used in the study were molecular biology grade and purchased from Sigma Aldrich.

Simulated body fluid (SBF) solution was prepared by dissolving the chemical reagents of NaCl, KCl, $CaCl_2$, $MgCl_2$, Na_2HPO_4, $NaHCO_3$, Na_2SO_4, $MgCl_2.6H_2O$ and $Na_2HPO_4 \cdot 12H_2O$ in distilled water. Preparation of 10x PBS was given in the Appendix A. The ion concentrations of SBF solution was given in Table 3.3. SBF solution simulates the human blood plasma.

Table 3.3. Ion concentrations of SBF

Na^+	K^+	Ca^{2+}	Mg^{2+}	Cl^-	HCO^{3-}	HPO_4^{2-}	SO_4^{2-}
142	5	2.5	1.5	103	27	1	0.5

In this study, three types of films were prepared which were dense chitosan films (Ch), dense chitosan film plasticized with glycerol (ChG) and asymmetric chitosan film (ACh).

3.1.2. Methods

In this study, chitosan based dense and asymmetric films were prepared. The prepared samples were ion implanted with C and $C+N_2$ hybrid ions. Implanted and un-implanted samples were characterized by TGA, DSC, SEM, FTIR-ATR, surface roughness, water absorption, contact angle, protein adsorption behavior and *in vitro* biodegradation.

3.2. Preparation of Films

In this study, 2% (w/v) chitosan solutions were used for the preparation of both dense and asymmetric films based on the preliminary experiments due to the repeatability of the constant film thickness by constant film volume, easy dissolution in acetic acid solution and tear-free behavior compared to other chitosan concentrations.

3.2.1. Preparation Dense Chitosan Films (Ch)

Dense chitosan films were prepared by using the solvent casting method. The dense film production steps were summarized below (Figure 3.1).

In the solvent casting method, 2% (w/v) chitosan powder dissolved in acetic acid 2% (v/v) in 24 hours with constant stirring. After 24 hr., solution filtered to remove the un-dissolved matter. After filtration, the solution was left to stand for 12 h without stirring for degassing. After all the bubbles had escaped, constant quantity of chitosan solution was poured onto the Petri dishes and then oven dried at 50˚C for 48h.

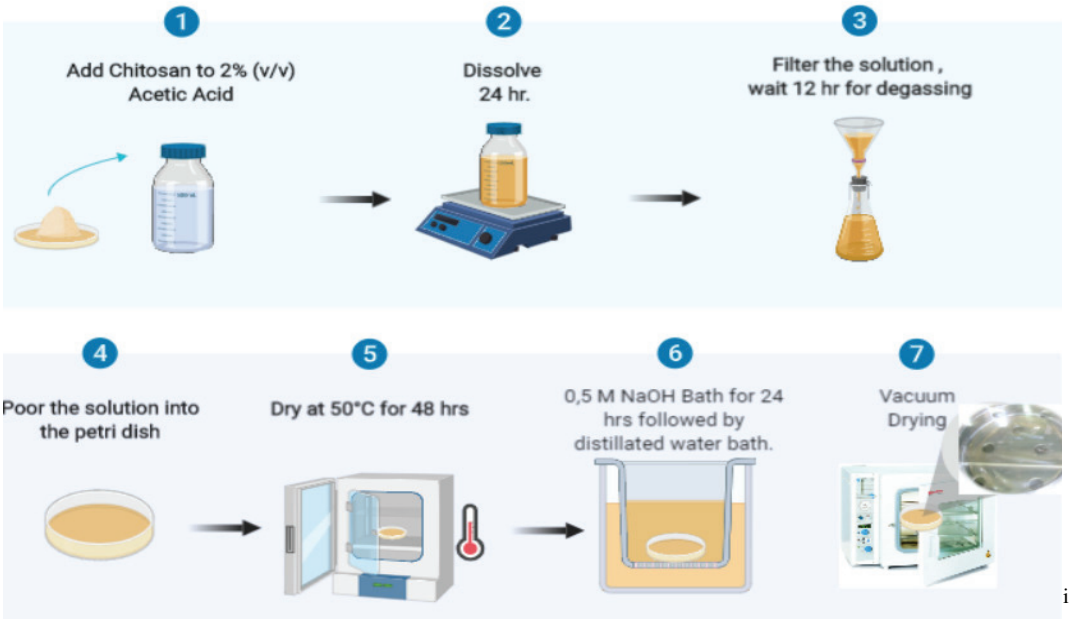

Figure 3.1. Dense Chitosan film preparation

After the drying step, the films were placed in 0,5M NaOH bath for 24h to neutralize. Then, the films were soaked in distilled water and dried again under vacuum to remove remaining NaOH on the films.

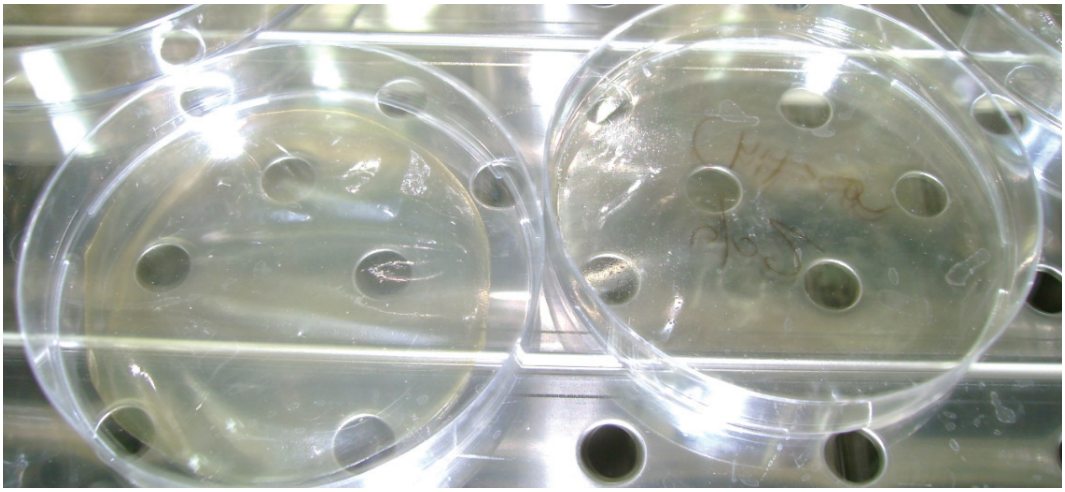

Figure 3.2. Produced Ch film

3.2.2. Preparation of Dense Chitosan Films Plasticized with Glycerol (ChG)

Glycerol plasticized dense chitosan film was prepared by almost the same procedure described in the Section 3.2.1. Only difference was the addition of the 2% (w/v) plasticizer before the filtration.

2% (w/v) chitosan powder dissolved in acetic acid 2% (v/v) in 24 hours with constant stirring. After dissolving the chitosan in acetic acid, 2% (w/v) glycerol was added and stirred for additional 24h.

After 24 hr., solution filtered to remove the un-dissolved matter. After filtration, the solution was left to stand for 12 h without stirring for degassing. After all the bubbles had escaped, constant quantity of chitosan solution was poured onto the Petri dishes and then oven dried at 50˚C for 48h. After the drying step, the films were placed in 0,5M NaOH bath for 24h to neutralize. Then, the films were soaked in distilled water and dried again under vacuum to remove remaining NaOH on the films.

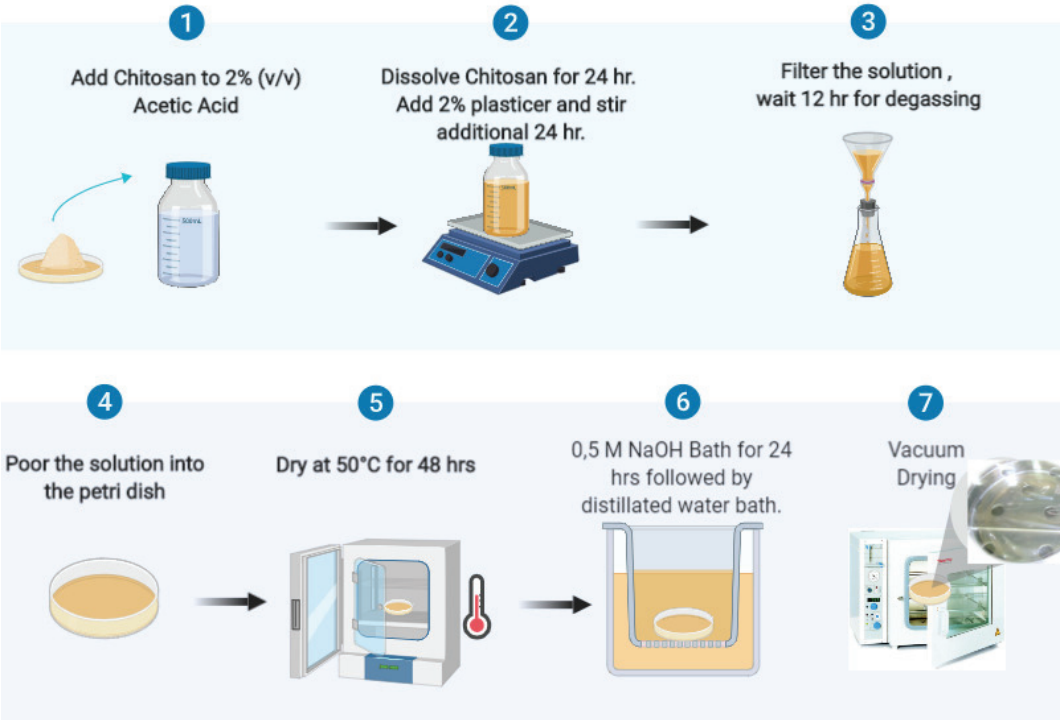

Figure 3.3. Dense Chitosan film preparation with plasticer

3.2.3. Preparation of Asymmetric Chitosan Films (ACh)

Asymmetric chitosan films were prepared by dry/wet phase separation. To produce 2% (w/v) asymmetric chitosan films 20 minutes pre-treatment time was studied. In dry/wet phase separation method, chitosan was dissolved in 2% (v/v) acetic acid for 24 hours. Insoluble substances were removed by filtration. In filtration a medium-pore-size glass funnel was used. After filtration, the solution waited for 12 hours without stirring for degassing. Constant quantity of chitosan solution was poured onto Petri dishes and pre-heated in an oven at 50˚C for 20 minutes for the dry phase separation.

After the dry phase separation, films were immersed into the coagulant tank for wet phase separation. In the study, 2% (wt/v) NaOH was used as coagulant. The pre-heated solutions were casted into aqueous NaOH solution for 24 hours for coagulation. After coagulation, the solidified chitosan film was soaked in distilled water to remove NaOH. Then, the sample was subsequently pre-conditioned and freeze-dried with a Labconco® shell freezer for 72 hours to obtain asymmetric films.

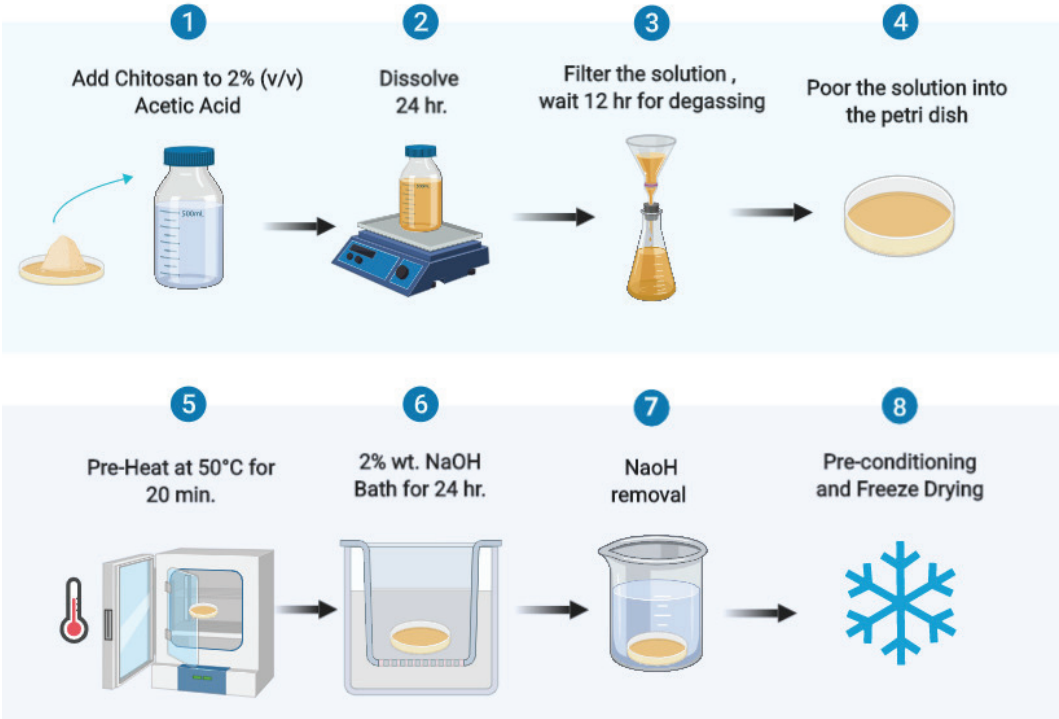

Figure 3.4. Asymmetric Chitosan film preparation

Asymmetric membrane pore distribution was studied by changing the pre-treatment time. Five different pre-treatment times (10, 15, 20, 30, and 40 minutes) were studied.

3.3. Surface Modification of Chitosan Films

Dense and asymmetric film surfaces were ion implanted by using the MEVVA ion implanter in Aegean University (Figure 3.5).

For ion implantation source, two types of ions were used. These ions are carbon, and a combination of both carbon and nitrogen hybrid ions. The ions are bombarded onto film surface with fluencies of $1x10^{15}$ ion/cm^2 with extraction volts of 20 kV, pulse rate of 1 Hz and ion energy of 60keV. In Figure 3.5, ion implantation facility in Aegean University is shown.

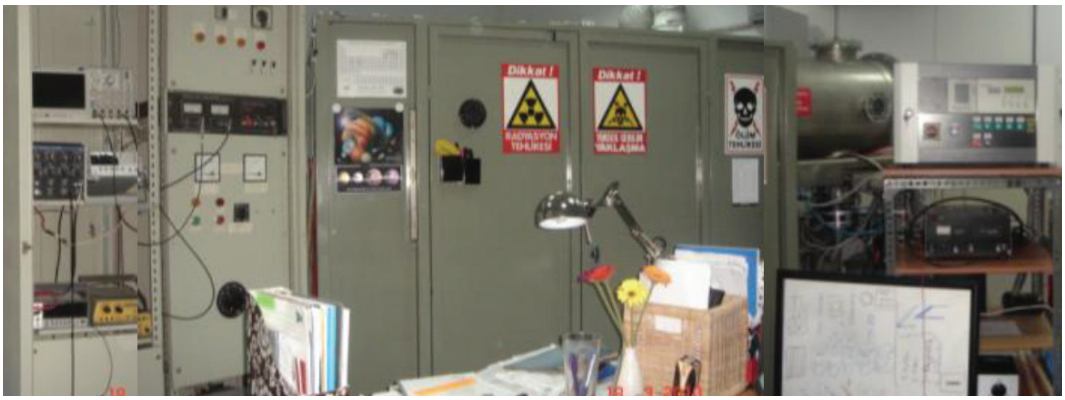

Figure 3.5. Ion implantation facility

3.4. Chemical and Thermal Characterization

In order to determine the chemical structural changes after ion implantation, Fourier transform infrared (FTIR-ATR) spectroscopy was used. Thermal analyses of untreated, C and C+N_2 ion implanted chitosan film samples were studied by DSC, and TGA.

3.4.1. Fourier Transform Infrared Spectrometer, FTIR-ATR

Chemical structure of chitosan films was investigated by using FTIR-ATR spectrometer (Perkin Elmer Spectrum 100) within a frequency range of 4000-650 cm^{-1}.

FTIR-ATR analysis was used for the detection of new chemical bonds formations on the surface. The spectra were collected in the materials by averaging 10 scans at 4 cm^{-1} resolution. Samples for FTIR-ATR were prepared by cutting the films rectangular with dimensions of 0. 9 x 9 cm.

3.4.2. Differential Scanning Calorimeter, DSC

Differential Scanning Calorimeter (DSC) is a technique which combines the ease measurement of heating and cooling curves of material as a function of

temperature and time with the quantitative features of calorimetry. Temperature is measured continuously and a differential technique is used to assess the heat flow into the sample and to equalize incidental heat gains and losses between the reference and sample.

Differential Scanning Calorimeter analysis was performed with Shimadzu DSC-50. The DSC curves were performed under a dynamic nitrogen atmosphere using sample mass as 2 to 5 mg at a heating rate of 10˚C/min from room temperature to 450˚C.

3.4.3. Thermal Gravimetry Analysis, TGA

Thermal gravimetric analysis measures the mass change of a sample as a function of temperature in the scanning mode or as a function of time in the isothermal mode. Experimental conditions affect the mass change characteristics. Factors such as sample mass, volume and physical form, the shape and nature of the sample holder, the nature and pressure of the atmosphere in the sample chamber and the scanning rate all have important influences on the characteristics of the recorded curve. From the thermo gravimetric curves, the characteristic temperature of decomposition is obtained.

- Temperature of initial decomposition (T_{di})
- Temperature at maximum decomposition rate (T_{max}).

In this study, the TGA analyses of the samples were performed in nitrogen atmosphere with 40 ml/min flow rate and at a temperature of between 25º C to 700º C at a rate of 10°C/min. The effect of ion implantation treatment on thermal stability was studied. The used sample weights were in between 9.8 mg to 10.1 mg.

3.5. Surface Characterization

In order to determine the morphology of the films, pore size in asymmetric films as well as changes in surface microstructure after ion implantation, scanning electron microscopy (SEM) was used. Contact angle measurements by sessile drop method were

performed in order to examine the surface wettability after ion implantation on film surfaces. Change in surface roughness was performed by atomic force microscopy measurement (AFM).

3.5.1. Scanning Electron Microscopy, SEM

SEM was used in order to see the morphology of the dense and asymmetric films, pore sizes in asymmetric films as well as surface morphology changes after ion implantation on chitosan films. The films were gold coated with a thin layer. The coated samples were examined by Philips XL30. The surface morphology of the protein adsorbed films was also investigated. The films were exposed to 0.1 µg/ml protein solution for 30 minutes. Then the films were taken from the protein solution and dried at 37ºC for 24 hours. Then the coated samples were analyzed by SEM.

3.5.2. Surface Wettability Measurement

Contact angle measurement of the prepared chitosan films were conducted using the initial contact angle method. During the analyses, 6µl of distillated water were dropped on the film surface by an automatic syringe (Figure 3.6).

Figure 3.6. Contact angle meter

The images of the droplet rapidly recorded by the camera by using attension program contact angle were calculated.

Contact angles of left and right sides were determined by a computer program digitally and the value of both sides was calculated and ten replications of the analyses were done for each sample and obtained values of the replications were reported. Contact angle measurements were performed by using Attension Theta Optical Tensiometer, KSV.

3.5.3 Surface Roughness Measurement

Effect of ion implantion of C and C+N_2 hybrid ions on surface roughness of the dense chitosan films was investigated by using Mitutoyo SJ 301 surface roughness equipment.

Asymmetric samples could not be measured with this equipment. Before measurements, the dense films were cut in a rectangular form and placed on a flat surface. Five measurements were done on each sample and the average data was reported.

3.5.4. Water Absorption

Samples were incubated at room temperature in 250 ml of water. Water absorption was conducted by using the equation given below. Water absorption amount as a function of time was measured.

$$WA\ \% = \frac{W_t - W_0}{W_0}\ x\ 100 \qquad (3.1)$$

In the equation;

- W_0 : The initial weight of the sample,
- W_t : The weight of the water aborbed sample after immersion time t.

3.5.5. Protein Adsorption Study

In this study, albumin and fibrinogen were used for a protein adsorption study. Absorbance of the samples was measured by using Perkin Elmer Lambda 45 spectrophotometer.

To study protein adsorption; firstly, protein concentration of unknown sample is found. To be able to find these concentrations the concentration of known samples is used. Calibration curves are used at this point. To be able to prepare calibration curves 1mg/ml concentration of albumin and fibrinogen was used. In the Appendix C, calibration curves of albumin and fibrinogen at pH: 4, pH: 5 and pH: 7.4 are given. Also, Appendix A, and B give detailed information about preparing PBS and BCA methods.

At first, films were cut as a weight of 0.01 grams. Since the films were in the same thickness, they were also had similar surface areas nearly 1.5 cm^2.

After that, films were suspended in 10 ml of protein solution for 3, 10, 15, 30, 45, 60, and 120 minutes for adsorption by orbital shaking at 150 rpm, 37°C. Protein solutions were freshly prepared by dissolving BSA and fibrinogen in PBS. Then, the samples were removed and rinsed with 10 ml of PBS solution to remove reversibly adsorbed protein. Irreversible adsorbed proteins were removed by 2 ml of 1% SDS solution in an hour. The adsorbed protein amount on the substrates was determined by a commercial protein assay kit, BCA (bicinchoninic acid) (Thermo – Pierce).

The amount of adsorbed protein onto Ch based film was determined by measuring the initial and final concentration of proteins from the absorbance at 562 nm of supernatant using a calibration curve previously prepared. The amount of protein, q, was calculated using Equation (3.2). Three repetitions were performed for all samples.

$$q = \frac{C_0 - C_f}{m} \times V \tag{3.2}$$

Where;

- q : The amount of adsorbed protein onto unit mass of adsorbents (mg/g),
- C_0: Initial concentration (mg/ml),
- C_f : Final concentration (mg/ml),
- m : The dry weight of adsorbents (g),

- V: Volume of protein solution (ml).

3.5.6. Molecular Weight Determination

Molecular weight determination studies were done by using Mark–Houwink equation. Average molecular weight of chitosan was calculated from intrinsic viscosity using Mark-Houwink Equation. Therefore, firstly, polymer solution was prepared by dissolving in solvent. Ubbelohde U-Tube capillary with C= 0.00924 cSt/s^2 was used in this study (Figure 3.7). Polymer solution as well as solvent were separately passed through the capillary viscometer. Tube placed into the PID controller temperature bath and filled with polymer solution. Flow time of the sample between the signed points was measured three times.

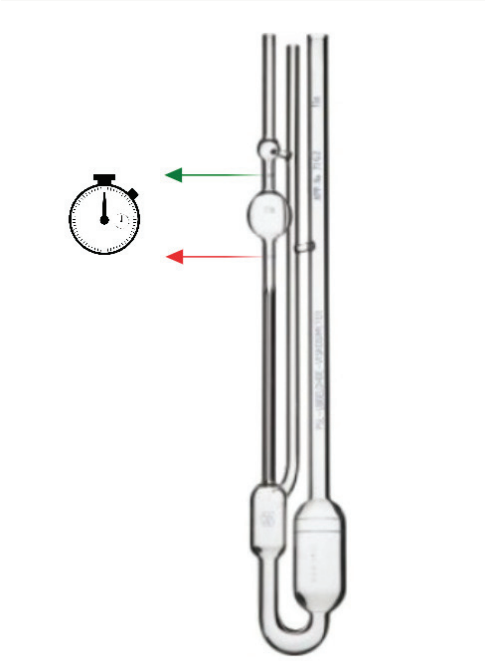

Figure 3.7. Kinematic viscosity measurement with Ubbelohde U-Tube capillary viscometer

Viscosity of polymer solution is affected by numerous determinants like ionic strength, deacetylation, molecular weight, pH, temperature and also concentration of the

polymer solution. Water bath was used to stabilize the temperature. Same batch of polymer was used at constant pH: 7.4.

The Mark Houwink equation (Equation 3.3) is given below:

$$[\eta] = K\, M_v^{\propto} \tag{3.3}$$

K and α value are constants. The constants determined in the study of the Wang et al. (K = 15.7×10^{-5} (dL/g) and α = 0.79) were used in the calculation of M_v (Wang, et al.1991).

Firstly, relative viscosity, η_{rel}, is calculated using Equation (3.4):

$$\eta_{\,rel} = t/t_s \tag{3.4}$$

Relative viscosity in this equation is defined as the ratio of time flow of polymer solution to time of solvent. Specific viscosity is calculated using Equation (3.5).

$$\eta_{sp} = (t/t_s) - 1 \tag{3.5}$$

Reduced viscosity is then calculated based on the ratio of specific viscosity to concentration of polymer solution as given in equation (3.6). Then, (In η_{red} – C) plot is drawn as a function of concentration (c) , and the intercept gives the intrinsic viscosity of polymer solution, η, (Eqn 3.7).

$$\eta_{red} = \eta_{sp}/c \tag{3.6}$$

$$\ln \eta_{rel}/C = \eta + k\eta 2\, C \tag{3.7}$$

3.5.7. In Vitro Biodegradation Study

The *in vitro* biodegradation can be monitored through molecular weight change as well as weight loss of sample. Biodegradation study of the chitosan films were

conducted with dense and aysmmetric chitosan film samples. Samples were firstly dried for 24 h at 50°C, and then weighted. *In vitro* test were performed by incubating the samples in pH 7.4 of phosphate-buffered saline (PBS) at 37ºC, orbital shaking at 150 rpm.

At pre-determined time intervals, 4, 7, 10, 14, 21 and 28 days, the films were taken out of the incubation medium, and weighed after films had completely dried. The percentage of weight loss was determined at different time intervals. M_v of samples at predetermined time intervals were determined from kinematic viscosity measurement by using the Mark Houwink equation (Equation 3.3).

CHAPTER 4

RESULTS AND DISCUSSION

4.1. Characterization Studies

4.1.1. FTIR-ATR

FTIR-ATR method was used to investigate chemical structural changes in the films. Figure 4.1 shows the chemical structure of the Ch, C-Ch, and CN_2-Ch films. Ion implantation dose for the films are $1x10^{15}$ ion/cm^2, 1Hz frequency and 20 kV voltage used.

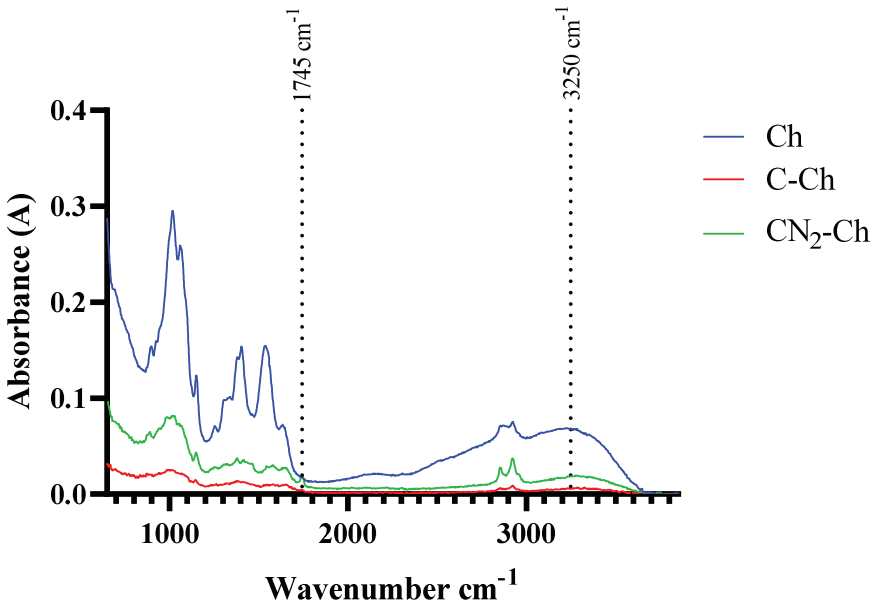

Figure 4.1. FTIR-ATR results of un-implanted and implanted chitosan films

The major characteristic peaks of chitosan can be seen in Figure 4.1. FTIR-ATR spectra show the stretching vibrations of carbonyl groups in the range 1650-1810 cm^{-1}. This is the effect of the C=O with different chemical environments presence. The band

at 1380 cm^{-1} was assigned to the C-H deformation of the CH_3 group, associated with few remaining acetamide groups present in the polymeric chain, as a result of the incomplete deacetylation of chitosan. Chitosan spectrum consists of characteristic bands appeared at around 3250cm^{-1} (O–H stretching) and at 2926 cm^{-1} (C–H stretch), at 1540 cm^{-1} (N-H bending (amide II), at 1155 cm^{-1} (bridge O stretch), and at 1070-1018 cm^{-1} (C–O stretch) and at 896 cm^{-1} (CH_2 bending) that are consistent with the literature finding (Escárcega-Galaz et al., 2018; Gomez Sanchez et al., 2018; Devi and Dutta 2019). As compared with the ion implanted samples, no new chemical bond formation was detected.

For the C implanted films, peak intensities of C-H stretch peaks at 2925 cm^{-1} , 1540 cm^{-1} N-H bending (amide II), C–H stretch of methyl group at 1380 cm^{-1} and C–O stretch at 1060 cm^{-1} and C=O at 1637 cm^{-1} decreased remarkably. Decrease in C-O and C=O band intensities related with decarbonylation/decarboxylation of polymer chains. On the other hand, decrease of C-H band intensities (at 2925 cm^{-1}) shows band breaking in polymer structure after ion implantation.

The spectral range between 2600 cm^{-1} and 1750 cm^{-1} chitosan does not present vibrational bands. Some weak -OH bonds increase in strength giving rise to a more well-defined value of the vibrational frequency in the 3430–3370 cm^{-1} range. Thus, the narrowing of OH band can be associated to increasing hydrogen bonding between chitosan chains. The OH stretching bands appear as a broad band between 3050 and 3600 cm^{-1} that can either be attributed to adsorbed water or hydroxyl groups on the film.

As can be seen for C-N_2 hybrid ion implanted samples, O–H stretch shifted from 3253 cm^{-1} to 3350 cm^{-1} and the N-H bending (amide II) shifted to 1550 cm^{-1} (from 1540 cm^{-1}) bridge O stretch and C-O stretch shifted to 1170 cm^{-1} and 998 cm^{-1}, respectively. All peak intensities decreased remarkably. This degradation is consistent with the changes in surface properties. Shifting to 1550cm^{-1} is likely related to observed high interaction between NH_3 groups of Ch and implanted C-N_2 ions (Sanchez et al., 2018).

Shifting of the peaks asserted the interaction of implanted ions with chitosan surface and also indicating the molecular miscibility of ion implantation. Similar peak shift results was reported (Patel et al., 2019).

A new band at 1745 cm^{-1} (C=O anhydride) appeared for C-N_2 ion implanted surfaces due to stretching absorption of carboxylic. This indicates the presence of a

carbonyl group in the film caused by ion implantation as suggested by (Xu et al., 2005, Mavropoulos et al., 2011).

The OH bond peak at 3250 cm^{-1} was expanded and shifted to higher frequency to 3262 cm^{-1} decreasing of intermolecular hydrogen bonds in chitosan ion implanted film due to the phenolic compounds. Also, amide II peak at 1541 cm^{-1} was expanded and shifted to a higher frequency by effecting of hydrogen bond formation of NH_2 group of CH and OH.

Ion implantation yields an overall fall of the intensities corresponding to all the vibrational bands. This confirms randomization of macromolecular chains, explicitly, the long chains cleave, degradation at backbones and side-chains of the macromolecular structure through extrication of hydrogen and carbon (Patel et al., 2019).

Table 4.1. Characteristic Bands of Chitosan Film

Sample	**Wavenumber (cm^{-1})**	**Assignment**
Chitosan Film	3250	O-H and N-H Stretching
	2926	Aliphatic C-H Stretch
	1745	C=O Anhydride
	1637	C=O Stretch (amide I)
	1541	N-H bend (amide II)
	1380	Symmetric CH_3 deformation
	1155	Glycosidic ring
	1060	C-O Stretch
	896	CH_2 bending

In the Figure 4.2, for the C and C-N_2 implanted Chitosan-Glycerol films, the peak intensities at 2925cm^{-1}, 1637cm^{-1}, 1380cm^{-1} and 1060cm^{-1} increased remarkably. The reverse behavior was observed compared to un-plasticized films. The new peak appeared for C ion implanted films at 1745 cm^{-1} could be due to some carbonyl formation resulting from surface oxidative degradation. In addition, the broadening of the peak may be due to increased concentration of free ions (Patel et al., 2017).

However, for both ion implanted films, the band at approximately 3240 cm^{-1} showed higher peak intensities indicating the higher number of water molecules

surrounding the film compared to un-implanted chitosan films. The OH stretching bands narrows 3050 cm^{-1} and 3600 cm^{-1} that can either be attributed to decrease in adsorbed water or hydroxyl groups on the un-implanted films. ChG film presents similar spectral bands with the Ch films (Figure 4.2). However, the presence of glycerol affects the position of the NH_3 band of Ch film. NH_3^+ band shifts from 1540 cm^{-1} to higher frequency, 1559 cm^{-1}. Shifting is likely related to observed high interaction between NH_3 groups of Ch films (Gomez Sanchez et al., 2018).

Comparison of the typical bands of Ch and ChG shows the shifts back with addition of glycerol. This shift indicates a change from symmetric deformation vibration of NH_3^+ to N-H bending vibration from NH_2 in the Ch molecules (Cobos et al., 2018) . This result confirms that glycerol displaces bound acetic acid from Ch.

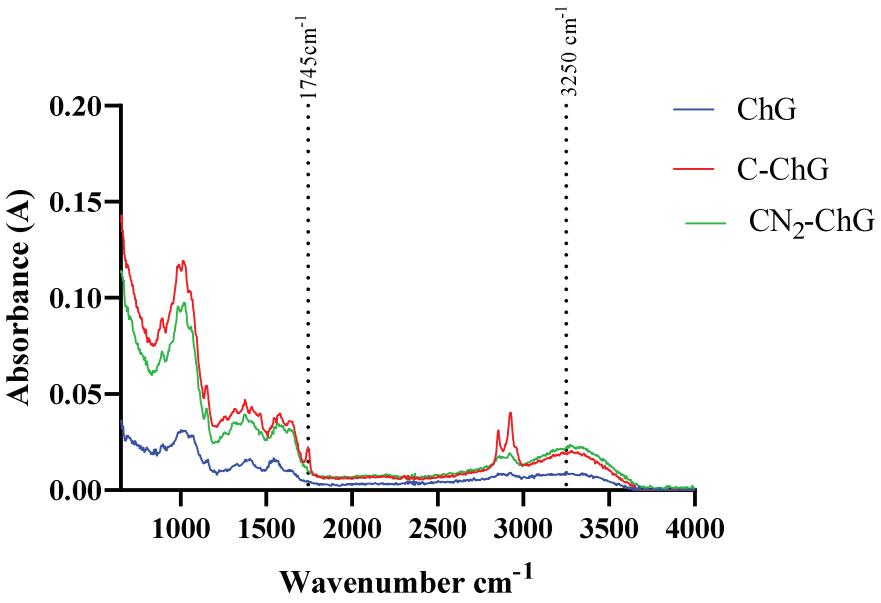

Figure 4. 2. FTIR-ATR results of un-implanted and implanted chitosan glycerol films

4.1.2. Differential Scanning Calorimeter, DSC

In all samples, an endothermic peak at given temperature that can be described to the loss of water. The second thermal event may be related to the decomposition of amine units with correspondent exothermic peaks.

According to DSC thermogram ion implantation to Ch film increases the Exothermic peak, and decreases the endothermic peak.

As given in the Table 4.2 ion implantation of ChG film does not improve its exothermic peak where as it degreases the endothermic peak. ACh and AChG does not show different endothermic and exothermic characterization. CN_2-ACh membrane show slight increase in endothermic peak whereas no change obtained in the exothermic peak.

As a result, ion implantation changes endothermic peak. For Ch and ChG films it degrades the endothermic peak which caused by the damage onto the surface by ion implantation. For the asymmetric membrane ion implantation increases the endothermic peak.

Table 4.2. DSC change of the chitosan films

Sample	**Endothermic Peak ˚C** (D_{min})	**Exothermic Peak ˚C** (D_{max})
Ch	97.80	280.45
C-Ch	89.60	296.70
CN_2-Ch	59.74	324.99
ChG	123.1	284.02
C-ChG	82.3	280.55
CN_2-ChG	85.40	283.60
ACh	51.76	323.94
AChG	52.59	322.05
CN_2-ACh	59.74	324.99

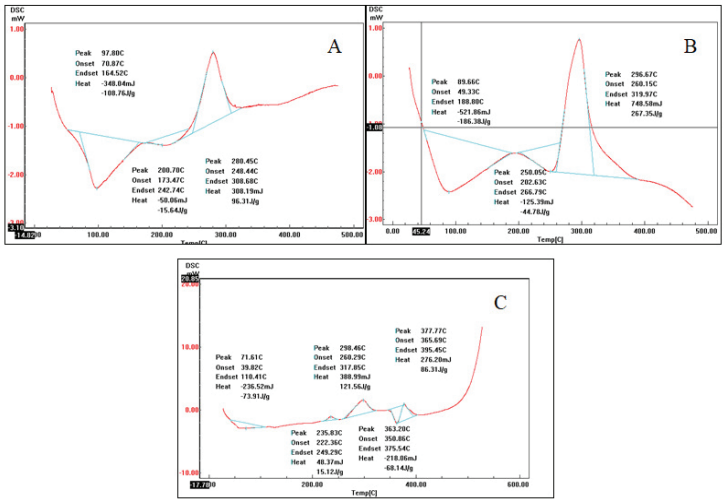

Figure 4. 3. DSC Thermogram of the Chitosan Films A: Ch; B: C-Ch; C: CN_2-Ch

4.1.3. Thermal Gravimetric Analysis

Thermal gravimetric analysis was studied for dense, asymmetric and glycerol plastized chitosan films before and after C and C+N_2 hybrid ion implantation. In the following TGA curves, mainly two major weight losses occurred. The first point of weight loss between 70°C – 110°C corresponds to the evaporation of water molecules adsorbed on the polar groups of chitosan, while the second point of weight loss at 250°C – 450°C corresponds to the thermal decomposition of chitosan. The loss of mass of the membranes shows no significant difference, indicating that the mass loss occurs in two stages (Takara et al., 2019). Following TGA curves shows the mass loss diagram of the films.

Figure 4.4 shows the two stage mass loss of the membranes. The first point 106.86°C was attributed to the evaporation of entrapped water. The weight loss curves were almost similar with a few differences. TGA results showed that the interactions between different ion implanted films were very small and did not significantly affect material's thermal degradation properties.

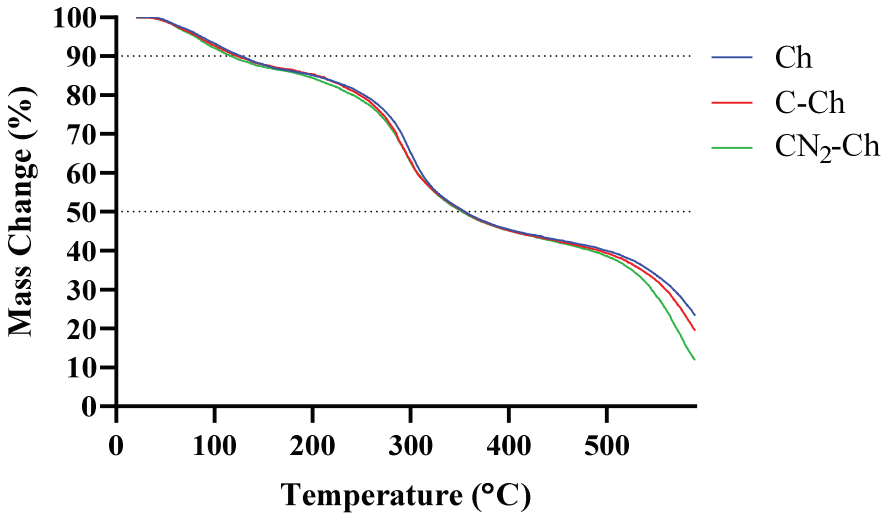

Figure 4.4. TGA results of Ion Implanted Ch film Samples

Initial 10% of the degradation starts a 127.4°C for Ch films and 126.7°C, 120.4°C for C-Ch and CN_2-Ch films. 50% percent of the Ch films loss at 355.5°C and C-Ch, CN_2-Ch films 358.5°C and 355.4°C respectively. The positions of the Ch were

higher than those of C-Ch and CN_2-Ch showing that the attractive interaction was weakened by C and CN_2 implantation. These results were in agreement with the results reported by M. Zhang et al., 2002.

Figure 4.5 shows the mass loss behavior of ChG films. The mass loss of C-ChG and CN_2-ChG were almost similar with a few differences. By ion implantation, ChG film surfaces were damaged so that the mass loss of the films becomes faster than the un-implanted ChG.

ChG film loss its initial 10% of the mass at 129.4°C and C-ChG and CN_2-ChG films loss 10% mass at 97.21°C and 91.25°C respectively.

ChG film loss its 50% of the mass at 377.9°C and C-ChG and CN_2-ChG films loss 50% mass at 260.1°C and 254.4°C respectively. As a consequence, after ion implantation the faster mass loss is seen.

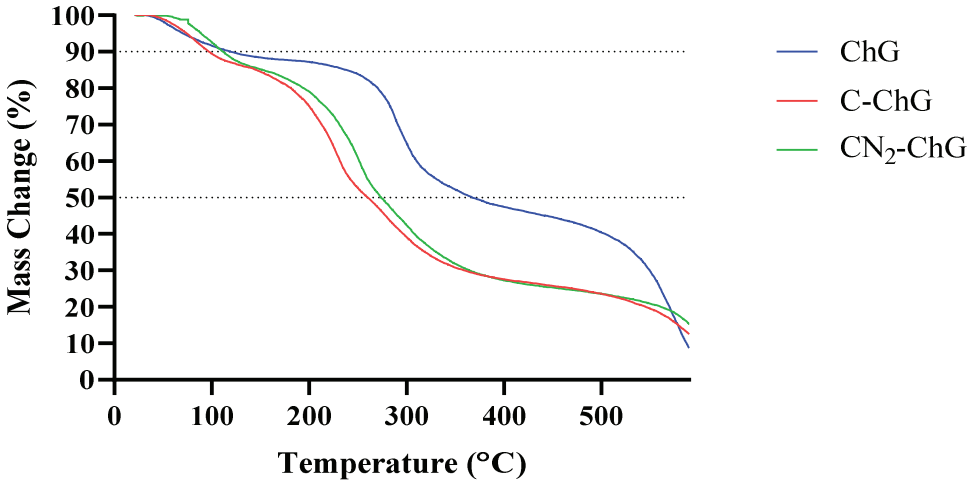

Figure 4.5. TGA results of Ion Implanted ChG film Samples

Figure 4.6 shows the mass loss diagram of asymmetric and ion implanted asymmetric films. At nearly 345°C 50% of both ACh and CN_2-ACh film mass loss obtained. Mass loss behavior does not show significant change after ion implantation. At nearly 230°C and 345°C un-implanted ACh sample slightly degradate faster.

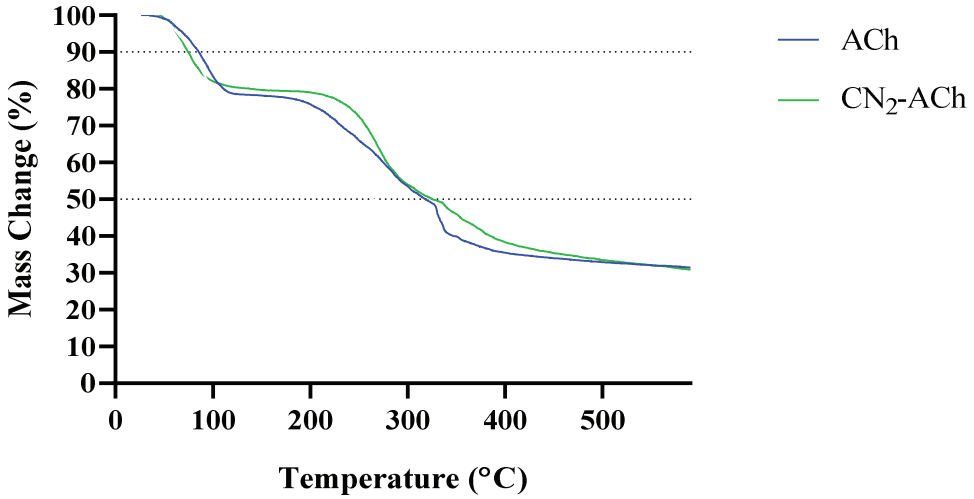

Figure 4.6. TGA results of ACh, and C-N_2 Ion Implanted ACh film Samples

Figure 4.7 shows the mass loss diagram of the ACh and AChG films. As seen from the figure, AChG film shows faster decomposition amount than the ACh. AChG film loss its 50% mass at 260°C whereas ACh loss the same amount at 320°C.

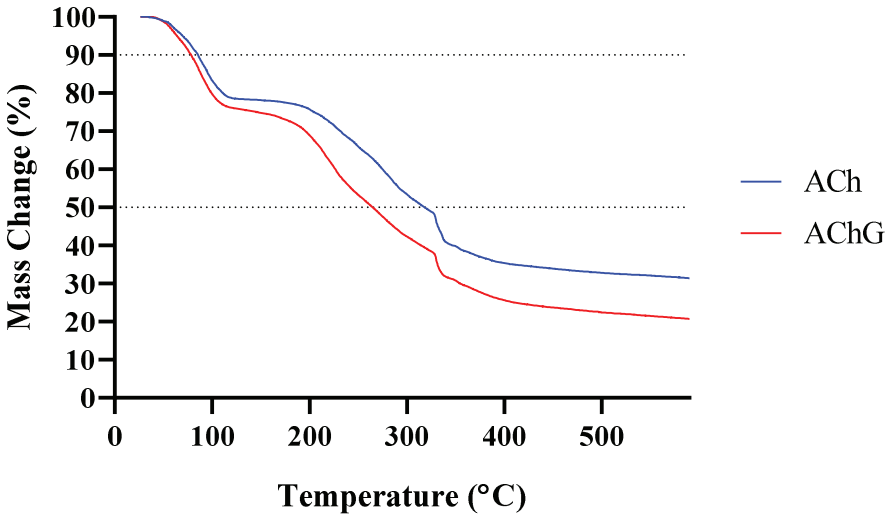

Figure 4.7. TGA results of ACh and AChG Samples

4.1.4. Scanning Electron Microscopy

The morphology of the dense, asymmetric and glycerol-plastized chitosan films was investigated by using Scanning Electron Microscopy. The film thickness *(dense and total)* and pore sizes of the asymmetric films were measured using ImageJ® software. Samples were controlled before and after C^+ and $C+N_2$ hybrid ion implantation. In the Figure 4.8, Figure 4.9 and Figure 4.10 shows the SEM image of The Ch, C-Ch and CN_2-Ch respectively.

In the Figure 4.8, in cross-section 500x magnifications was used. The film thickness of Ch measured as 49.24 ± 15.59 µm and no pores detected. The Figure 4.8.b was taken from surface of the film with 5000x magnification. In these images again no pores are detected as excepted and similarly with the literature (Silva et al., 2008).

Figure 4.9.a and 4.9.b shows C-Ch with ion implantation dose of $1x10^{15}$ kV from 500x and 10000x respectively. After ion implantation chitosan film becomes rougher and exhibits some protuberances (Chang and Chian 2013). In the literature Afzal et al. (2018) modified the Al surfaces with Carbon ions. In this study, some surface deformations were detected. They were controlled with XRD and found that these dispersions are Al_4C_3 precipitates. In our SEM figures, similar surface formations were also detected but unfortunately XRD tests were not applied to the sample so that we cannot exactly determine the cause of the precipitation. And also, there is no literature about C ion implantation on chitosan surfaces. So that, no prediction can be done to these precipitations.

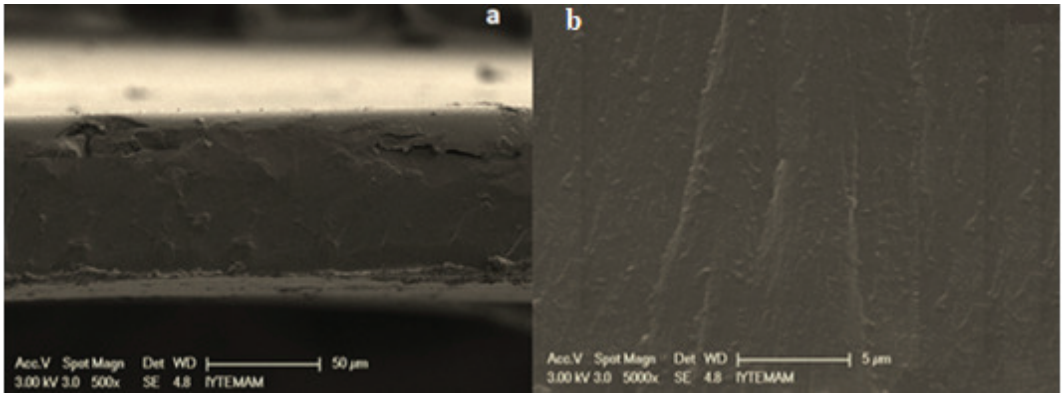

Figure 4.8**.** SEM images of Ch films

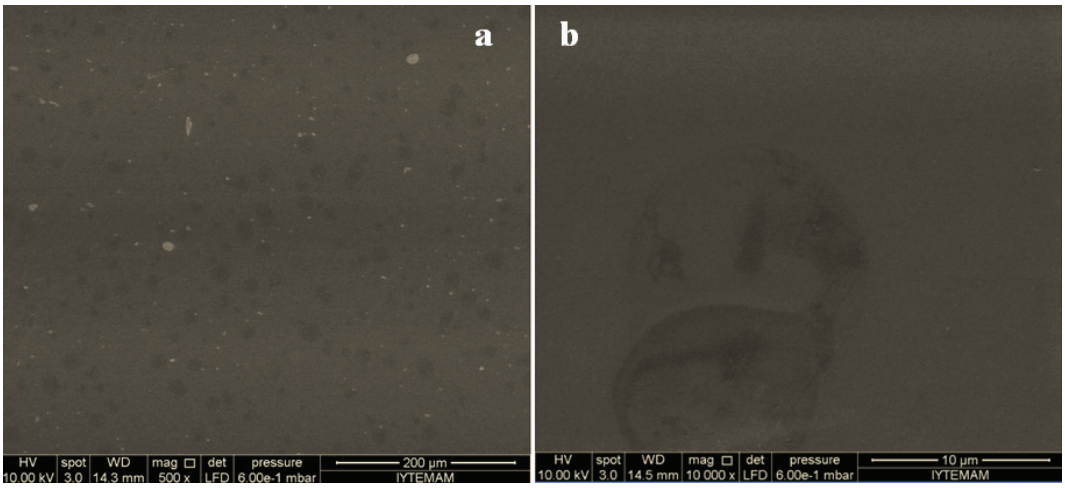

Figure 4.9. SEM images of C-Ch films

Figure 4.10 show surface morphology of CN_2-Ch film with ion implantation dose of $1x10^{15}$ kV at two different magnifications (500X and 5000X). As seen in Figure 4.9, the untreated and implanted samples had a smooth surface. There were several kinds of cracks on implanted surfaces. These types of micro-cracks were also found in the previous studies and it was reported that the structure of these micro-cracks changed according to the type of ion and metal–gas mixtures (Öktem et al., 2008).

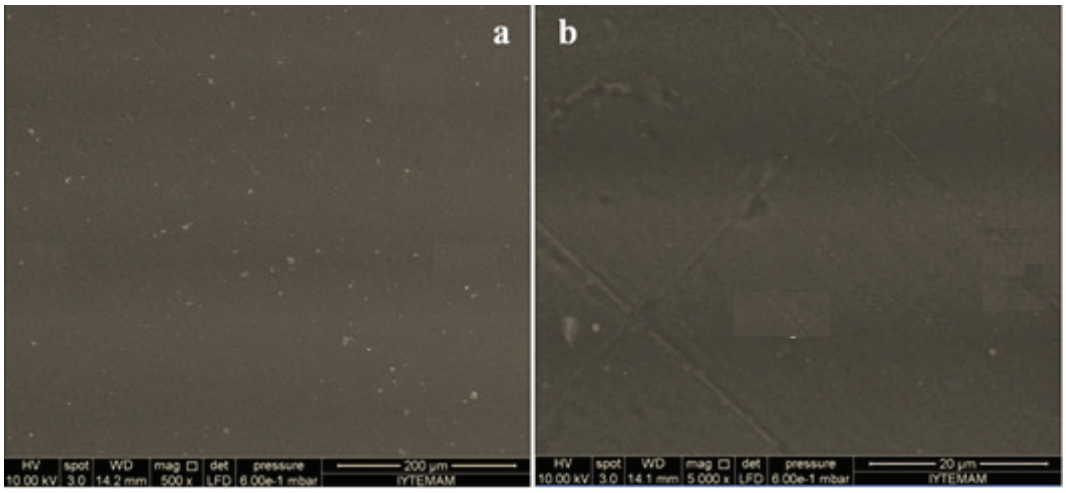

Figure 4.10. SEM images of CN_2-Ch, ion implanted film

Figure 4.11 shows the surface morphology of implanted chitosan films, C-ChG and CN_2-ChG films, at the ion implantation dose of $1x10^{15}$ kV. As seen from the images, the surface of the CN_2-ChG films was defected by implanted ions. Similar surface effect also reported on the literature by Dhawan and Sharma,(2019).

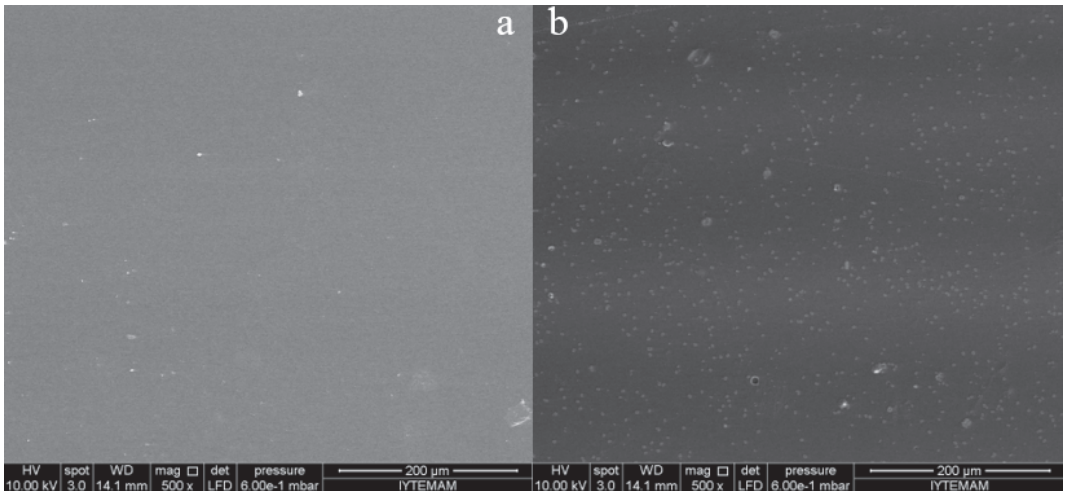

Figure 4.11. SEM images of C-ChG, and CN_2-ChG films

Figure 4.12 (a) illustrates the cross sectional SEM image of asymmetric chitosan film (ACh) prepared for 20 minutes pre heating time.

Total thickness of the ACh film is about 538.15 ± 14.35 µm and dense section' thickness is 49.24 ± 15.59 µm. the average pore size is calculated as 134.0 ± 87.9 µm. ACh films were also prepared at different pre-heating times and effect of pre-heating time on the morphology of Ach films was studied. Table 4.3 tabulates pore size distribution of ACh films prepared at different pre-heating times. As seen in the Table 4.3, thicknesses of the films decrease in contrast to an increase in pre-treatment time. Dense film thickness increased with an increasing pretreatment time. In the study of Mi et al., similarly dense film thickness was found to be proportional with pre-treatment time.

Figure 4.12 (b) shows the surface of ion implanted Ach films, CN_2-ACh, with dose of $1x10^{15}$ kV. As seen from the figure, the local spots were observed in the surface of the CN_2-ACh film due to the implantation effect.

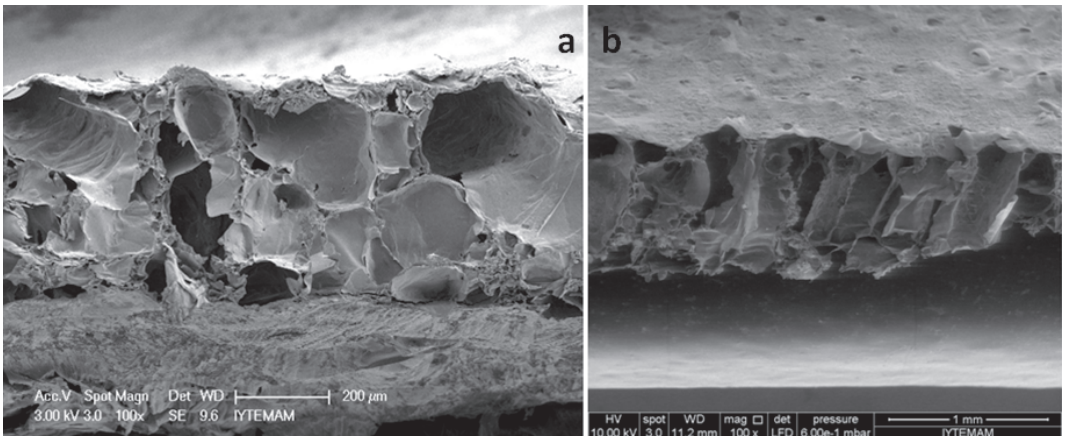

Figure 4.12. SEM images of ACh and CN_2-ACh film

Table 4.3. Film thickness and pore size change with respect to pre treatment time

Pre treatment time	**Film Thickness, µm**	**Dense Thickness, µm**	**Ave. Pore Size, µm**
10 Min	874.9 ± 15.5	15.7 ± 3.7	129.5 ± 56.4
15 Min	604.7 ± 20.1	21.6 ± 13.5	173.5 ± 63.7
20 Min	538.1 ± 14.3	49.2 ± 15.5	134.0 ± 87.9
30 Min	364.7 ± 3.3	64.0 ± 11.2	67.7 ± 60.4
40 Min	355.9 ± 29.7	78.1 ± 16.1	174.0 ± 90.6

4.1.5. Surface Wettability

Contact angle, θ, higher than 90° shows the formation of hydrophobic surface of material. To observe the contact angle / surface property changes after ion implantation, initial contact angle measurement was conducted. At hydrophilic surfaces, water molecules tend to spread on the surface. In a hydrophobic interaction, it seems that the hydrophobic molecules are rejecting water. In fact, water is rejecting the hydrophobic molecules in favor of bonding itself. Basically, the angle between the surface and the

water drop was calculated and measured, water contact angles of chitosan films gives us the surface properties.

Table 4.4 summarizes the water contact angles of chitosan films. According to results, contact angle of chitosan increased with ion implantation. Contact angle of the chitosan - glycerol film decrease with ion implantation.

Contact angle of the chitosan found as 58.39 ± 3.82 θ. Similar Chitosan contact angle literature results were reported by (Alhwaige et al., 2019). After C-N_2 hybrid ion implantation surface of the film changes and contact angle of the film increases to 72.24 ± 2.01 θ. By C ion implantation contact angle is increase to 84.82 ± 4.88 θ.

Increasing the contact angle of chitosan indicate that chitosan films increased in hydrophobic behavior after the plasma treatment. For untreated chitosan samples water is attracted to the film surface stronger than other samples. For hydrophobic surfaces the contact angle will be larger than 90° as in the ChG film. The contact angle of the ChG film was found as 100.00 ± 2.35 θ. The contact angle of this hydrophobic surface decreased after ion implantation. Both Carbon and Nitrogen implantation decreased the contact angle of Chitosan Glycerol film but the surface still behaves hydrophobic after the plasma treatment.

Table 4.4. Contact angle change after ion implantation

Sample	**Contact Angle Θ**	**Sample**	**Contact Angle**
Ch	58.39 ± 3.82	ChG	100.0 ± 2.35
CN_2 –Ch	72.24 ± 2.01	CN_2-ChG	96.24 ± 5.10
C-Ch	84.82 ± 4.88	C-ChG	85.67 ± 4.56

4.1.6. Surface Roughness

As seen in the Figure 4.13 ion implantation increases the surface roughness of samples. Ch film surface roughness was found as 0.097 . Our result was found be good aggrement with the study of Chou et al. as 0.09 Ra for chitosan having degree of acetylation of 96 (DD_{96}).

C and CN_2 hybrid ion implantation increased surface roughness of both Ch and ChG films. ChG films are more rough compared to Ch films. Surface roughness value of CN_2 ion implanted ChG films is the highest among all films and increased to from 0.28 ηm upto 0.41 ηm.

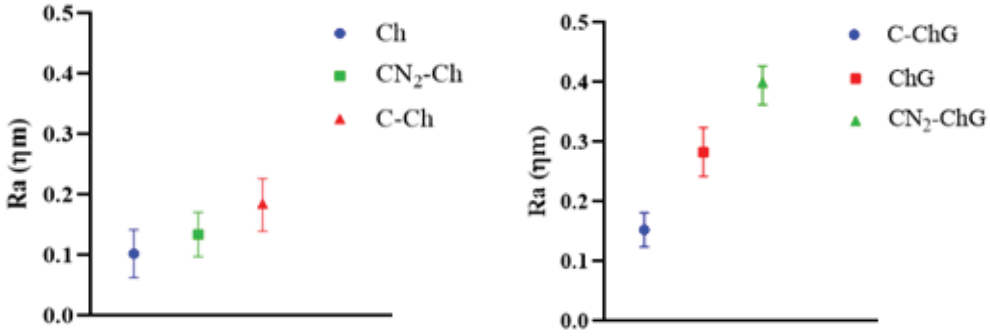

Figure 4.13. Surface Roughness of Unimplanted and Implanted Chitosan Films

As reported in the literature, surface roughness is changing depending on the implanted ions. Some investigators have reported that the surface roughness increases the hydrophobicity of the polymer's surface. In this study, after ion implantation, surface roughness of the implanted Ch and ChG films increased. However, only contact angle of the Ch films increased with an increase of surface roughness

4.1.7. Water Absorption

Chitosan is a hydrophilic material and it absorbs water in large amounts. In the Table 4.5, water absorption changes of dense and asymmetric films are listed as a function of time from the 1st day to 45th day. Since the asymmetric chitosan films are porous films, they absorb larger amounts of water than the dense chitosan film. Absorption of the water increases by time for both types of the films. Y. Ma et al studied Ch film water absorption ratio after 30 minutes and they found 111.95%. The decrease in the swelling values for ACh films could be explained by a higher crosslinking degree, which reduced free volume and chain mobility, thus, hindering the water entry into the network (Guerrero et al., 2019).

Table 4.5. Water Absorption of Ch, ChG, ACh films

Water Absorption %			
Days	**Ch**	**ChG**	**ACh**
1	137.3 ± 1.2	72.1 ± 2.7	407.0 ± 3.6
7	150.5 ± 1.1	89.9 ± 2.5	472.6 ± 5.1
14	147.9 ± 0.9	90.4 ± 1.9	561.4 ± 5.9
21	141.5 ± 2.5	97.2 ± 1.2	621.6 ± 6.2
28	144.1 ± 3.1	95.1 ± 2.5	606.9 ± 5.7
45	165.8 ± 2.9	100.8 ± 2.1	672.2 ± 8.9

In this study, ion implantation effect on the water absorption properties of chitosan films was also studied. Percent water absorption of the films soaked in 6 hours was tabulated in Table 4.6.

As seen in the Table, Ch film absorbs 157.32% water because of the highly swelling property of chitosan polymer.

C and CN_2 implanted Ch films absorb less amount of water as 125.66% and 127.97% water, respectively due to change in surface hydrophobicity of Ch films after ion implantation as observed in Section 4.1.5. Glycerol addition makes the films hydrophobic and ChG films absorbs 60.92% water after 6 hours.

Asymmetric membranes adsorb more water because of the porous structure. Water absorption results of the Ch, ChG and ACh films are in good agreement with contact angle results.

Table 4.6. Water absorption change after ion implantation

	Sample	**Water Absorption % (after 6 hours)**
Dense Chitosan	Ch	157.32
	C-Ch	125.66
	CN_2-Ch	127.97

(Cont. on next page)

Table 4.6. (Cont.)

Glycerol	ChG	60.92
	C-ChG	168.29
	CN_2-ChG	150.00
Asymmetric	ACh	489.56
	CN_2-ACh	569.17
	AChG	444.79

4.1.8. *In Vitro* Protein Adsorption Study

In this study, albumin and fibrinogen were used as model proteins to study protein adsorption of chitosan films. Effects of pH change as well as implantation ion effect on protein adsorption of chitosan films were also studied. Firstly calibration curves of albumin and fibrinogen proteins were prepared using 1mg/ml concentration of protein. In the Appendix C, calibration curves of albumin and fibrinogen at pH: 4, pH: 5 and pH: 7.4 are given. Also, Appendix A, and Appendix B give detailed information about preparation of PBS and BCA methods.

Figure 4.14 illustrates adsorption isotherms of the albumin onto the Ch films. The maximum adsorption amount is reached at pH: 7.4. Adsorption amount is decreased slightly with a decrease in pH.

This decrease with pH can be explained after considering many factors. First of all, Albumin is a small size protein and tent to re-arrange its structure to increase the adsorption. Also, iso-electric point of the Albumin is 4,8 and albumin becomes positively charged when the pH < pI. Albumin is an carboxylic acid rich protein and due to the charge-charge repulsion it must be less adsorbed at pH: 7.4.

So, it is obvious that the BSA undergoes conformational changes or deformations that are highly dependent on the surface polarity and inter-protein interactions since the maximum absorption seen at pH: 7.4 as previously reported (Ouberai et al., 2014)

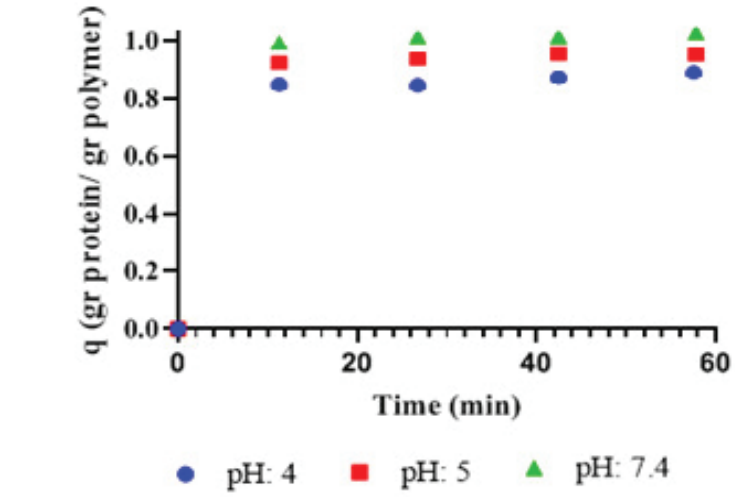

Figure 4.14. pH effect on Albumin adsorption onto Ch film

Figure 4.15 shows protein adsorption results at different pHs after C ion implantation on Ch films. As sen in the figure except pH 7.4, C implanted Ch films have higher protein adsorption (Table 4.7, Figure 4.15). Our findings are in good agreement with the reported studies in the literature (Tangpasuthadol et al., 2003; Ramya et al., 2018; Chang and Chian 2013). And also, Albumin is an carboxylic acid rich protein and due to the charge-charge repulsion it must be less adsorbed onto the C-Ch film at pH:7.4 than pH:5 and pH:4.

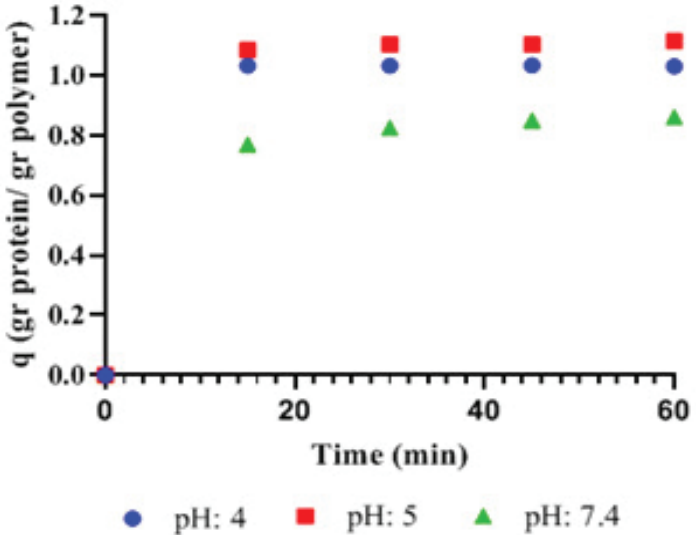

Figure 4.15. pH effect on albumin adsorption onto C-Ch film

Figure 4.16 shows effect of pH on fibrinogen adsorption for Ch film. Fibrinogen is a medium size protein. Also, iso-electric point of the Fibrinogen is 5.5 and Fibrinogen becomes positively charged when the pH < pI. Structural behavior mechanism of the adsorption graph is similar with BSA adsorption. Maximum adsorption occurred at pH 5 compared to pH 4 and pH 7.4 (Table 4.16). Our findings were in good agreement with the study of Rabe et al. (Rabe et al., 2008).

Figure 4.17 shows effect of pH on fibrinogen adsorption of C-Ch film. C implanted Ch film adsorption behavior is very similar with the unimplanted Ch film. Maximum adsorption is seen again at pH:5 followed by pH:4 and pH: 7.4 as given in the Figure 4.17 and Table 4.7.

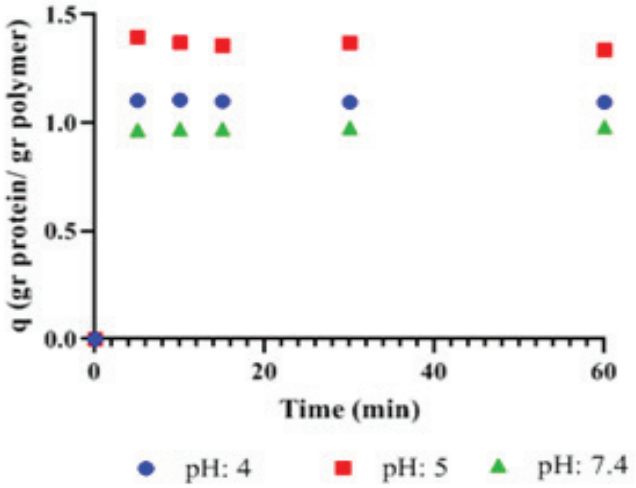

Figure 4.16. pH effect on Fibrinogen adsorption onto Ch film

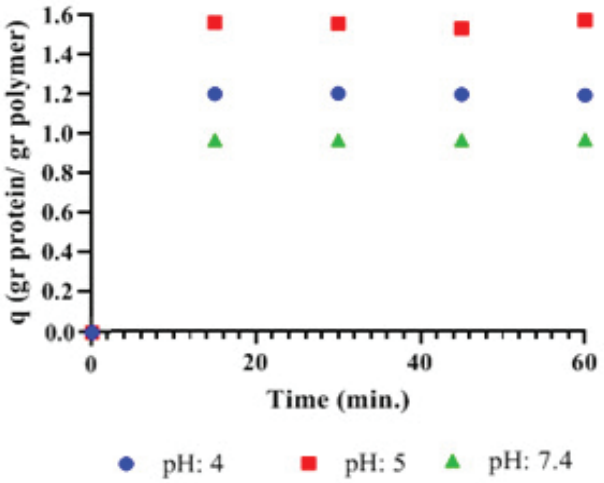

Figure 4.17. pH Effect on Fibrinogen Adsorption onto C-Ch film

Table 4.7. Relationship between pH, pI of proteins, and surface charge

Sample	Contact Angle	Ch Charge	pI =4.8 Albumin Charge	q Albumin (t=60min)	pI = 5.5 Fibrinogen Charge	Q Fibrinogen (t=60min)
Ch pH:4	58.39 ± 3.82	+	+	0.945	+	1.09
Ch pH:5		+	-	0.969	+	1.33
Ch pH:7.4		-	-	0.988	-	0.98
C-Ch pH:4	84.82 ± 4.88	+	+	1.030	+	1.19
C-Ch pH:5		+	-	1.11	+	1.57
C-Ch pH:7.4		-	-	0.86	-	0.97

Effect of ion implantation on albumin adsorption of Ch films at pH: 7.4 were shown in Figure 4.18. Initial slope is high, it caused fast adsorption.

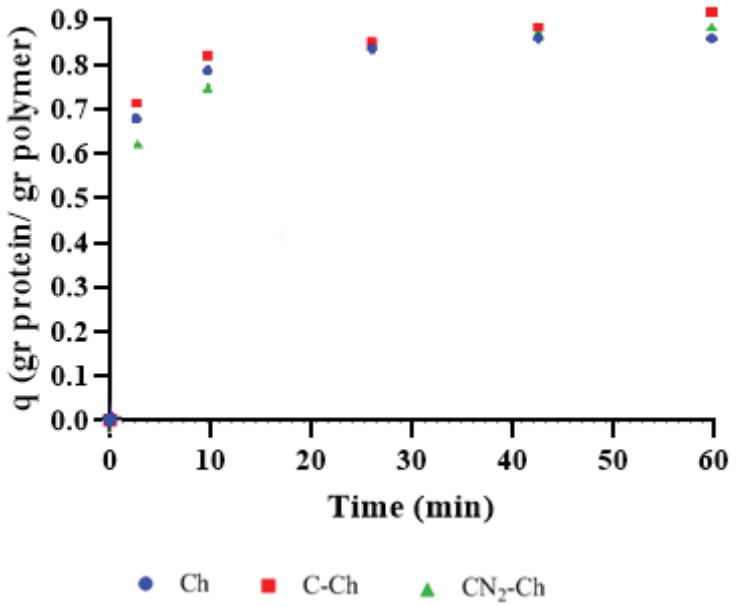

Figure 4.18. Albumin adsorption change on implanted and un-implanted Ch films at pH:7.4

Both C and CN_2 ion implanted Ch films adsorbed slightly higher amount of protein due to the higher contact angles of the surface as found in the literature (Tangpasuthadol et al., 2003).

As seen in the Figure 4.19, fibrinogen adsorption amount reaches the highest value for C-Ch film. Although the overall charge of the fibrinogen molecule is negative at pH = 7.4, the distribution along the macromolecule is not homogeneous and some parts of it are positively charged. Hydrogen bonding and charge-charge attraction could be responsible for the lower protein adsorption of CN_2-Ch compared to un-implanted Ch.

It has been found that the isoelectric point and adsorption amount are related with each other. The maximum adsorption occurs near its isoelectric point since protein surface interaction becomes weaker.

In the Table 4.8, amount of protein adsorption on un-implanted and ion implanted films for 60 minutes at pH: 4; pH: 5 and pH: 7.4 are given. At pH: 4, fibrinogen adsorption amount is higher than albumin. Maximum protein adsorption amount obtained after CN_2 ion implantation. At pH: 7.4, plasticer addition effect to protein adsorption is seen.

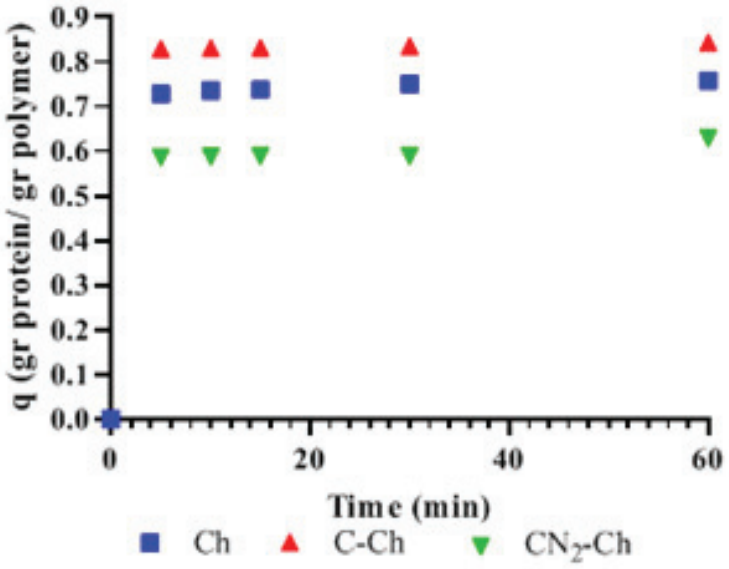

Figure 4.19. Fibrinogen adsorption change on implanted and un-implanted Ch films at pH:7.4.

Table 4.8. Protein adsorption results of Albumin and Fibrinogen

	pH:4			pH:5			pH:7.4		
	Ch	**C-Ch**	**CN_2-Ch**	**Ch**	**C-Ch**	**CN_2-Ch**	**Ch**	**C-Ch**	**CN_2-Ch**
Albumin	0.945	1.031	-	0.969	1.115	-	0.988	0.861	0.861
Fibrinogen	1.096	0.918	1.238	1.336	0.150	0.783	0.758	0.844	0.629
	ChG	**C-ChG**	**CN_2ChG**	**ChG**	**CChG**	**CN_2ChG**	**ChG**	**C-ChG**	**CN_2ChG**
Albumin	0.579	0.521	0.550	0.984	0.836	0.974	0.384	0.334	0.368
Fibrinogen	0.733	0.796	1.606	0.578	0.424	0.387	0.464	0.424	0.387

Figure 4.20 shows SEM images of dense and C and CN_2 implanted chitosan films and CN_2 implanted ACh film. Images taken after 60 minutes for fibrinogen adsorption at pH: 7.4. Figure shows the adsorbed proteins on the surface of the films.

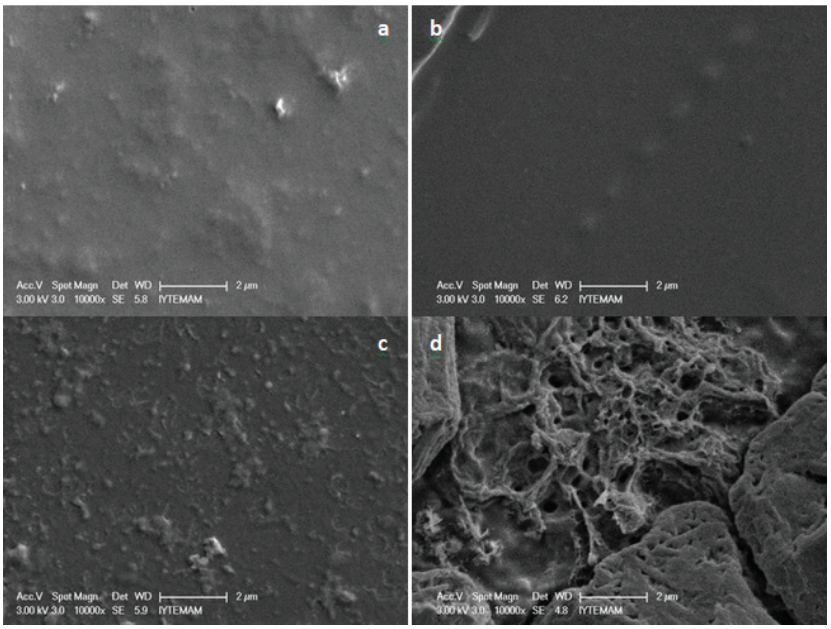

Figure 4.20. SEM images of films after 60 min. Fibrinogen adsorption at pH: 7.4
a) Ch, b) C-Ch , c) CN_2-Ch, d) CN_2-ACh

4.1.8.1. Adsorption Kinetics

Number of models has been developed to describe kinetics of polymer biosorption in batch test. Conformity between experimental results and a predicted model values is expressed by correlation coefficients (R^2). When the R^2 values close or equal to 1, that indicates the model successfully described.

In this thesis, two adsorption kinetic models were investigated to explain adsorption mechanism:

Lagergren Equation (Pseudo-First-Order)

This kinetic model is expressed as;

$$\frac{dq_t}{dt} = k_l(q_e - q_t) \qquad \text{(Eqn.4.1)}$$

$$\log (q_e\text{-}q_t) = \log q_e - \frac{k_1 t}{2.303} \qquad \text{(Eqn. 4.2)}$$

Where q_e and q_t (mg/g) are the adsorption capacity at equilibrium and at time *t,* and k_1 is the rate constant of adsorption (min^{-1}). Plot of log (q_e-q_t) versus t gives a straight line and k_1 can be calculated from the graph.

In the Figure 4.21 plot of log (q_e-q_t) versus t plot is given. The calculated linear regression correlation coefficient for Ch film was found as 0,984. The experimental q_e value did not agree with the calculated values obtained from the linear plot (Table 4.9). So, pseudo-first-order equation did not fit well with experimental result and therefore, could not be used to describe the adsorption kinetics of BSA onto Ch film.

Table 4.9. Pseudo-First-Order Model Constants

	Pseudo-First-Order Model		
T (K) = 310	**Constants**		
	k_1 (min^{-1})	**q_e (mg/g)**	**R^2**
Ch	0.0255	87.6	0.984
C-Ch	0.0148	90.4	0.942
CN_2-Ch	0.0163	89.3	0.979

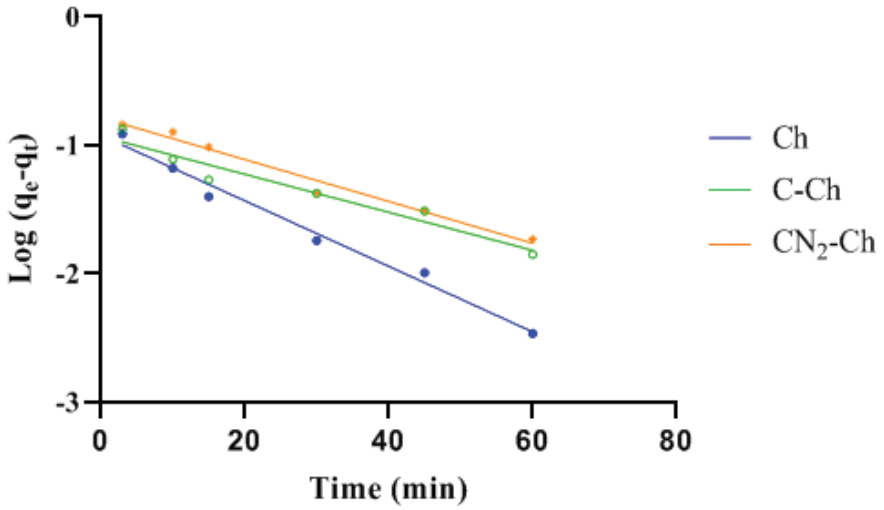

Figure 4.21. Pseudo First Order Equation Graph

Ho and McKay Equation (Pseudo-second order equation)

Adsorption kinetics rate is expressed according to sorption kinetic model developed by Ho & McKay equation as; and

$$\frac{t}{q_t} = \frac{1}{k_2\, q_{e^2}} + \frac{t}{q_e} \qquad \text{(Eqn.4.3)}$$

Where k_2 is the pseudo-second order rate constant (g/(mg*min)). The equilibrium adsorption capacity (q_e) and the model constants (k_2) can be determined experimentally from the slope and intercept of plot t/q_t versus t.

In the Figure 4.22, plot of log (q_e-q_t) versus t plot is given. The calculated linear regression correlation coefficient for Ch film was found as 1. The experimental q_e value agrees with the calculated values obtained from the linear plot with a high R^2 value (Table 4.10), so pseudo-second order kinetics agreed well with that of the experimental values. These results indicated that the adsorption of BSA on Ch followed pseudo-second order kinetics.

Table 4.10. Pseudo-Second-Order Model Constants

Pseudo-Second-Order Model		
T (K) = 310	**Constants**	
	k_1 (min $^{-1}$)	**R^2**
Ch	1.1349	1
C-Ch	1.1174	0.9998
CN_2-Ch	1.1114	0.9996

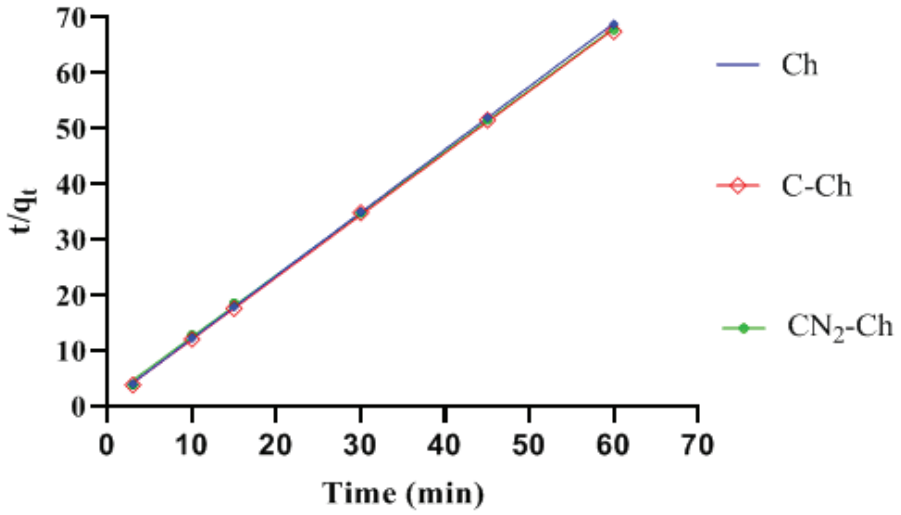

Figure 4.22. Pseudo Second Order Equation Graph

Our experimental protein adsorption kinetic data is well correlated with the Pseudo Second Order model. Table 4.11 gives the correlation results with the comparison with the first order model.

Table 4.11. Comparison of Adsorption Kinetic Models

T (K) = 310	Pseudo First Order	Pseudo-Second-Order
	R^2	
Ch	0.984	1
C-Ch	0.942	0.9998
CN_2-Ch	0.979	0.9996

4.1.9. *In Vitro* Biodegradation Study

In vitro biodegradation of Ch films was studied by monitoring change of MW change as well as % weight loss as a function of time. Figure 4.23 shows η_{spec} /c vs. concentration graph where the intrinsic viscosity of commercial chitosan was determined from the intercept of the plot as 5.235 mL/g at 0.2M acetic acid/ 0.1M sodium acetate (0.2M CH_3COOH/ 0.1M CH_3COONa) solvent system. Molecular weight is then calculated by using equation (Equation 3.3), Mark Houwink Equation, and found as 531297.8 (g/mol). Mw of chitosan in the literature found between 500000

to 600000 (ref), therefore our experimental finding is in good agreement with the literature.

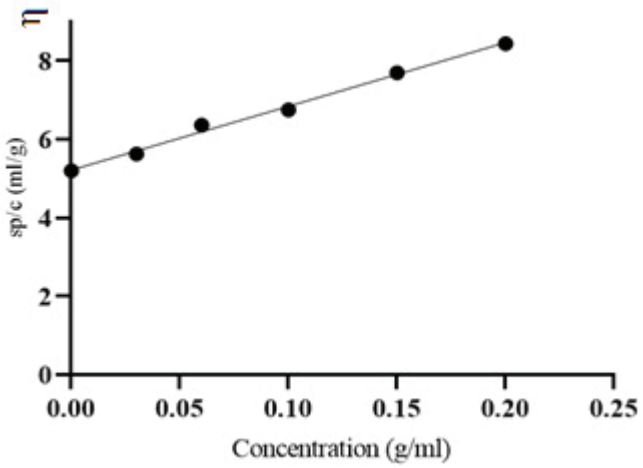

Figure 4.23. Intrinsic Viscosity curve of Low Molecular Weight Chitosan

Molecular weight change as a function of time was studied for dense and asymmetric Ch films. At the end of the 21st day, 82.19% decrease in molecular weight is obtained, however, this decrease was only 54.02% for dense films.

In vitro degradation of dense Ch and ACh films as well as implanted Ch films were also studied by % weight loss and compared each other. Figure 4.25 shows % weight loss for both dense Ch and ACh films. After 3 weeks, 40% of Ch film was degraded whereas 65% of ACh films degraded due to the porous structure. However, for ion implanted samples, the slower degradation of the films were obtained (Figure 4.25). At the end of the 21th day, only 17.7% weight loss was observed for C-Ch films, whereas 30% for CN_2-Ch films as compared to 40% for dense Ch films.

In contrast to dense films, asymmetric films degraded much faster after ion implantation. Un-implanted ACh sample degrades 57.43% whereas CN_2 hybrid ion implanted ACh degrades 65% at the end of the 21th day.

Weight loss of the films in SBF solution was studied (Figure 4.25). *In vitro* degradation results shows that ACh films degrades much faster (mass loss: 57%) than dense chitosan films (mass loss: 40%) due to the porous structure at the end of 21 days. However, the ion implanted samples degraded much slower compared to un-implanted chitosan films. C+N_2 and C implanted samples having mass loss of 30% and 17.7% respectively at the end of 21 days. The results are in good agreement with water

sorption and surface hydrophobicity of the implanted films after ion implantation due to the cleavage of the bonds and new band formations, implanted films degrade faster.

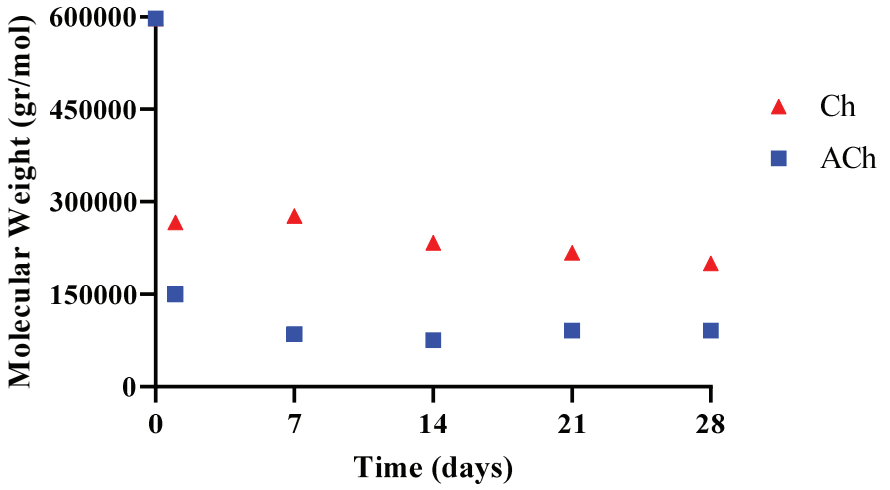

Figure 4. 24. Determination of the Molecular Weight Change of Chitosan

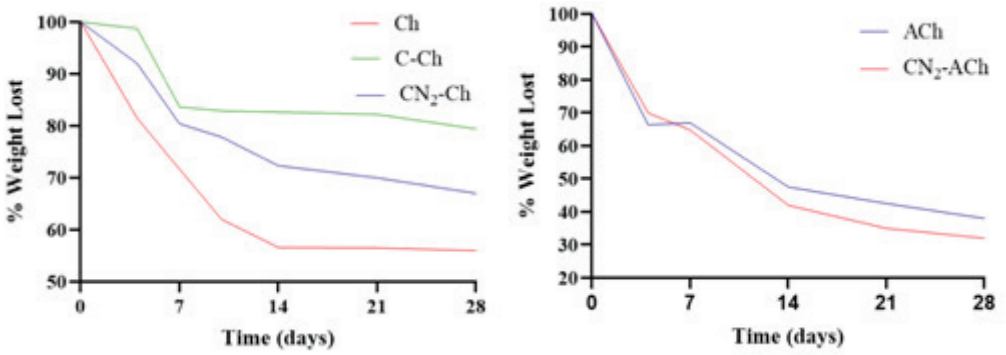

(a) Ch film and ion implantanted Ch films**.** **(b)** ACh film and ion implantanted ACh film.

Figure 4. 25 *In Vitro* biodegradation of Ch and ACh films with respect to % weight loss

CHAPTER 5

CONCLUSION

In this study, preparation and characterization of dense and asymmetric chitosan films for biomaterial applications was investigated. Surface of the chitosan films was modified by Metal Gas (MEVVA) ion implantation method. The study comprises the effect of ion implantation on chitosan film characteristics, parametric optimization of Ch and ACh film production, protein absorption kinetics, water absorption kinetics, and in *vitro* biodegradation kinetics of the Ch based films.

First of all, Ch film production parameters were optimized by evaluating the effect of chitosan concentration on thermal degradation and water absorption. To prepare chitosan films, 2% chitosan concentration were selected. Then, ACh film production parameters were optimized by evaluating the effect of pre-treatment time on pore size, thickness of the film (porous and dense layers). Pre-treatment time was selected as 20 minutes. By changing the pre-treatment time, pore size and dense/porous layer thickness of the film changes. In other words, changing the pre-treatment time relative to the target area provides an alternative method of adjusting the pore size.

Similarly, the effects of ion implantation on film-contact-angles were investigated to determine the change in surface wettability. A surface with moderate hydrophobicity characterized by a water contact angle of about 90º was considered to be most effective for preventing bacterial adhesion by M. Wang, T. Tang, (2018). To be able to prevent bacterial adhesion ion implantation method could be used. Application of ion implantation method to biomaterials may also cause a decrease in post-operational bacterial-induced death, post-operative maintenance cost, high fever etc.

Results show that the ion implantation not only changes the surface properties, but also changes protein adsorption and degradation behavior of the material. Changing of the degradation mechanism by ion implantation is very important since it provides an alternative method for mass biomaterial production after the transition from theoretical studies to medical applications. Similarly, protein adsorption behavior change makes it easy to adjust the biomaterial for the application area.

Protein adsorption studies show that maximum BSA adsorbed at pH 7.4 onto Ch film, and at pH 5 onto ChG film. Maximum Fibrinogen adsorbed at pH 5 onto Ch film, however adsorbed at pH 4 onto ChG film. Protein adsorption enhanced for C and $C+N_2$ ion implanted samples for BSA and fibrinogen, respectively due to the hydrophobic protein surface interaction effect. According to protein adsorption kinetic studies, adsorption kinetic matches with pseudo-second-order mechanism similarly with previous study reported by Wang et al.

To investigate the degradation kinetics enzymatic degradation was examined by using PBS solution for 21 days by tracking mass change. The mass of Ch, C-Ch, CN_2-Ch and ACh, CN_2-ACh samples were measured at 4^{th}, 7^{th}, 10^{th}, 14^{th} and 21^{st} days and their degradation rate evaluated. Enzymatic environment was remained as steady state by keeping the pH value stable. All samples indicated a decrease on their mass starting from the first control point at the 4^{th} day. Similarly, molecular weight degradation was seen from the first control point at the end of the 1^{st} day. When Ch and ACh samples were compared, ACh samples shows significantly higher degradation rate both by mass and molecular weight. CN_2-ACh and ACh films were degraded after 21 days 65% and 57% percent respectively. Ch, C-Ch and CN_2-Ch films were degraded after 21 days 43%, 21% and 30% percent respectively. So, healing time of the target tissue must be taken into consideration. Moreover, implantation processes modify the surface properties by re-creating the surface topology via adding new molecular bonding on the surface when C and $C+N_2$ ion bombarded into the polymer surface. Therefore, Ch ion implanted samples were started to degrade slower. Because of the porous structure of the ACh and CN_2-ACh films faster degradation of the CN_2-ACh films were not explained. This could be occurred because of the implantation process broke the bonds between monomers and form new chemical bonds between monomers and the ions. For instance, in the SEM images of the CN_2 implanted samples surface integrity corruption was seen like punctured surface.

Further studies could comprise dose effect of the ion implantation.

REFERENCES

Afzal, Naveed, Mohsin Rafique, Wajeeha Javaid, R. Ahmad, Ameeq Farooq, Murtaza Saleem, and Zubair Khaliq. 2018. "Influence of Carbon Ion Implantation Energy on Aluminum Carbide Precipitation and Electrochemical Corrosion Resistance of Aluminum." *Nuclear Instruments and Methods in Physics Research, Section B: Beam Interactions with Materials and Atoms* 436 (June): 84–91. https://doi.org/10.1016/j.nimb.2018.09.008.

Ahmed, Shakeel, Annu, Akbar Ali, and Javed Sheikh. 2018. "A Review on Chitosan Centred Scaffolds and Their Applications in Tissue Engineering." *International Journal of Biological Macromolecules*. Elsevier B.V. https://doi.org/10.1016/j.ijbiomac.2018.04.176.

Ahn, Jungho, Jihoon Ko, Somin Lee, James Yu, Yong Tae Kim, and Noo Li Jeon. 2018. "Microfluidics in Nanoparticle Drug Delivery; From Synthesis to Pre-Clinical Screening." *Advanced Drug Delivery Reviews* 128: 29–53. https://doi.org/10.1016/j.addr.2018.04.001.

AIBA, S. 2007. "Application of Chitosan Medical Care." *Gels Handbook*, 221–29. https://doi.org/10.1016/b978-012394690-4/50114-6.

Aider, Mohammed. 2010. "Chitosan Application for Active Bio-Based Films Production and Potential in the Food Industry: Review." *LWT - Food Science and Technology*. https://doi.org/10.1016/j.lwt.2010.01.021.

Alhwaige, Almahdi A., Hatsuo Ishida, and Syed Qutubuddin. 2019. "Poly(Benzoxazine-f-Chitosan) Films: The Role of Aldehyde Neighboring Groups on Chemical Interaction of Benzoxazine Precursors with Chitosan." *Carbohydrate Polymers* 209 (January): 122–29. https://doi.org/10.1016/j.carbpol.2019.01.016.

Ali, Akbar, and Shakeel Ahmed. 2018. "A Review on Chitosan and Its Nanocomposites in Drug Delivery." *International Journal of Biological Macromolecules* 109: 273–

86. https://doi.org/10.1016/j.ijbiomac.2017.12.078.

Björnmalm, Mattias, Yan Yan, and Frank Caruso. 2014. "Engineering and Evaluating Drug Delivery Particles in Microfluidic Devices." *Journal of Controlled Release* 190: 139–49. https://doi.org/10.1016/j.jconrel.2014.04.030.

Bostancioglu, R. Beklem, Mevlut Gurbuz, Ayse Gul Akyurekli, Aydin Dogan, A. Savas Koparal, and A. Tansu Koparal. 2017. "Adhesion Profile and Differentiation Capacity of Human Adipose Tissue Derived Mesenchymal Stem Cells Grown on Metal Ion (Zn, Ag and Cu) Doped Hydroxyapatite Nano-Coated Surfaces." *Colloids and Surfaces B: Biointerfaces* 155: 415–28. https://doi.org/10.1016/j.colsurfb.2017.04.015.

Bowman, Shaun M., and Stephen J. Free. 2006. "The Structure and Synthesis of the Fungal Cell Wall." *BioEssays* 28 (8): 799–808. https://doi.org/10.1002/bies.20441.

Chang, Shih Hang, and Chin He Chian. 2013. "Plasma Surface Modification Effects on Biodegradability and Protein Adsorption Properties of Chitosan Films." *Applied Surface Science* 282: 735–40. https://doi.org/10.1016/j.apsusc.2013.06.044.

Chen, Suting, Rui Feng, Chuang Zhang, and Yanyan Zhang. 2018. "Surface Roughness Measurement Method Based on Multi-Parameter Modeling Learning." *Measurement: Journal of the International Measurement Confederation* 129 (July): 664–76. https://doi.org/10.1016/j.measurement.2018.07.071.

Cheong, Hogyun, Jimin Kim, Bum Jin Kim, Eunjin Kim, Hae Yeon Park, Bong Hyuk Choi, Kye Il Joo, et al., 2019. "Multi-Dimensional Bioinspired Tactics Using an Engineered Mussel Protein Glue-Based Nanofiber Conduit for Accelerated Functional Nerve Regeneration." *Acta Biomaterialia* 90: 87–99. https://doi.org/10.1016/j.actbio.2019.04.018.

Chou, Shih Feng, Jui Yang Lai, Ching Hsien Cho, and Chih Hung Lee. 2016. "Relationships between Surface Roughness/Stiffness of Chitosan Coatings and Fabrication of Corneal Keratocyte Spheroids: Effect of Degree of Deacetylation."

Colloids and Surfaces B: Biointerfaces 142: 105–13. https://doi.org/10.1016/j.colsurfb.2016.02.051.

Cobos, Mónica, Bernardina González, M. Jesús Fernández, and M. Dolores Fernández. 2018. "Study on the Effect of Graphene and Glycerol Plasticizer on the Properties of Chitosan-Graphene Nanocomposites via in Situ Green Chemical Reduction of Graphene Oxide." *International Journal of Biological Macromolecules* 114: 599–613. https://doi.org/10.1016/j.ijbiomac.2018.03.129.

Dash, M., F. Chiellini, R. M. Ottenbrite, and E. Chiellini. 2011. "Chitosan - A Versatile Semi-Synthetic Polymer in Biomedical Applications." *Progress in Polymer Science (Oxford)* 36 (8): 981–1014. https://doi.org/10.1016/j.progpolymsci.2011.02.001.

Deb, Payel, Ashish B. Deoghare, Animesh Borah, Emon Barua, and Sumit Das Lala. 2018. "Scaffold Development Using Biomaterials: A Review." *Materials Today: Proceedings* 5 (5): 12909–19. https://doi.org/10.1016/j.matpr.2018.02.276.

Devi, Nirmla, and Joydeep Dutta. 2019. "Development and in Vitro Characterization of Chitosan/Starch/Halloysite Nanotubes Ternary Nanocomposite Films." *International Journal of Biological Macromolecules* 127 (April): 222–31. https://doi.org/10.1016/j.ijbiomac.2019.01.047.

Elshoky, Hisham A., Taher A. Salaheldin, Maha A. Ali, and Mohamed H. Gaber. 2018. "Ascorbic Acid Prevents Cellular Uptake and Improves Biocompatibility of Chitosan Nanoparticles." *International Journal of Biological Macromolecules* 115 (August): 358–66. https://doi.org/10.1016/j.ijbiomac.2018.04.055.

Escárcega-Galaz, Ana A., Dalia I. Sánchez-Machado, Jaime López-Cervantes, Ana Sanches-Silva, Tomás J. Madera-Santana, and Perfecto Paseiro-Losada. 2018. "Mechanical, Structural and Physical Aspects of Chitosan-Based Films as Antimicrobial Dressings." *International Journal of Biological Macromolecules* 116 (September): 472–81. https://doi.org/10.1016/j.ijbiomac.2018.04.149.

Fonseca-Santos, Bruno, and Marlus Chorilli. 2017. “An Overview of Carboxymethyl Derivatives of Chitosan: Their Use as Biomaterials and Drug Delivery Systems.” *Materials Science and Engineering C* 77: 1349–62. https://doi.org/10.1016/j.msec.2017.03.198.

Ghosh, Arun, M. Azam Ali, and Richard Walls. 2010. “Modification of Microstructural Morphology and Physical Performance of Chitosan Films.” *International Journal of Biological Macromolecules* 46 (2): 179–86. https://doi.org/10.1016/j.ijbiomac.2009.11.006.

Gomez Sanchez, Alejandro, Evgen Prokhorov, Gabriel Luna-Barcenas, Alma G. Mora-García, Yuriy Kovalenko, Eric M. Rivera-Muñoz, Maria Grazia Raucci, and Giovanna Buonocore. 2018. “Chitosan-Hydroxyapatite Nanocomposites: Effect of Interfacial Layer on Mechanical and Dielectric Properties.” *Materials Chemistry and Physics* 217 (June): 151–59. https://doi.org/10.1016/j.matchemphys.2018.06.062.

Guerrero, P., A. Muxika, I. Zarandona, and K. de la Caba. 2019. “Crosslinking of Chitosan Films Processed by Compression Molding.” *Carbohydrate Polymers* 206 (November 2018): 820–26. https://doi.org/10.1016/j.carbpol.2018.11.064.

Güneş, Seda, and Funda Tıhmınlıoğlu. 2017. “Hypericum Perforatum Incorporated Chitosan Films as Potential Bioactive Wound Dressing Material.” *International Journal of Biological Macromolecules* 102: 933–43. https://doi.org/10.1016/j.ijbiomac.2017.04.080.

Harish Prashanth, K. V., and R. N. Tharanathan. 2007. “Chitin/Chitosan: Modifications and Their Unlimited Application Potential-an Overview.” *Trends in Food Science and Technology* 18 (3): 117–31. https://doi.org/10.1016/j.tifs.2006.10.022.

He, Haisheng, Yi Lu, Jianping Qi, Quangang Zhu, Zhongjian Chen, and Wei Wu. 2019. “Adapting Liposomes for Oral Drug Delivery.” *Acta Pharmaceutica Sinica B* 9 (1): 36–48. https://doi.org/10.1016/j.apsb.2018.06.005.

Ho, Ming H., Chih Chien Hsieh, Sheng W. Hsiao, and Doan Van Hong Thien. 2010. "Fabrication of Asymmetric Chitosan GTR Membranes for the Treatment of Periodontal Disease." *Carbohydrate Polymers* 79 (4): 955–63. https://doi.org/10.1016/j.carbpol.2009.10.031.

Hollister, S J, R D Maddox, and J M Taboas. 2002. "1-S2.0-S0142961202001485-Main.Pdf" 23: 4095–4103. https://doi.org/10.1016/S0142-9612(02)00148-5.

Homez-Jara, Angie, Luis Daniel Daza, Diana Marcela Aguirre, José Aldemar Muñoz, José Fernando Solanilla, and Henry Alexander Váquiro. 2018. "Characterization of Chitosan Edible Films Obtained with Various Polymer Concentrations and Drying Temperatures." *International Journal of Biological Macromolecules* 113 (July): 1233–40. https://doi.org/10.1016/j.ijbiomac.2018.03.057.

Hong, Hua, Jie Wei, and Changsheng Liu. 2007. "Development of Asymmetric Gradational-Changed Porous Chitosan Membrane for Guided Periodontal Tissue Regeneration." *Composites Part B: Engineering* 38 (3): 311–16. https://doi.org/10.1016/j.compositesb.2006.05.005.

Hu, Shihao, Shichao Bi, Dong Yan, Zhongzheng Zhou, Guohui Sun, Xiaojie Cheng, and Xiguang Chen. 2018. "Preparation of Composite Hydroxybutyl Chitosan Sponge and Its Role in Promoting Wound Healing." *Carbohydrate Polymers* 184 (March): 154–63. https://doi.org/10.1016/j.carbpol.2017.12.033.

Jeong, Hyo Jin, Sang June Nam, Jin Young Song, and Soo Nam Park. 2019. "Synthesis and Physicochemical Properties of PH-Sensitive Hydrogel Based on Carboxymethyl Chitosan/2-Hydroxyethyl Acrylate for Transdermal Delivery of Nobiletin." *Journal of Drug Delivery Science and Technology* 51 (October 2018): 194–203. https://doi.org/10.1016/j.jddst.2019.02.029.

Jiang, Bo, Zhihong Wu, Huichuan Zhao, Fangyuan Tang, Jian Lu, Qingrong Wei, and Xingdong Zhang. 2006. "Electron Beam Irradiation Modification of Collagen Membrane." *Biomaterials* 27 (1): 15–23. https://doi.org/10.1016/j.biomaterials.2005.05.091.

Jing, Wei, Qiang Ao, Lin Wang, Zirong Huang, Qing Cai, Guoqiang Chen, Xiaoping Yang, and Weihong Zhong. 2018. “Constructing Conductive Conduit with Conductive Fibrous Infilling for Peripheral Nerve Regeneration.” *Chemical Engineering Journal* 345 (April): 566–77. https://doi.org/10.1016/j.cej.2018.04.044.

Joon B. Park ; Bronzino, Joseph D. 2003. *Biomaterials: Principles and Applications*. Edited by Joseph D. Bronzino. 2nd ed.,. New York.

Kara, Aylin, Sedef Tamburaci, Funda Tihminlioglu, and Hasan Havitcioglu. 2019. “Bioactive Fish Scale Incorporated Chitosan Biocomposite Scaffolds for Bone Tissue Engineering.” *International Journal of Biological Macromolecules* 130: 266–79. https://doi.org/10.1016/j.ijbiomac.2019.02.067.

Kaya, Murat, Preethi Ravikumar, Sedef Ilk, Muhammad Mujtaba, Lalehan Akyuz, Jalel Labidi, Asier M. Salaberria, Yavuz S. Cakmak, and Seher Karaman Erkul. 2018. “Production and Characterization of Chitosan Based Edible Films from Berberis Crataegina’s Fruit Extract and Seed Oil.” *Innovative Food Science and Emerging Technologies* 45 (February): 287–97. https://doi.org/10.1016/j.ifset.2017.11.013.

Kaya, N., Ahmet M. Oztarhan, E. S. Urkac, D. Ila, S. Budak, E. Oks, A. Nikolaev, et al., 2007. “Polymeric Thermal Analysis of C + H and C + H + Ar Ion Implanted UHMWPE Samples.” *Nuclear Instruments and Methods in Physics Research, Section B: Beam Interactions with Materials and Atoms* 261 (1-2 SPEC. ISS.): 711–14. https://doi.org/10.1016/j.nimb.2007.04.098.

Kondyurina, I., I. Shardakov, G. Nechitailo, V. Terpugov, and A. Kondyurin. 2014. “Cell Growing on Ion Implanted Polytetrafluorethylene.” *Applied Surface Science* 314 (September): 670–78. https://doi.org/10.1016/j.apsusc.2014.07.057.

Konwarh, Rocktotpal, Prerak Gupta, and Biman B. Mandal. 2016. “Silk-Microfluidics for Advanced Biotechnological Applications: A Progressive Review.” *Biotechnology Advances* 34 (5): 845–58. https://doi.org/10.1016/j.biotechadv.2016.05.001.

Kotwal, Arundhati, and Christine E. Schmidt. 2001. “Electrical Stimulation Alters Protein Adsorption and Nerve Cell Interactions with Electrically Conducting Biomaterials.” *Biomaterials* 22 (10): 1055–64. https://doi.org/10.1016/S0142-9612(00)00344-6.

Lavon, Ilana, and Joseph Kost. 2004. “Ultrasound and Transdermal Drug Delivery.” *Drug Discovery Today* 9 (15): 670–76. https://doi.org/10.1016/S1359-6446(04)03170-8.

Lee, Jong Hyun, Abhishek Sahu, Won Il Choi, Jae Young Lee, and Giyoong Tae. 2016. “ZOT-Derived Peptide and Chitosan Functionalized Nanocarrier for Oral Delivery of Protein Drug.” *Biomaterials* 103: 160–69. https://doi.org/10.1016/j.biomaterials.2016.06.059.

Liu, Lei, Yingcong He, Xuetao Shi, Huichang Gao, Yingjun Wang, and Zhengmei Lin. 2018. “Phosphocreatine-Modified Chitosan Porous Scaffolds Promote Mineralization and Osteogenesis in Vitro and in Vivo.” *Applied Materials Today* 12 (September): 21–33. https://doi.org/10.1016/j.apmt.2018.03.010.

Liu, Xu, Yang Wang, Zheng Cheng, Jie Sheng, and Rendang Yang. 2019. “Nano-Sized Fibrils Dispersed from Bacterial Cellulose Grafted with Chitosan.” *Carbohydrate Polymers* 214 (March): 311–16. https://doi.org/10.1016/j.carbpol.2019.03.055.

Lulli, G. 2014. “Introduction to Ion Implantation.” *CNR Institute for Microelectronics and Microsystems (IMM)*, no. Imm: 135–52. https://doi.org/10.5772/67458.

Mahajan, A., and S. S. Sidhu. 2018. “Surface Modification of Metallic Biomaterials for Enhanced Functionality: A Review.” *Materials Technology* 33 (2): 93–105. https://doi.org/10.1080/10667857.2017.1377971.

Malyer, Elif, and Ahmet Oztarhan. 2005. “Wear Behavior of Nitrogen Implanted PVD-Coated Hard Metal Cutting Inserts.” *Surface and Coatings Technology* 196 (1-3 SPEC. ISS.): 369–72. https://doi.org/10.1016/j.surfcoat.2004.08.205.

Martínez-Camacho, A. P., M. O. Cortez-Rocha, J. M. Ezquerra-Brauer, A. Z. Graciano-Verdugo, F. Rodriguez-Félix, M. M. Castillo-Ortega, M. S. Yépiz-Gómez, and M. Plascencia-Jatomea. 2010. "Chitosan Composite Films: Thermal, Structural, Mechanical and Antifungal Properties." *Carbohydrate Polymers* 82 (2): 305–15. https://doi.org/10.1016/j.carbpol.2010.04.069.

Martínez-Martínez, Mayte, Guillermo Rodríguez-Berna, Marival Bermejo, Isabel Gonzalez-Alvarez, Marta Gonzalez-Alvarez, and Virginia Merino. 2019. "Covalently Crosslinked Organophosphorous Derivatives-Chitosan Hydrogel as a Drug Delivery System for Oral Administration of Camptothecin." *European Journal of Pharmaceutics and Biopharmaceutics* 136 (January): 174–83. https://doi.org/10.1016/j.ejpb.2019.01.009.

Mavropoulos, Elena, Andréa M Costa, Lilian T Costa, Carlos A Achete, Alexandre Mello, José M Granjeiro, and Alexandre M Rossi. 2011. "Colloids and Surfaces B : Biointerfaces Adsorption and Bioactivity Studies of Albumin onto Hydroxyapatite Surface." *Colloids and Surfaces B: Biointerfaces* 83 (1): 1–9. https://doi.org/10.1016/j.colsurfb.2010.10.025.

Mi, Fwu Long, Shin Shing Shyu, Yu Bey Wu, Sung Tao Lee, Jen Yeu Shyong, and Rong Nan Huang. 2001. "Fabrication and Characterization of a Sponge-like Asymmetric Chitosan Membrane as a Wound Dressing." *Biomaterials* 22 (2): 165–73. https://doi.org/10.1016/S0142-9612(00)00167-8.

Mi, Fwu Long, Yu Bey Wu, Shin Shing Shyu, An Chong Chao, Juin Yih Lai, and Chia Ching Su. 2003. "Asymmetric Chitosan Membranes Prepared by Dry/Wet Phase Separation: A New Type of Wound Dressing for Controlled Antibacterial Release." *Journal of Membrane Science* 212 (1–2): 237–54. https://doi.org/10.1016/S0376-7388(02)00505-7.

Miguel, Sónia P., André F. Moreira, and Ilídio J. Correia. 2019. "Chitosan Based-Asymmetric Membranes for Wound Healing: A Review." *International Journal of Biological Macromolecules* 127: 460–75. https://doi.org/10.1016/j.ijbiomac.2019.01.072.

Mohandas, Annapoorna, S. Deepthi, Raja Biswas, and R. Jayakumar. 2018. “Chitosan Based Metallic Nanocomposite Scaffolds as Antimicrobial Wound Dressings.” *Bioactive Materials*. KeAi Communications Co. https://doi.org/10.1016/j.bioactmat.2017.11.003.

Monte, Micheli L., Matheus L. Moreno, Janaina Senna, Leonardo S. Arrieche, and Luiz A.A. Pinto. 2018. “Moisture Sorption Isotherms of Chitosan-Glycerol Films: Thermodynamic Properties and Microstructure.” *Food Bioscience* 22 (April): 170–77. https://doi.org/10.1016/j.fbio.2018.02.004.

Mukherjee, Dhrubojyoti, Md Azamthulla, S. Santhosh, Guru Dath, Arijit Ghosh, Rahul Natholia, J. Anbu, B. Venkatesh Teja, and K. Mohammed Muzammil. 2018. “Development and Characterization of Chitosan-Based Hydrogels as Wound Dressing Materials.” *Journal of Drug Delivery Science and Technology* 46 (August): 498–510. https://doi.org/10.1016/j.jddst.2018.06.008.

Nedela, Oldrich, Petr Slepicka, and Václav Švorcík. 2017. “Surface Modification of Polymer Substrates for Biomedical Applications.” *Materials* 10 (10). https://doi.org/10.3390/ma10101115.

Ning, Ruizhi, Feng Wang, and Ling Lin. 2016. “Biomaterial-Based Microfluidics for Cell Culture and Analysis.” *TrAC - Trends in Analytical Chemistry* 80: 255–65. https://doi.org/10.1016/j.trac.2015.08.017.

Oks, E. M., G. Yu Yushkov, P. J. Evans, A. Oztarhan, I. G. Brown, M. R. Dickinson, F. Liu, R. A. MacGill, O. R. Monteiro, and Z. Wang. 1997. “Hybrid Gas-Metal Co-Implantation with a Modified Vacuum Arc Ion Source.” *Nuclear Instruments and Methods in Physics Research, Section B: Beam Interactions with Materials and Atoms* 127–128: 782–86. https://doi.org/10.1016/S0168-583X(97)00007-4.

Öktem, T., I. Tarakçioğlu, E. Özdoğan, A. Öztarhan, E. S. Namligöz, A. Karaaslan, and Z. Tek. 2008. “Modification of Friction and Wear Properties of PET Membrane Fabrics by MEVVA Ion Implantation.” *Materials Chemistry and Physics* 108 (2–3): 208–13. https://doi.org/10.1016/j.matchemphys.2007.09.032.

Ouberai, Myriam M, Kairuo Xu, and Mark E Welland. 2014. “Biomaterials Effect of the Interplay between Protein and Surface on the Properties of Adsorbed Protein Layers.” *Biomaterials* 35 (24): 6157–63. https://doi.org/10.1016/j.biomaterials.2014.04.012.

Öztarhan, A., I. Brown, C. Bakkaloglu, G. Watt, P. Evans, E. Oks, A. Nikolaev, and Z. Tek. 2005. “Metal Vapour Vacuum Arc Ion Implantation Facility in Turkey.” *Surface and Coatings Technology* 196 (1-3 SPEC. ISS.): 327–32. https://doi.org/10.1016/j.surfcoat.2004.08.178.

Patel, Gnansagar B., N. L. Singh, and Fouran Singh. 2017. “Modification of Chitosan-Based Biodegradable Polymer by Irradiation with MeV Ions for Electrolyte Applications.” *Materials Science and Engineering B: Solid-State Materials for Advanced Technology* 225 (September): 150–59. https://doi.org/10.1016/j.mseb.2017.08.023.

Patel, Gnansagar B., N. L. Singh, Fouran Singh, and P. K. Kulriya. 2019. “Effects of MeV Ions on Physicochemical and Dielectric Properties of Chitosan/PEO Polymeric Blend.” *Nuclear Instruments and Methods in Physics Research, Section B: Beam Interactions with Materials and Atoms* 447 (December 2018): 68–78. https://doi.org/10.1016/j.nimb.2019.03.052.

Pomory, Christopher M. 2008. “Color Development Time of the Lowry Protein Assay.” *Analytical Biochemistry* 378 (2): 216–17. https://doi.org/10.1016/j.ab.2008.04.015.

Prakrajang, K., P. Wanichapichart, S. Anuntalabhochai, S. Pitakrattananukool, and L. D. Yu. 2009. “Ion Beam Modification of Chitosan and Cellulose Membranes for Simulation of Ion Bombardment of Plant Cell Envelope.” *Nuclear Instruments and Methods in Physics Research, Section B: Beam Interactions with Materials and Atoms* 267 (8–9): 1645–49. https://doi.org/10.1016/j.nimb.2009.01.094.

Quan, Qi, Haoye Meng, Biao Chang, Lei Hong, Rui Li, Guang Bo Liu, Xiao Qing Cheng, et al., 2019. “Novel 3-D Helix-Flexible Nerve Guide Conduits Repair Nerve Defects.” *Biomaterials* 207 (March): 49–60.

https://doi.org/10.1016/j.biomaterials.2019.03.040.

Rabe, Michael, Dorinel Verdes, Jan Zimmermann, and Stefan Seeger. 2008. "Surface Organization and Cooperativity during Nonspecific Protein Adsorption Events." *Journal of Physical Chemistry B* 112 (44): 13971–80. https://doi.org/10.1021/jp804532v.

Rahmani, Soheila, Shirin Hakimi, Azam Esmaeily, Fatemeh Yazdi Samadi, Elaheh Mortazavian, Mahboobeh Nazari, Zohreh Mohammadi, Niyousha Rafiee Tehrani, and Morteza Rafiee Tehrani. 2019. "Novel Chitosan Based Nanoparticles as Gene Delivery Systems to Cancerous and Noncancerous Cells." *International Journal of Pharmaceutics* 560 (October 2018): 306–14. https://doi.org/10.1016/j.ijpharm.2019.02.016.

Ramya, R., P. Muthukumaran, and J. Wilson. 2018. "Electron Beam-Irradiated Polypyrrole Decorated with Bovine Serum Albumin Pores: Simultaneous Determination of Epinephrine and L-Tyrosine." *Biosensors and Bioelectronics* 108 (October 2017): 53–61. https://doi.org/10.1016/j.bios.2018.02.044.

Ranjith, R., S. Balraj, J. Ganesh, and M.C. John Milton. 2019. "Therapeutic Agents Loaded Chitosan-Based Nanofibrous Mats as Potential Wound Dressings: A Review." *Materials Today Chemistry* 12: 386–95. https://doi.org/10.1016/j.mtchem.2019.03.008.

Ratner, Buddy D., Allan S. Hoffman, Frederick J. Schoen, and Jack E. Lemons. Biomaterials science : an introduction to materials in medicine. Washington: Elsevier Academic Press, 1996.

Rautray, Tapash R., R. Narayanan, and Kyo Han Kim. 2011. "Ion Implantation of Titanium Based Biomaterials." *Progress in Materials Science* 56 (8): 1137–77. https://doi.org/10.1016/j.pmatsci.2011.03.002

Sahoo, Debasish, Sarmila Sahoo, Priyanka Mohanty, S. Sasmal, and P. L. Nayak. 2009. "Chitosan: A New Versatile Bio-Polymer for Various Applications." *Designed*

Monomers and Polymers 12 (5): 377–404. https://doi.org/10.1163/138577209X12486896623418

Sanhueza, Claudia, Francisca Acevedo, Sebastian Rocha, Pamela Villegas, Michael Seeger, and Rodrigo Navia. 2019. "Polyhydroxyalkanoates as Biomaterial for Electrospun Scaffolds." *International Journal of Biological Macromolecules* 124: 102–10. https://doi.org/10.1016/j.ijbiomac.2018.11.068.

Santos, D. E.S., C. G.T. Neto, J. L.C. Fonseca, and M. R. Pereira. 2008. "Chitosan Macroporous Asymmetric Membranes-Preparation, Characterization and Transport of Drugs." *Journal of Membrane Science* 325 (1): 362–70. https://doi.org/10.1016/j.memsci.2008.07.050.

Saporito, Francesca, Giuseppina Sandri, Silvia Rossi, Maria Cristina Bonferoni, Federica Riva, Lorenzo Malavasi, Carla Caramella, and Franca Ferrari. 2018. "Freeze Dried Chitosan Acetate Dressings with Glycosaminoglycans and Traxenamic Acid." *Carbohydrate Polymers* 184 (August 2017): 408–17. https://doi.org/10.1016/j.carbpol.2017.12.066.

Selvi, S., Z. Tek, A. Öztarhan, N. Akbaş, and I. G. Brown. 2005. "High Fluence Effects on Ion Implantation Stopping and Range." *Nuclear Instruments and Methods in Physics Research, Section B: Beam Interactions with Materials and Atoms* 229 (1): 60–64. https://doi.org/10.1016/j.nimb.2004.11.015.

Shalaby W. Shalaby and Karen JL Burg. 2004. *Absorbable and Biodegradable Polymers*. CRC Press.

Shamekhi, Fatemeh, Elnaz Tamjid, and Khosro Khajeh. 2018. "Development of Chitosan Coated Calcium-Alginate Nanocapsules for Oral Delivery of Liraglutide to Diabetic Patients." *International Journal of Biological Macromolecules* 120: 460–67. https://doi.org/10.1016/j.ijbiomac.2018.08.078.

Sharma, Poonam, Anil Dhawan, and S. K. Sharma. 2019. "Influence of Nitrogen Ion Implantation on Corrosion Behavior of Zr 55 Cu 30 Ni 5 Al 10 Amorphous Alloy."

Journal of Non-Crystalline Solids 511 (February): 186–93. https://doi.org/10.1016/j.jnoncrysol.2019.02.009.

Shen, Chiung Chyi, Yi Chin Yang, and Bai Shuan Liu. 2011. "Large-Area Irradiated Low-Level Laser Effect in a Biodegradable Nerve Guide Conduit on Neural Regeneration of Peripheral Nerve Injury in Rats." *Injury* 42 (8): 803–13. https://doi.org/10.1016/j.injury.2011.02.005.

Shi, Chunmeng, Ying Zhu, Xinze Ran, Meng Wang, Yongping Su, and Tianmin Cheng. 2006. "Therapeutic Potential of Chitosan and Its Derivatives in Regenerative Medicine 1 1 This Work Was Supported by '973' Programs on Severe Trauma (NO. 1999054205 and NO. 2005CB522605) from the Ministry of Science and Technology of China." *Journal of Surgical Research*. https://doi.org/10.1016/j.jss.2005.12.013.

Shin, Jin Wook, Joon Pyo Jeun, and Phil Hyun Kang. 2010. "Surface Modification and Characterization of N+ Ion Implantation on Polyimide Film." *Macromolecular Research* 18 (3): 227–32. https://doi.org/10.1007/s13233-010-0310-x.

Silva, Simone S., Sandra M. Luna, Manuela E. Gomes, Johan Benesch, Iva Pashkuleva, João F. Mano, and Rui L. Reis. 2008. "Plasma Surface Modification of Chitosan Membranes: Characterization and Preliminary Cell Response Studies." *Macromolecular Bioscience* 8 (6): 568–76. https://doi.org/10.1002/mabi.200700264.

Singh, Dharaminder, Adam J. Harding, Emad Albadawi, Fiona M. Boissonade, John W. Haycock, and Frederik Claeyssens. 2018. "Additive Manufactured Biodegradable Poly(Glycerol Sebacate Methacrylate) Nerve Guidance Conduits." *Acta Biomaterialia* 78: 48–63. https://doi.org/10.1016/j.actbio.2018.07.055.

Siow, Kim S. 2018. "Low Pressure Plasma Modifications for the Generation of Hydrophobic Coatings for Biomaterials Applications." *Plasma Processes and Polymers* 15 (9): 1–19. https://doi.org/10.1002/ppap.201800059.

Sokullu Urkac, E., A. Oztarhan, F. Tihminlioglu, N. Kaya, D. Ila, C. Muntele, S. Budak, et al., 2007. “Thermal Characterization of Ag and Ag + N Ion Implanted Ultra-High Molecular Weight Polyethylene (UHMWPE).” *Nuclear Instruments and Methods in Physics Research, Section B: Beam Interactions with Materials and Atoms* 261 (1-2 SPEC. ISS.): 699–703. https://doi.org/10.1016/j.nimb.2007.04.102.

Srinivasa, P. C., M. N. Ramesh, and R. N. Tharanathan. 2007. “Effect of Plasticizers and Fatty Acids on Mechanical and Permeability Characteristics of Chitosan Films.” *Food Hydrocolloids* 21 (7): 1113–22. https://doi.org/10.1016/j.foodhyd.2006.08.005.

Sun, Xiumin, Ying Bai, Hong Zhai, Sheng Liu, Chi Zhang, Yiwei Xu, Jianlong Zou, et al., 2019. “Devising Micro/Nano-Architectures in Multi-Channel Nerve Conduits towards a pro-Regenerative Matrix for the Repair of Spinal Cord Injury.” *Acta Biomaterialia* 86: 194–206. https://doi.org/10.1016/j.actbio.2018.12.032.

Sun, Xun, Yan Fang, Zonghao Tang, Zhengchao Wang, Xinqing Liu, and Haiqing Liu. 2019. “Mesoporous Silica Nanoparticles Carried on Chitosan Microspheres for Traumatic Bleeding Control.” *International Journal of Biological Macromolecules* 127: 311–19. https://doi.org/10.1016/j.ijbiomac.2019.01.039.

Takano, Ichiro, Yoshiharu Arai, Michiko Sasaki, Yoshio Sawada, Kaori Yamada, Takayoshi Yagasaki, and Yuji Kimura. 2006. “Surface Modification of Biodegradable Plastics by Ion Beams.” *Vacuum* 80 (7 SPEC. ISS.): 788–92. https://doi.org/10.1016/j.vacuum.2005.11.003.

Takara, Eduardo A., Esteban G. Vega-Hissi, Juan C. Garro-Martinez, José Marchese, and Nelio A. Ochoa. 2019. “About Endothermic Sorption of Tyrosine on Chitosan Films.” *Carbohydrate Polymers* 206 (June 2018): 57–64. https://doi.org/10.1016/j.carbpol.2018.10.102.

Takeuchi, Issei, Tomoyoshi Takeshita, Takaaki Suzuki, and Kimiko Makino. 2017. “Iontophoretic Transdermal Delivery Using Chitosan-Coated PLGA Nanoparticles for Positively Charged Drugs.” *Colloids and Surfaces B: Biointerfaces* 160: 520–

26. https://doi.org/10.1016/j.colsurfb.2017.10.011.

Tamburaci, Sedef, Ceren Kimna, and Funda Tihminlioglu. 2019. “Bioactive Diatomite and POSS Silica Cage Reinforced Chitosan/Na-Carboxymethyl Cellulose Polyelectrolyte Scaffolds for Hard Tissue Regeneration.” *Materials Science and Engineering C* 100 (March): 196–208. https://doi.org/10.1016/j.msec.2019.02.104.

Tamburaci, Sedef, and Funda Tihminlioglu. 2017. “Diatomite Reinforced Chitosan Composite Membrane as Potential Scaffold for Guided Bone Regeneration.” *Materials Science and Engineering C* 80: 222–31. https://doi.org/10.1016/j.msec.2017.05.069.

Tamburaci, Sedef, and Funda Tihminlioglu. 2018. “Biosilica Incorporated 3D Porous Scaffolds for Bone Tissue Engineering Applications.” *Materials Science and Engineering C* 91 (May): 274–91. https://doi.org/10.1016/j.msec.2018.05.040.

Tanaka, Toshiyuki, Rena Ujiie, Hirofumi Yajima, Kyoichiro Mizutani, Yoshiaki Suzuki, and Hitoshi Sakuragi. 2011. “Ion-Beam Irradiation into Biodegradable Nanofibers for Tissue Engineering Scaffolds.” *Surface and Coatings Technology* 206 (5): 889–92. https://doi.org/10.1016/j.surfcoat.2011.04.049.

Tangpasuthadol, Varawut, Noppong Pongchaisirikul, and Vipavee P. Hoven. 2003. “Surface Modification of Chitosan Films. Effects of Hydrophobicity on Protein Adsorption.” *Carbohydrate Research* 338 (9): 937–42. https://doi.org/10.1016/S0008-6215(03)00038-7.

Tek, Z., A. Öztarhan, and S. Selvi. 2007. “Characterization of Ti + N and Zr Ion Implanted 316 L Stainless Steel.” *Surface and Coatings Technology* 201 (19-20 SPEC. ISS.): 8303–7. https://doi.org/10.1016/j.surfcoat.2006.09.334.

Tinwala, Hussain, and Sarika Wairkar. 2019. “Production, Surface Modification and Biomedical Applications of Nanodiamonds: A Sparkling Tool for Theranostics.” *Materials Science and Engineering C*. Elsevier Ltd. https://doi.org/10.1016/j.msec.2018.12.073.

Tsai, Li Chu, Chien Ho Chen, Cheng Wei Lin, Yi Cheng Ho, and Fwu Long Mi. 2019. "Development of Mutlifunctional Nanoparticles Self-Assembled from Trimethyl Chitosan and Fucoidan for Enhanced Oral Delivery of Insulin." *International Journal of Biological Macromolecules* 126: 141–50. https://doi.org/10.1016/j.ijbiomac.2018.12.182.

Ugwoke, Michael I., Remigius U. Agu, Norbert Verbeke, and Renaat Kinget. 2005. "Nasal Mucoadhesive Drug Delivery: Background, Applications, Trends and Future Perspectives." *Advanced Drug Delivery Reviews* 57 (11): 1640–65. https://doi.org/10.1016/j.addr.2005.07.009.

Uragami, Tadashi. 2006. *Material Science of Chitin and Chitosan*. Vol. 62. Tokyo: Kodansha - Springer.

Varma, Ratna, Fabio G. Aoki, Kayla Soon, Golnaz Karoubi, and Thomas K. Waddell. 2018. "Optimal Biomaterials for Tracheal Epithelial Grafts: An in Vitro Systematic Comparative Analysis." *Acta Biomaterialia* 81: 146–57. https://doi.org/10.1016/j.actbio.2018.09.048.

Vasenina, I. V., K. P. Savkin, O. A. Laput, D. N. Lytkina, V. V. Botvin, A. V. Medovnik, and I. A. Kurzina. 2018. "Effects of Ion- and Electron-Beam Treatment on Surface Physicochemical Properties of Polytetrafluoroethylene." *Surface and Coatings Technology* 334 (January): 134–41. https://doi.org/10.1016/j.surfcoat.2017.11.035.

Vijayavenkataraman, Sanjairaj, Siti Thaharah, Shuo Zhang, Wen Feng Lu, and Jerry Ying Hsi Fuh. 2019. "Electrohydrodynamic Jet 3D-Printed PCL/PAA Conductive Scaffolds with Tunable Biodegradability as Nerve Guide Conduits (NGCs) for Peripheral Nerve Injury Repair." *Materials and Design* 162: 171–84. https://doi.org/10.1016/j.matdes.2018.11.044.

Wang, Guo Wu, Hui Yang, Wei Feng Wu, Ping Zhang, and Jin Ye Wang. 2017. "Design and Optimization of a Biodegradable Porous Zein Conduit Using Microtubes as a Guide for Rat Sciatic Nerve Defect Repair." *Biomaterials* 131:

145–59. https://doi.org/10.1016/j.biomaterials.2017.03.038.

Wang, Qianwen, Zhong Zuo, Cheuk Kit Chucky Cheung, and Sharon Shui Yee Leung. 2019. “Updates on Thermosensitive Hydrogel for Nasal, Ocular and Cutaneous Delivery.” *International Journal of Pharmaceutics* 559 (October 2018): 86–101. https://doi.org/10.1016/j.ijpharm.2019.01.030.

Wang, Wei, Soichiro Itoh, Naoki Yamamoto, Atsushi Okawa, Akiko Nagai, and Kimihiro Yamashita. 2010. “Enhancement of Nerve Regeneration along a Chitosan Nanofiber Mesh Tube on Which Electrically Polarized β-Tricalcium Phosphate Particles Are Immobilized.” *Acta Biomaterialia* 6 (10): 4027–33. https://doi.org/10.1016/j.actbio.2010.04.027.

Wu, Jie, Wei Wei, Lian Yan Wang, Zhi Guo Su, and Guang Hui Ma. 2007. “A Thermosensitive Hydrogel Based on Quaternized Chitosan and Poly(Ethylene Glycol) for Nasal Drug Delivery System.” *Biomaterials* 28 (13): 2220–32. https://doi.org/10.1016/j.biomaterials.2006.12.024.

Y.X. Xu, K.M. Kim, M.A Hanna, D. Nag. 2005. “Chitosan-Starch Composite Film: Preparation and Characterization.” *Industrial Crops Anf Products 21*, 185–92.

Yotoriyama, Tasuku, Yoshiaki Suzuki, Takaya Mise, Takeyo Tsukamoto, and Masaya Iwaki. 2005. “Surface Characterization of Thin Film Induced by He+ Ion-Beam Irradiation into PLLA.” *Surface and Coatings Technology* 196 (1-3 SPEC. ISS.): 383–88. https://doi.org/10.1016/j.surfcoat.2004.08.157.

Younes, Islem, and Marguerite Rinaudo. 2015. “Chitin and Chitosan Preparation from Marine Sources. Structure, Properties and Applications.” *Marine Drugs*. https://doi.org/10.3390/md13031133.

Yu, Fang, and Deepak Choudhury. 2019. “Microfluidic Bioprinting for Organ-on-a-Chip Models.” *Drug Discovery Today* 00 (00). https://doi.org/10.1016/j.drudis.2019.03.025.

Zhang, Shumin, Rong Li, Dan Huang, Xuehong Ren, and Tung Shi Huang. 2018. "Antibacterial Modification of PET with Quaternary Ammonium Salt and Silver Particles via Electron-Beam Irradiation." *Materials Science and Engineering C* 85 (June 2017): 123–29. https://doi.org/10.1016/j.msec.2017.12.010.

Zhang, Xiwen, Masaya Kotaki, Satoko Okubayashi, and Sachiko Sukigara. 2010. "Effect of Electron Beam Irradiation on the Structure and Properties of Electrospun PLLA and PLLA/PDLA Blend Nanofibers." *Acta Biomaterialia* 6 (1): 123–29. https://doi.org/10.1016/j.actbio.2009.06.007.

Zhou, Wenting, Jian Le, Yang Chen, Ying Cai, Zhanying Hong, and Yifeng Chai. 2019. "Recent Advances in Microfluidic Devices for Bacteria and Fungus Research." *TrAC - Trends in Analytical Chemistry* 112: 175–95. https://doi.org/10.1016/j.trac.2018.12.024.

Zimet, Patricia, Álvro W. Mombrú, Dominique Mombrú, Analía Castro, Juan Pablo Villanueva, Helena Pardo, and Caterina Rufo. 2019. "Physico-Chemical and Antilisterial Properties of Nisin-Incorporated Chitosan/Carboxymethyl Chitosan Films." *Carbohydrate Polymers*. https://doi.org/10.1016/j.carbpol.2019.05.013.

APPENDIX A

10X PBS SOLUTION PREPARATION

(Ca^{2+}, Mg^{2+} free) Stock Solution, pH 7.4 (4ºC)

Prepare 10X using deionized H_2O, filter through Millipore filter, store at room temperature. Dilute 1:10 just before use with 4º water.

10X: 1 liter

- Make 0.2M phosphates (20X), 500 ml each:
    - 13.8 g/500 ml monobasic
        - Add 13.8 g to 400 ml deionized H_2O**.**
        - Dissolve by stirring at room temperature.
        - Bring volume up to 500 ml in graduated cylinder.
    - 14.2 g/500 ml dibasic anhydrous or 26.81 g/500 ml dibasic heptahydrate
- To 500 ml dibasic, add enough monobasic (< 100 ml) to reach pH 7.4.
- To 500 ml dibasic/monobasic mixture (pH 7.4), add 500 ml water containing 90 g NaCl.

APPENDIX B

TEST TUBE PROCEDURE OF BCA METHOD

- 0.1 ml of each standard and unknown sample putted into test tube.
- 2.0 ml working reagent was added to test tubes and mixed.
- Cover and incubate tubes at 37°C for 30 minutes.
- Tubes are cooled to room temperature.
- Spectrophotometer settled to 562 nm.
- Zero the spectrophotometer on a cuvette filled with deionized H_2O. Subsequently, measure the absorbance of all the samples within 10 minutes.
- Subtract the average 562 nm absorbance measurement of the Blank standard replicates from the 562 nm absorbance measurement of all other individual standard and unknown sample replicates.
- Prepare a standard curve by plotting the average Blank-corrected 562 nm measurement for each BSA standard vs. its concentration in μg/ml.
- Use the standard curve to determine the protein concentration of each unknown sample.

APPENDIX C

CALIBRATION CURVES

Calibration curves are used for the read unknown sample concentration by its absorbance reading. Calibration curves were prepared by using bovine serum albumin (BSA) and fibrinogen.

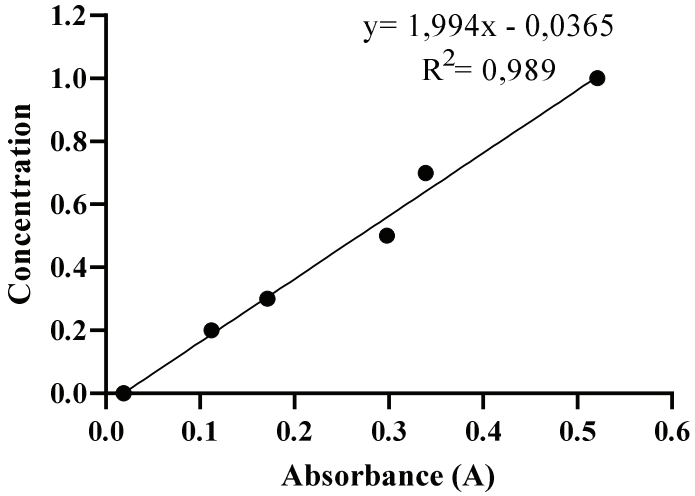

Figure C.1. Calibration curve with Albumin at pH: 4 buffer

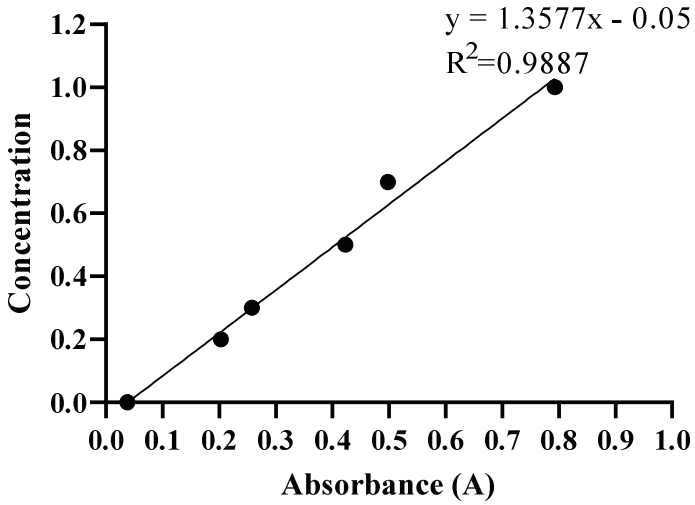

Figure C.2. Calibration curve with Albumin at pH: 5 buffer

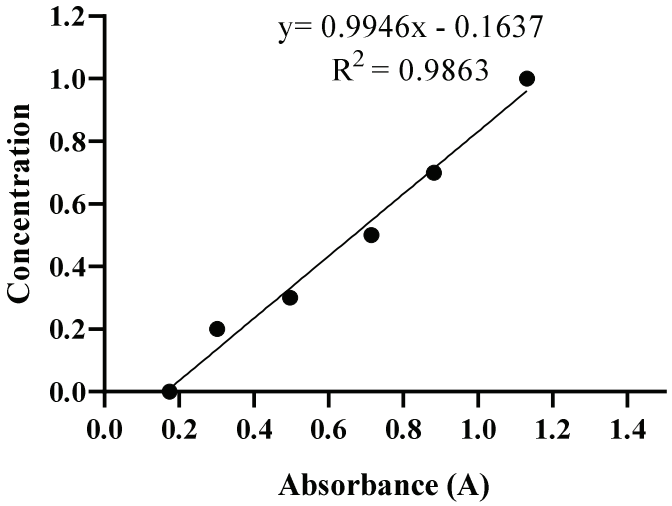

Figure C.3. Calibration curve with Albumin at pH: 7.4 buffer

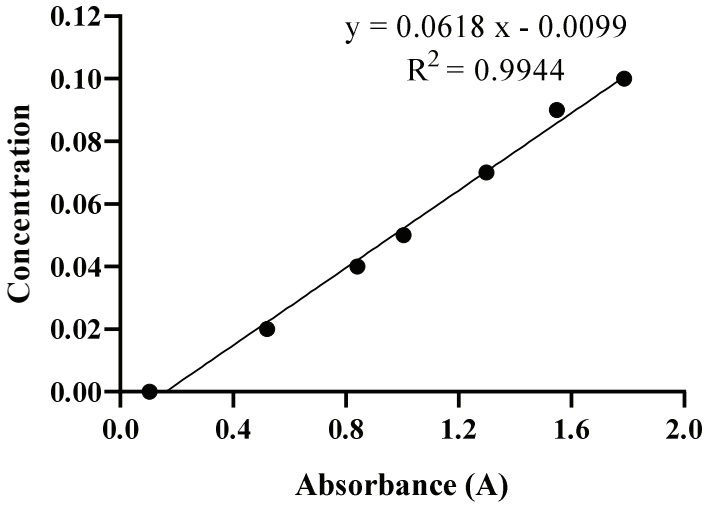

Figure C.4. Calibration curve with Fibrinogen at pH: 4 buffer

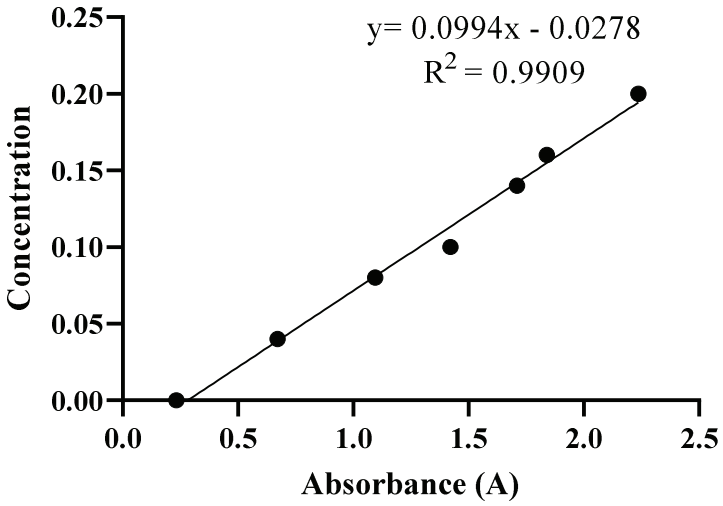

Figure C.5. Calibration curve with Fibrinogen at pH: 5 buffer

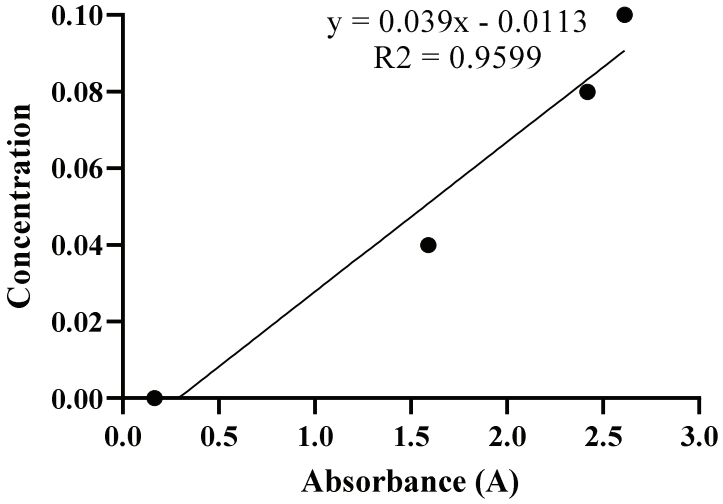

Figure C.6. Calibration curve with Fibrinogen at pH: 7.4 buffer

APPENDIX D

PROTEIN ADSORPTION RESULTS

Table D.1. Protein Adsorption Amounts

Sample q @ 60 minutes	**pH:4 ALM**	**pH:5 ALM**	**pH:7.4 ALM**	**pH:4 LYZ**	**pH:5 LYZ**	**pH:7.4 LYZ**
Ch	0.945	0.969	0.988	1.096	1.336	0.982
C-Ch	1.031	1.115	0.861	0.918	0.150	0.975
CN_2-Ch	-	-	0.861	1.238	0.783	0.629
ChG	0.579	0.984	0.384	0.733	0.578	0.463
C-ChG	0.521	0.837	0.334	0.796	0.341	0.424
CN_2- ChG	0.551	0.974	0.368	1.606	0.446	0.387
ACh	0.305	0.616	0.888	0.226	0.215	0.368
AChG	-	-	-	0.306	0.497	0.636
CN_2-ACh	-	-	0.897	0.799	1.139	0.544

APPENDIX E

MOLECULAR WEIGHT DETERMINATION

Molecular weight (Mw) determination can be studied by using viscometer. According to Mark-Houwink-Sakurada relation, by using intrinsic viscosity of polymer molecular weight is found by using following equations (Equation (E.1) (Kasaai, et al., 2007)

$$[\eta] = KM_v^a \tag{E.1}$$

Where, [η]*:* the intrinsic viscosity,

- M_υ : the average Mw,
- K and α are constants.

K and α equations were given below. They are constants changed by deacetylation degree (DD), used solvent system and also temperature. These constants were previously calculated by Kasaai et al. (2000) by equations (E.2) and (E.3). In this study constant K = $15.7*10^{-5}$ and α = 0.79 values were used for 75% DD values.

$$K = 1.64\ x\ 10^{-30}\ x\ DD^{14} \tag{E.2}$$

$$\alpha = -1.02\ x\ 10^{-2} x\ DD + 1.82 \tag{E.3}$$

Kasaai et al. (2000) were used acetic acid/sodium acetate (0.25 M /0.25 M) at 25°C for DD 75% as solvent system.

Stock solution of chitosan was prepared by dissolving 0.20 gram chitosan in 200 mL of 0.25M HAc / 0.25M NaAc. Then the stock solution diluted to lower concentrations of 0.0000, 0.0100, 0.0125, 0.0250, 0.0400, 0.0600, 0.0800, 0.1000, 0.1500, 0.2000 (w/v) with the 0.25M HAc / 0.25M NaAc solvent system.

PETROTEST kinematic viscosity device was used for kinematic viscosity measurements of chitosan solutions. In the kinematic viscosity measurements, an

Ubbelohde U-Tube capillary tube was used. Viscosimeter constant (C) of the tube is given below.

$$C = 0.00924\ cSt/s^2$$

Measurement method basically based on the multiplication of time and known C value. The sample, solvent and reduced viscosity calculation equations were given by Equation (E.4), Equation (E.5), and Equation (E.6). In the equation (4.6) "c" is the chitosan solution concentration used in viscosity measurement.

$$\eta_{sample/solvent} = C\ \left(\frac{mm^2}{sec^2}\right) t\ (sec) \tag{E.4}$$

$$\eta_{sample/solvent} = \frac{(\eta_{sample} - \eta_{solvent})}{\eta_{solvent}} \tag{E.5}$$

$$\eta_{reduced} = \frac{\eta_{specific}}{c} \tag{E.6}$$

First of all, U-Tube capillary viscometer is filled with the sample solution. The running time between the signed areas on the tube was taken. Time measurements were repeated for three times for all concentrations.

For the calculation of intrinsic viscosity, Equation (E.7) was used.

$$\eta_{reduced} = [\eta] + k[\eta]^2 c \tag{E.7}$$

APPENDIX F

DSC GRAPHS

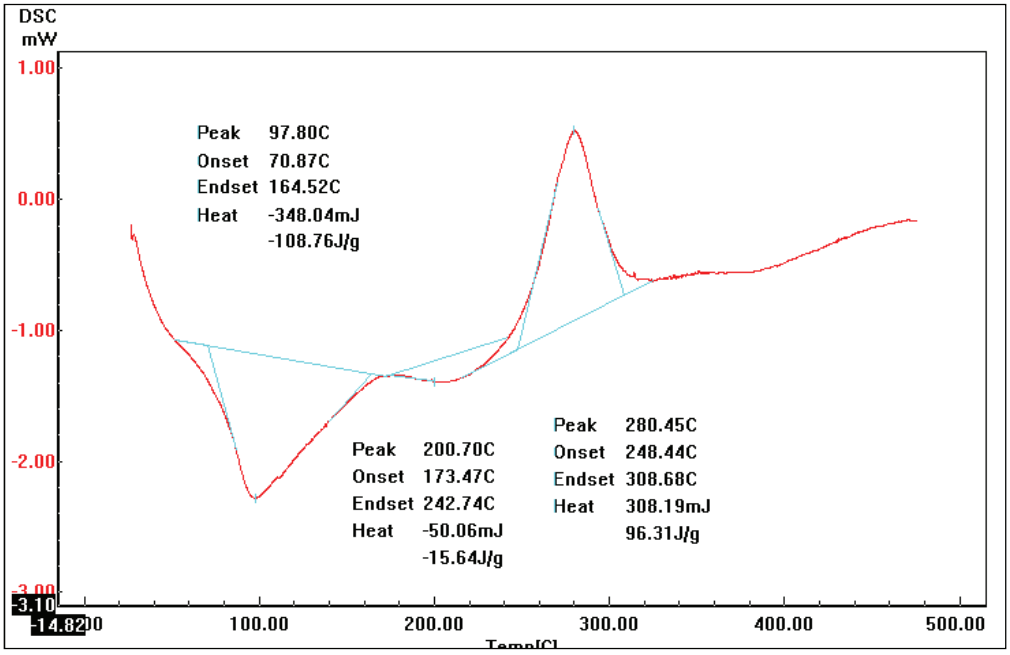

Figure F.1. DSC Graph of Ch film

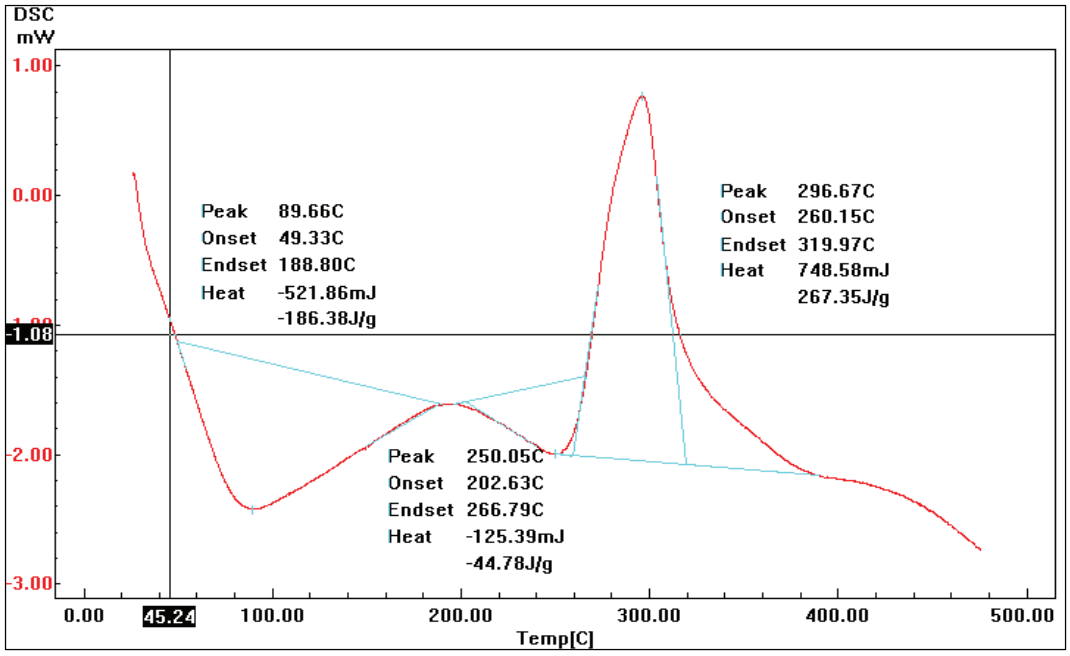

Figure F.2. DSC Graph of C-Ch film

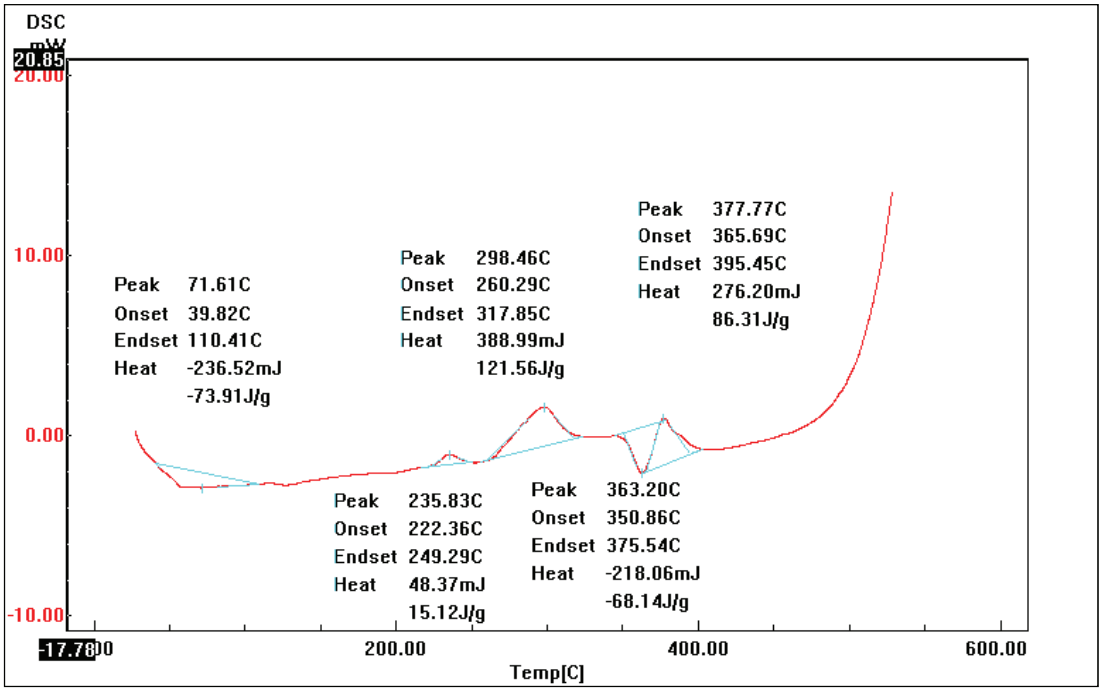

Figure F.3. DSC Graph of CN_2-Ch film

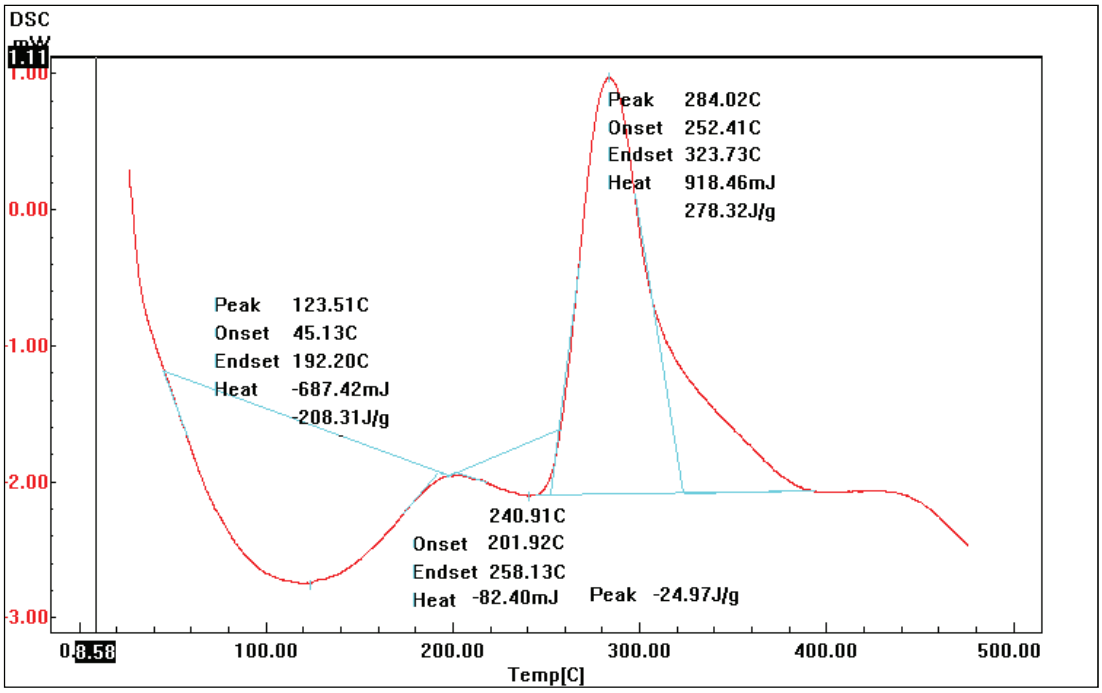

Figure F.4. DSC Graph of ChG film

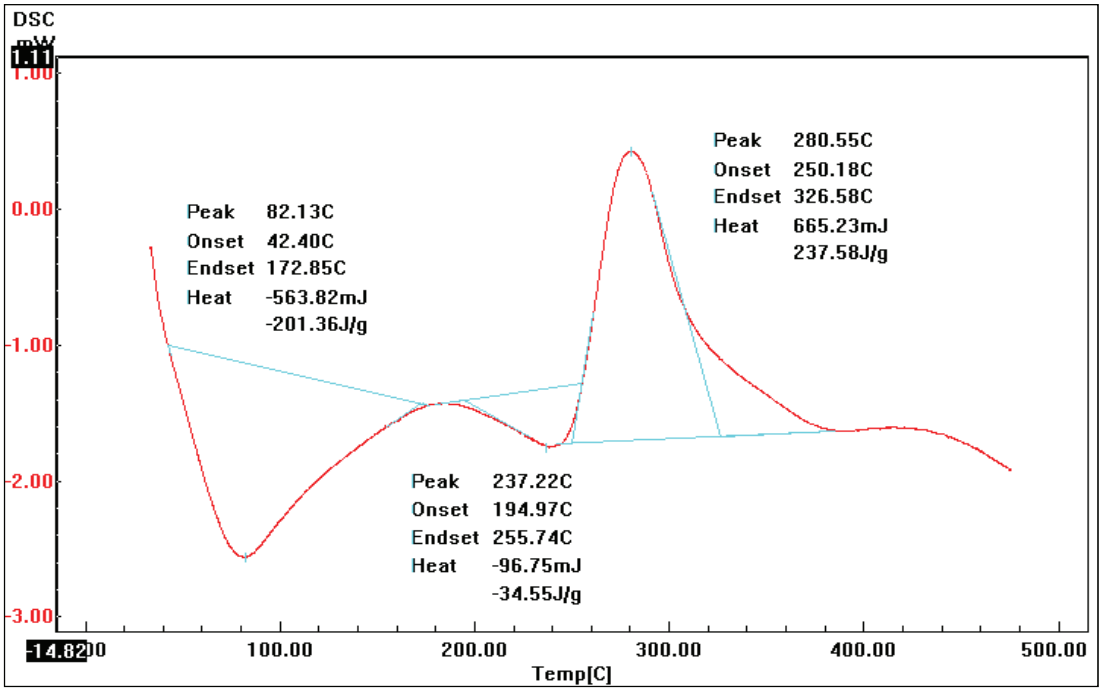

Figure F.5. DSC Graph of C-ChG film

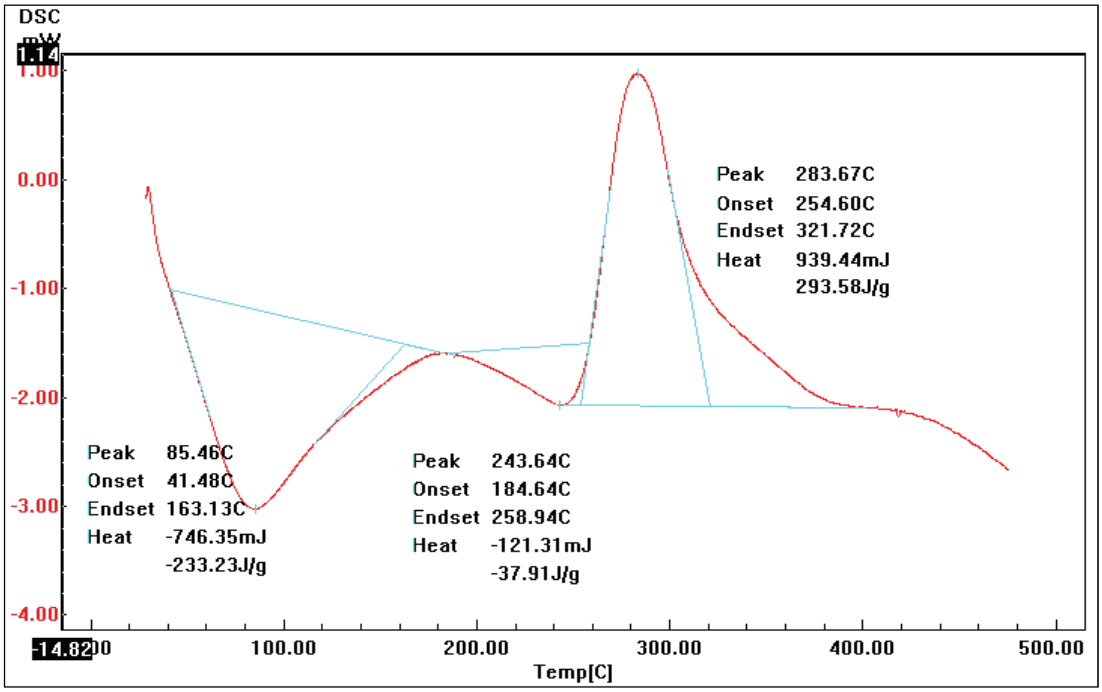

Figure F.6. DSC Graph of CN_2-ChG film

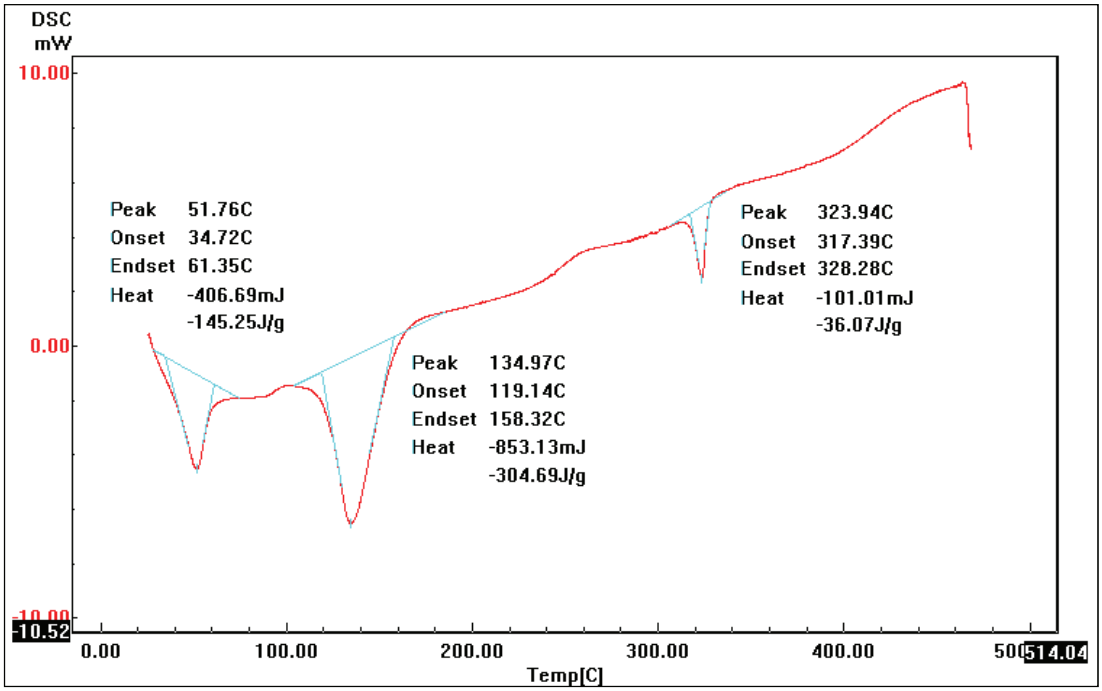

Figure F.7. DSC Graph of ACh mesh

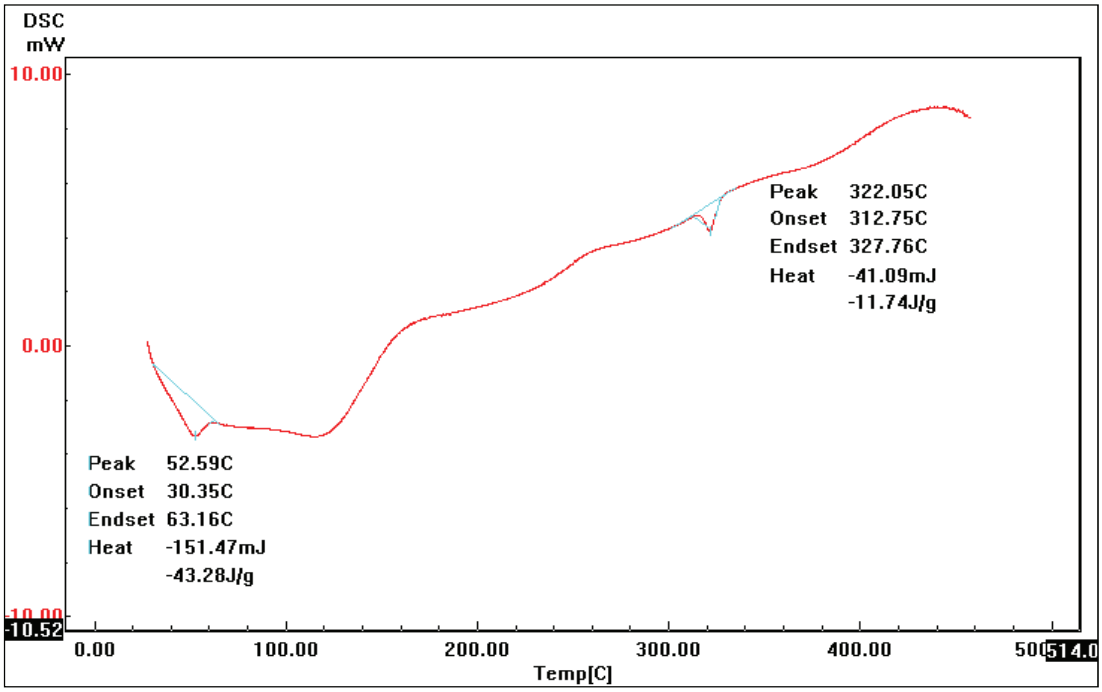

Figure F. 7. DSC Graph of AChG mesh

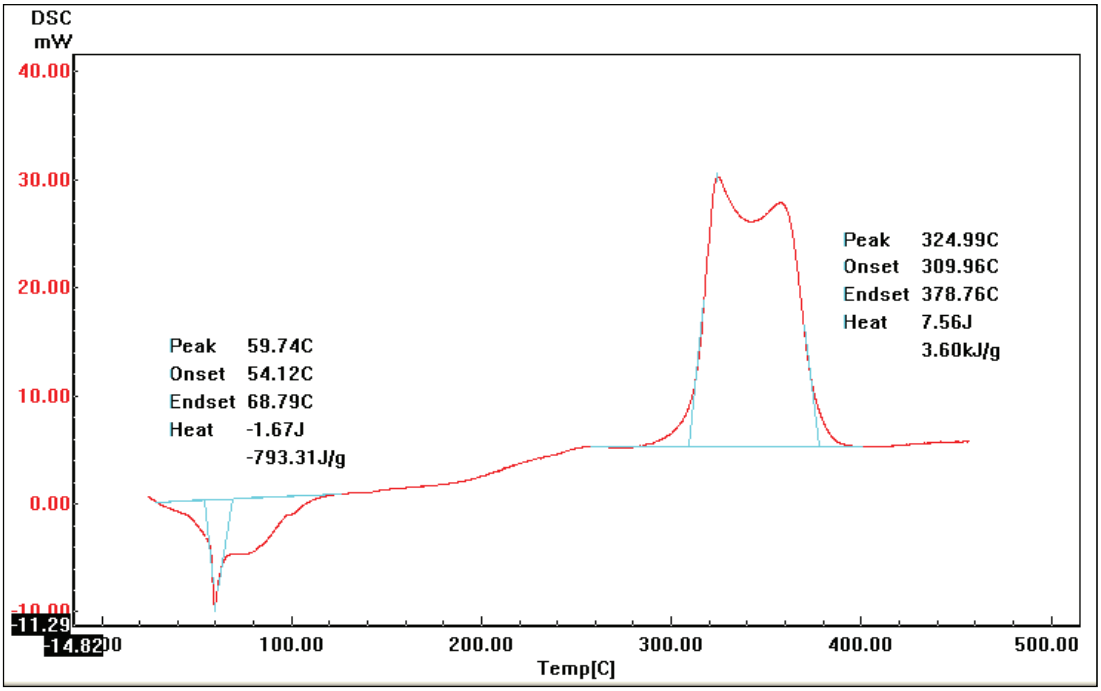

Figure F.8. DSC Graph of CN_2-AChG mesh

APPENDIX G

PRETREATMENT TIME EFFECT TO ASYMMETRIC MESHES

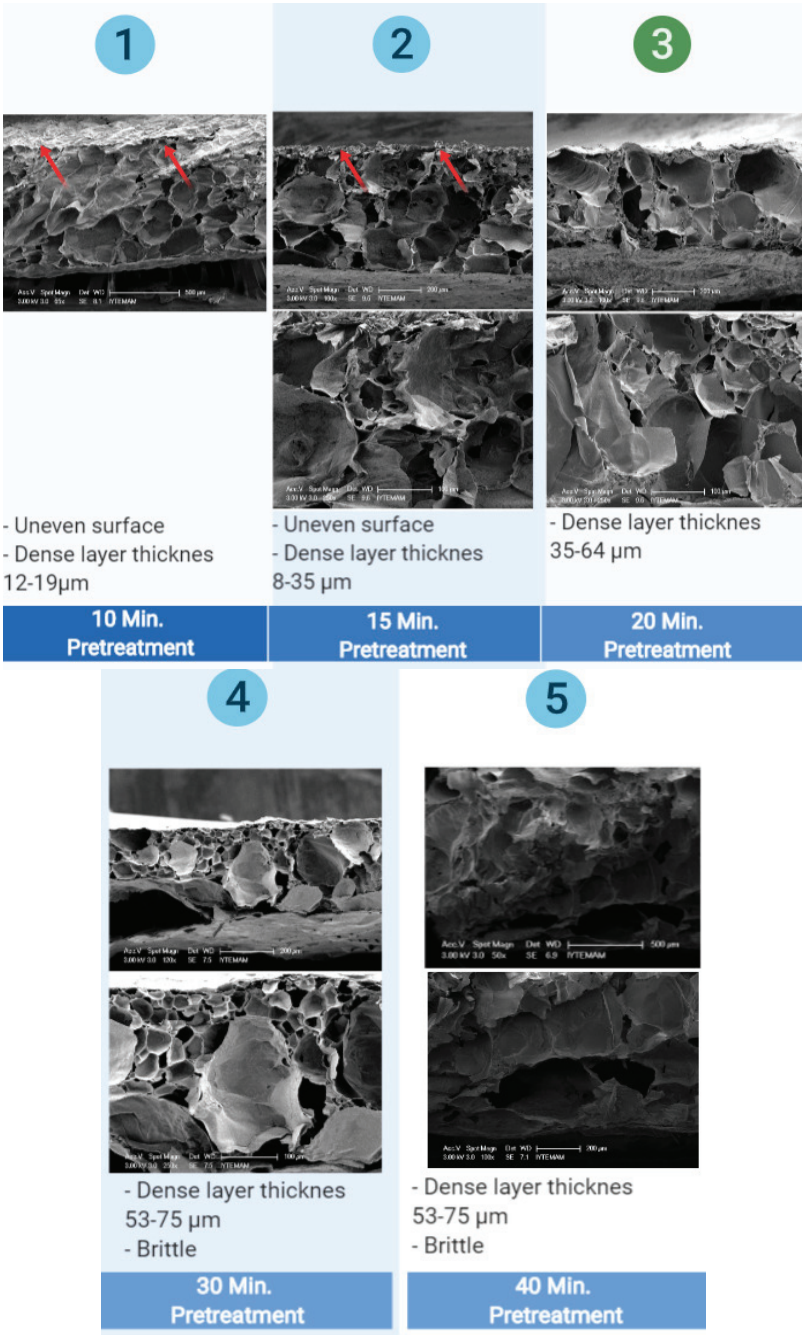

Figure G. 1 Pretreatment time effect to Asymmetric Meshes